



Astrophysical smooth particle hydrodynamics

Stephan Rosswog

School of Engineering and Science, Jacobs University Bremen, Campus Ring 1, 28759 Bremen, Germany

ARTICLE INFO

Article history:

Accepted 6 August 2009

Available online 3 September 2009

Keywords:

Hydrodynamics
Variational principles
Conservation
Shocks
Relativity

ABSTRACT

The paper presents a detailed review of the smooth particle hydrodynamics (SPH) method with particular focus on its astrophysical applications. We start by introducing the basic ideas and concepts and thereby outline all ingredients that are necessary for a practical implementation of the method in a working SPH code. Much of SPH's success relies on its excellent conservation properties and therefore the numerical conservation of physical invariants receives much attention throughout this review. The self-consistent derivation of the SPH equations from the Lagrangian of an ideal fluid is the common theme of the remainder of the text. We derive a modern, Newtonian SPH formulation from the Lagrangian of an ideal fluid. It accounts for changes of the local resolution lengths which result in corrective, so-called "grad-h-terms". We extend this strategy to special relativity for which we derive the corresponding grad-h equation set. The variational approach is further applied to a general-relativistic fluid evolving in a fixed, curved background space-time. Particular care is taken to explicitly derive all relevant equations in a coherent way.

© 2009 Elsevier B.V. All rights reserved.

1. Introduction

Much of what we observe in the physical Universe has been shaped by fluid dynamical processes. From the hot gas in galaxy clusters to the internal structures of their constituent galaxies down to their stars and planets, all has been formed by the interplay between gravity, gas dynamics and further physical processes such as the interaction with radiation, nuclear burning or magnetic fields. The latter processes often involve intrinsic length and time scales that are dramatically different from those of the gas dynamical processes, therefore many astrophysical problems are prime examples of multi-scale and multi-physics challenges. The complexity of the involved physical processes and the lack of symmetry usually prohibit analytical treatments and only numerical approaches are feasible.

Although fluid dynamics is also crucial for many technical applications, their requirements usually differ substantially from those of astrophysics and this also enters the design of the numerical methods. Typical astrophysical requirements include:

- Since fixed boundaries are usually absent, flow geometries are determined by the interplay between different physical processes such as gas dynamics and (self-)gravity which often lead to complicated, dynamically changing flow geometries. Thus, a high spatial adaptivity is often required from astrophysical hydrodynamics schemes.

- Shocks often crucially determine the evolution of cosmic objects. Examples include in supernova remnants or the Earth's magnetosphere.
- Physical quantities can vary by many orders of magnitudes between different regions of the simulation domain. This requires a particularly high robustness of the numerical scheme.
- In many astrophysical problems the numerical conservation of physically conserved quantities determines the success and the reliability of a computer simulation. Consider, for example, a molecular gas cloud that collapses under the influence of its own gravity to form stars. If the simulation for some reason dissipates angular momentum, a collapsing, self-gravitating portion of gas may form just a single stellar object instead of a multiple system of stars and it will thus produce a qualitatively wrong result.
- Many astrophysical questions require dealing with physical processes beyond gas dynamics and self-gravity. A physically intuitive and flexible formulation of the numerics can substantially facilitate the implementation of new physics modules into existing codes.

No numerical method performs equally well at each of the above requirements, therefore, the choice of the best-suited numerical approach can often save a tremendous amount of effort in obtaining reliable results. Therefore: *horses for courses*.

In the following, the smooth particle hydrodynamics (SPH) method (Lucy, 1977; Gingold and Monaghan, 1977; Hernquist and Katz, 1989; Benz, 1990; Monaghan, 1992, 2005), a completely mesh-free approach to solve the hydrodynamic equations is

E-mail address: s.rosswog@jacobs-university.de

discussed in detail. Its conservation properties are a major strength of SPH, therefore “hard-wired” conservation receives much attention throughout this text. The derivation of the SPH equations (in the absence of dissipation) requires nothing more than a suitable Lagrangian, a density prescription that depends on the coordinates and the first law of thermodynamics. The resulting equations conserve the physically conserved quantities even in their discretized form, provided that the original Lagrangian possessed the correct symmetries. Therefore, derivations from Lagrangians play a central role in our discussion of the subject.

This review has emerged from a lecture series on “Computational relativistic astrophysics” as part of a Doctoral Training Programme on the “Physics of Compact Stars” that was held in summer 2007 at the European Centre for Theoretical Studies in Nuclear Physics and Related Areas (ECT^{*}) in Trento, Italy. In the pedagogical spirit of this lecture series the text is kept in “lecture” rather than “paper” style, i.e. even rather trivial steps are written down explicitly. The goal is to pave a broad and smooth avenue to a deep understanding of the smooth particle hydrodynamics method rather than just to provide a bumpy trail. Due to this pedagogical scope, the focus of this review needs to be clear-cut, but rather narrow: it only discusses the numerical solution of the inviscid hydrodynamics equations, in the Newtonian, special-relativistic and general-relativistic (fixed metric) case.

For practical astrophysical simulations often sophisticated additional physics modules are required and their implementation may pose additional numerical challenges which are beyond the scope of this review. In the following we provide a brief list of additional physics that has been implemented into SPH and point to references that are intended as starting points for further reading.

1.1. Gravity

Self-gravity is for many astrophysical problems a key ingredient. A straight forward calculation of pairwise gravitational forces between N particles requires a prohibitively large $O(N^2)$ number of operations and therefore such an approach is not feasible for realistic problems. The most natural gravitational force evaluation for a purely meshfree method like SPH is the use of a tree, either in the form of an oct-tree (Barnes and Hut, 1986; Hernquist and Katz, 1989; Warren and Salmon, 1995; Dave et al., 1997; Carraro et al., 1998; Springel et al., 2001; Springel, 2005) or a binary tree (Benz et al., 1990; Wadsley et al., 2004; Nelson et al., 2008) both of which require only $O(N \log(N))$ operations. Other possibilities include particle-mesh methods (Hockney and Eastwood, 1988; Klypin and Holtzman, 1997; Dubinski et al., 2004) in which the particles are mapped onto a mesh. The latter is used to efficiently solve Poisson’s equation and to subsequently calculate the accelerations at the particle positions. Dehnen (2000, 2002) has used ideas from the Fast Multipole Method (FMM) (Greengard and Rokhlin, 1987) for a fast tree code which scales proportional to $O(N)$. Several hybrid approaches which combine elements of different methods exist (Theuns, 1994; Theuns et al., 1998; Bode et al., 2000; Knebe et al., 2001; Bode and Ostriker, 2003).

1.2. Equations of state

For some problems polytropic equations of state (EOS), $p = K\rho^\Gamma$, with K being a function of entropy, ρ the matter density and Γ the adiabatic exponent, are sufficiently accurate. Other problems require more sophisticated approaches. This is particularly true in cases where the matter compressibility depends on the density regime, as, for example, in neutron stars where the effective polytropic exponent above nuclear matter density is $\Gamma \approx 2.5$, but drops to values close to $4/3$ at lower densities. Different nuclear EOSs have been used (Herant et al., 1994; Fryer et al., 1999,

2006; Rosswog et al., 1999; Rosswog and Davies, 2002) in the context of neutron stars, at lower densities and in cases where the matter composition is important for other processes further physical EOSs have been applied (Guerrero et al., 2004; Lee et al., 2004, 2005; Yoon et al., 2007; Rosswog et al., 2008).

1.3. Solid state mechanics

In the context of planetary impacts additional concepts such as material stresses, fracture physics or plasticity criteria need to be implemented into SPH. This branch of development was initiated by the work of Libersky and Petschek (1990) and further continued by Libersky et al. (1993), Benz and Asphaug (1994, 1995), Asphaug and Benz (1996), Randles and Libersky (1996), Hicks et al. (1997), Vignjevic et al. (2000), Schäfer et al. (2007). More recently, also porosity models were included in SPH (Sirono, 2004; Jutzi et al., 2008).

1.4. Physical viscosity

For some applications the solution of the non-dissipative hydrodynamics equations is inadequate and physical (as opposed to artificial) viscosity needs to be modelled. Examples include the angular momentum transport in accretion disks, see e.g. (Frank et al., 2002), or the dissipation of sound waves as a mechanism to heat intra-cluster media (Fabian et al., 2003). Various authors have implemented the viscous stress tensor into SPH (Flebbe et al., 1994; Takeda et al., 1994; Watkins et al., 1996; Morris and Monaghan, 1997; Lee and Ramirez-Ruiz, 2002; Schäfer et al., 2004; Sijacki and Springel, 2006). This requires particular care in the implementation of higher order derivatives which – in a straight forward kernel approximation – can be sensitive to particle disorder.

1.5. Thermal conduction

Thermal conduction has, for example, been proposed as a possible heating mechanism for offsetting central cooling losses in rich clusters of galaxies. Its implementation poses some challenges due to second derivatives that enter the conductive term of the energy equation. Usually, a particular discretization of the second derivative due to Brookshaw (1985) is used in modelling thermal conduction (Cleary and Monaghan, 1999; Jubelgas et al., 2004).

1.6. Nuclear burning

Often the energy release due to nuclear reactions is too slow to influence gas flows substantially on a dynamical time scale. Under special circumstances, however, explosive nuclear burning can be triggered and in such cases the nuclear energy release can become the main driver of the dynamical gas evolution. In such cases the coupling between the hydrodynamics and the nuclear reactions is challenging due to the huge difference in their intrinsic time scales. The first implementation of a nuclear reaction network into SPH goes back to Benz et al. (1989). The 14 isotope α -chain network of this first study has also been used with updated nuclear reaction rates in studies of white dwarf coalescences (Guerrero et al., 2004). More recently, further small networks (Hix et al., 1998; Timmes, 1999) have been coupled with SPH (Rosswog et al., 2008) to study white dwarf coalescences (Yoon et al., 2007; Dan et al., 2009), collisions between them (Rosswog et al., 2009; Raskin et al., 2009) and tidal disruptions of white dwarfs by black holes (Rosswog et al., 2008, 2009).

1.7. Chemistry

Chemical abundances carry the imprints of the past evolutionary processes that shaped today's galaxies. Their chemical enrichment is inseparably interwoven with the formation of structure in galaxies since – being closely related to supernovae – it drives local energy feedback and gas expansion, but on the other hand it also triggers – via metallicity-dependent cooling – the contraction and collapse of local gas structures. A large variety of chemical evolution approaches has been implemented into SPH, for a starting point one may want to consult (Steinmetz and Müeller, 1994, 1995; Raiteri et al., 1996; Carraro et al., 1998; Berczik, 1999; Kawata and Gibson, 2003; Kobayashi, 2004; Tornatore et al., 2004; Scannapieco et al., 2005; Martinez-Serrano et al., 2008; Greif et al., 2009; Wiersma et al., 2009).

1.8. Radiation: photons and neutrinos

Closely related to chemical species is the interaction between photons and the ambient gas. For some problems relatively simple cooling and heating recipes can be applied, e.g. (Hernquist and Katz, 1989; Katz et al., 1996; Springel, 2005). Optically thick diffusion has in fact already been implemented in one of the very first SPH-papers (Lucy, 1977). Later, more sophisticated approaches to calculate the required second derivatives were suggested (Brookshaw, 1985). For a recent implicit diffusion approach, see (Viau et al., 2006). Flux-limited diffusion schemes have been suggested by Whitehouse et al. (2005), Whitehouse and Bate (2006) and Mayer et al. (2007), Monte-Carlo-type approaches have been followed by Oxley and Woolfson (2003), Stamatellos and Whitworth (2005), Semelin et al. (2007), and Croft and Altay (2008) and ray-tracing has been applied by Kessel-Deynet and Burkert (2000), Alvarez et al. (2006) and Altay et al. (2008). Several further methods to treat radiation in SPH do exist (Dale et al., 2007; Johnson et al., 2007; Susa, 2006; Pawlik and Schaye, 2008; Gritschneider et al., 2009; Forgan et al., 2009).

When matter densities are so large that photons are “trapped”, neutrinos can become the only cooling agents. For white dwarfs and less compact stars matter is transparent to neutrinos and they can just be treated as a local drain of thermal energy. For higher densities, say in a neutron star or the inner regions of the disk around a hyper-accreting black hole, opacity effects may prohibit the free escape of neutrinos. A further example of the astrophysical importance of neutrino physics is the delayed explosion mechanism (Wilson, 1982; Bethe and Wilson, 1985) of core-collapse supernovae where the energy deposition via neutrinos is thought to be vital to re-energize the stalled shock after it has crossed the outer layers of the stellar iron core. In this context, multi-flavour neutrino cooling and heating has been implemented into SPH (Herant et al., 1994; Fryer et al., 2006) in an entirely particle-based, flux-limited diffusion approach. To model compact object mergers, neutrinos have been implemented into SPH via a hybrid, particle-mesh approach (Rosswog and Liebendörfer, 2003) and by using local disk scale heights to estimate neutrino opacities (Lee et al., 2004, 2005).

1.9. Magnetic fields

Magnetic fields are prevalent everywhere in the cosmos, but they pose a notorious numerical challenge not least because of the difficulty in fulfilling the $\nabla \cdot \vec{B} = 0$ -constraint.

The most obvious approach is a straight-forward SPH discretization of the ideal MHD equations (Gingold and Monaghan, 1977; Phillips and Monaghan, 1985; Dolag et al., 2002; Price and

Monaghan, 2004a,b, 2005; Price, 2004). While it performs reasonably well in some problems, particle disorder and finite $\nabla \cdot \vec{B}$ values can trigger numerical instabilities (Price, 2004).

Several approaches have been developed that apply regularization techniques to overcome the problems related to particle disorder (Børve et al., 2001, 2004, 2005, 2006; Dolag and Stasyszyn, 2009).

Recently, an approach has been implemented (Rosswog and Price, 2007, 2008) that advects so-called Euler-potentials, α and β , with the SPH particles. The magnetic field can be reconstructed from the values of these potentials at the particle positions via $\vec{B} = \nabla\alpha \times \nabla\beta$. This approach guarantees the fulfillment of the $\nabla \cdot \vec{B} = 0$ -constraint by construction and has shown excellent results in a large number of test cases (Rosswog and Price, 2007).

1.10. Further “subgrid” models

Often, numerical models of astrophysical processes require the feedback from physical processes on sub-resolution scales. Such processes are usually implemented as (parametrized) “subgrid” models that transmit the main effects from the unresolved processes to the fluid.

Cosmic rays present one such example. They contribute significantly to the pressure of the interstellar medium in our Galaxy and therefore they may be important in regulating star formation during the formation and evolution of galaxies. For the implementation of the effects of cosmic rays into SPH see (Enßlin et al., 2007; Jubelgas et al., 2008; Pfrommer et al., 2008a,b; Sijacki et al., 2008).

Another example is the modelling of the feedback of (unresolvable) accretion-driven outflows during the merger of galaxies to study the self-regulation of black hole growth (Di Matteo et al., 2005; Springel et al., 2005).

In simulations on galactic scales stars – their birth, feedback via outflows and possible supernova explosions – also need to be modelled as effective sub-scale models. By their very nature such approaches are closely linked to those of radiative transfer and chemical enrichment. For the various approaches we refer to the literature (Navarro and White, 1993; Mihos and Hernquist, 1994; Bate et al., 1995, 2003; Gerritsen and Icke, 1997; Sommer-Larsen et al., 1999; Springel, 2000, 2005; Springel et al., 2001; Thacker and Couchman, 2000; Scannapieco et al., 2001; Thacker et al., 2001; Kay et al., 2002; Ascasibar et al., 2002; Theuns et al., 2002; Springel and Hernquist, 2003; Bonnell et al., 2003; Marri and White, 2003; Tornatore et al., 2003; van den Bosch et al., 2003; Clark and Bonnell, 2004; Kay, 2004; Cox et al., 2004; Dale et al., 2005; Hoeft et al., 2006; Cattaneo et al., 2007).

The remainder of this review is organized as follows. In Section 2 the most basic form of SPH (“vanilla ice”) is derived by discretizing the equations of Lagrangian hydrodynamics. This form is somewhat ad hoc, yet it performs well in practice and it is at the heart of many SPH codes that are regularly used in the astrophysics community. In Section 3, the Lagrangian of an ideal fluid is discretized and subsequently used to derive a modern version of SPH. Since it follows from a variational principle, this formulation avoids any ambiguity with respect to a symmetrization of the equations and it naturally leads to additional terms that result from derivatives of the local hydrodynamic resolution length, the so-called “grad-h-terms”, (Springel and Hernquist, 2002; Monaghan, 2002). Armed with this gadgetery suitable Lagrangians are used to elegantly derive the SPH-equations both for the special- and the general-relativistic case, see Section 4. The summary and a brief outlook are presented in Section 5.

2. Basic concepts of smooth particle hydrodynamics

2.1. Lagrangian hydrodynamics

In contrast to grid-based (Eulerian) methods, Smooth Particle Hydrodynamics (SPH) is purely Lagrangian. In the Eulerian picture, derivatives are calculated at a fixed point in space while, in the Lagrangian description, they are evaluated in a coordinate system attached to a moving fluid element. Thus in the Lagrangian approach we follow individual fish rather than staring at the pond and watch the swarm pass by. The Lagrangian (or substantial) time derivative, d/dt , is related to the Eulerian time derivative, $\partial/\partial t$, by

$$\frac{d}{dt} = \frac{dx^i}{dt} \frac{\partial}{\partial x^i} + \frac{\partial}{\partial t} = \vec{v} \cdot \nabla + \frac{\partial}{\partial t}. \quad (1)$$

Applied to the Eulerian continuity equation,

$$\frac{\partial \rho}{\partial t} + \nabla \cdot (\rho \vec{v}) = 0, \quad (2)$$

one finds, using $d\rho/dt = \vec{v} \cdot \nabla \rho + \partial\rho/\partial t$, the Lagrangian form

$$\frac{d\rho}{dt} = -\rho \nabla \cdot \vec{v}. \quad (3)$$

The momentum conservation equation for a non-viscous fluid, the so-called Euler equation, reads in Lagrangian form

$$\frac{d\vec{v}}{dt} = -\frac{\nabla P}{\rho} + \vec{f}, \quad (4)$$

i.e. apart from “body forces” such as gravity or magnetic fields embodied in the quantity \vec{f} , the fluid is accelerated by gradients of the pressure P . The energy equation follows directly from the (adiabatic) first law of thermodynamics, Eq. (7), together with Eq. (3):

$$\frac{du}{dt} = \frac{P}{\rho^2} \frac{d\rho}{dt} = -\frac{P}{\rho} \nabla \cdot \vec{v}. \quad (5)$$

First law of thermodynamics

For SPH one needs the first law of thermodynamics, $dU = dQ - PdV$, in terms of “specific” quantities. Restriction to adiabatic processes allows to drop the dQ -term. On a “per mass basis”, the energy U becomes u (“energy per mass”) and the volume, V , becomes “volume per mass”, i.e. $1/\rho$, with $dV \rightarrow d(1/\rho) = -d\rho/\rho^2$. For the case without entropy generation the first law reads

$$du = \frac{P}{\rho^2} d\rho, \quad (6)$$

from which

$$\frac{du}{dt} = \frac{P}{\rho^2} \frac{d\rho}{dt} \quad \text{and} \quad \left(\frac{\partial u}{\partial \rho}\right)_s = \frac{P}{\rho^2}, \quad (7)$$

follow. In a relativistic context it can be advantageous to work with quantities “per baryon”:

$$\left(\frac{\partial u}{\partial n}\right)_s = \frac{P}{n^2}, \quad (8)$$

where n is the baryon number density in the local rest frame.

The set of Eqs. (3)–(5) must be closed by an equation of state that relates quantities such as the pressure, P , or the speed of sound, c_s , to macroscopic fluid quantities such as density or temperature. All the microphysics, say whether the pressure is produced by collisions in a Maxwell–Boltzmann gas or by

degenerate electrons due to the Pauli principle, is embodied in the equation of state. It can be as simple as a polytrope, or, for more complicated cases, say for hot nuclear matter, it may only be available in tabular form, see the introduction for a link to the existing literature.

2.2. The SPH kernel interpolation

In the following, discrete representations of the continuous Lagrangian hydrodynamics equations are derived. In SPH, the interpolation points (“particles”) are moved with the local fluid velocity¹, derivatives are calculated via a kernel approximation without the need for finite differences. In this way the partial differential equations of Lagrangian fluid dynamics are transformed into ordinary differential equations.

In principle, there is some freedom in discretizing the fluid equations. But to ensure that the physically conserved quantities are also conserved *by construction* in the discretized particle equations the latter need to possess the correct symmetries in the particle indices. In the simplest, “vanilla ice” version of SPH, the symmetrization is imposed somewhat *ad hoc*, yet, it works well in practice and it is commonly used throughout astrophysics, see e.g. (Benz, 1990; Steinmetz, 1996; Klessen and Burkert, 2000; Bate et al., 2003; Wadsley et al., 2004; Rosswog and Davies, 2002; Wetzstein et al., 2008). For different symmetrization possibilities see (Hernquist and Katz, 1989; Thomas and Couchman, 1992; Flebbe et al., 1994; Kunze et al., 1997) and Section 2.5.

2.2.1. Interpolating function values

At the heart of SPH is a kernel approximation in which a function $f(\vec{r})$ is approximated by

$$\tilde{f}_h(\vec{r}) = \int f(\vec{r}') W(\vec{r} - \vec{r}', h) d^3 r', \quad (9)$$

where W is the so-called smoothing kernel (or window function) and the smoothing length, h , determines the width of this kernel. Obviously, one would like to recover the original function in the limit of an infinitely small smoothing region and therefore the kernel should fulfill

$$\lim_{h \rightarrow 0} \tilde{f}_h(\vec{r}) = f(\vec{r}) \quad \text{and} \quad \int W(\vec{r} - \vec{r}', h) d^3 r' = 1, \quad (10)$$

i.e. apart from being normalized, the kernel should have the δ -distribution property in the limit of vanishing smoothing length.

To arrive at a discrete approximation, one can write the integral as

$$\tilde{f}_h(\vec{r}) = \int \frac{f(\vec{r}')}{\rho(\vec{r}')} W(\vec{r} - \vec{r}', h) \rho(\vec{r}') d^3 r', \quad (11)$$

where ρ is the mass density and subsequently one can replace the integral by a sum over a set of interpolation points (“particles”), whose masses, m_b , result from the $\rho(\vec{r}') d^3 r'$ term²

$$f(\vec{r}) = \sum_b \frac{m_b}{\rho_b} f_b W(\vec{r} - \vec{r}_b, h). \quad (12)$$

The summation interpolant Eq. (12) of the density then reads

$$\rho(\vec{r}) = \sum_b m_b W(\vec{r} - \vec{r}_b, h). \quad (13)$$

¹ Variants that use local averages of fluid velocities exist, see the “XSPH”-approach of Monaghan (1989).

² For simplicity, we are omitting the subscript h in what follows. We also drop the distinction between the function to be interpolated and the interpolant, i.e. we use the same symbol f on both sides of the equal signs. Throughout the article subscripts such as A_b refer to the values at a particle position, i.e. $A_b \equiv A(\vec{r}_b)$.

This density estimate by summing up kernel-weighted masses in the neighborhood of the point \vec{r} plays a central role in the derivation of the SPH equations from a Lagrangian, see Section 3. Note that h has not been specified yet, this will be addressed at a later point. In practice, the density can also be calculated via integration of a discretized version of Eq. (3) via Eq. (31), see below. In most applications the difference between integrated and summed density estimates is completely negligible. The summation form, however, is certainly numerically more robust, integration can, in extremely underresolved regions, produce negative density values. The summation form does not assume the density to be a differentiable function while Eqs. (3) and (31) do so (Price, 2008). The standard practice in SPH is to keep the particle masses fixed so that the mass conservation is perfect and there is no need to solve the continuity equation.

2.2.2. Approximating derivatives

To calculate derivatives, one takes the analytical expression of the summation approximation, Eq. (12),

$$\nabla f(\vec{r}) = \sum_b \frac{m_b}{\rho_b} f_b \nabla W(\vec{r} - \vec{r}_b, h), \quad (14)$$

i.e. the exact derivative of the approximated function is used. The kernel function is known analytically, therefore there is no need for finite difference approximations.

Processes such as diffusion or thermal conduction require second derivatives. One could now proceed in a straight forward manner and take another derivative of Eq. (14). Yet, this estimate is rather sensitive to particle disorder and therefore not recommended for practical use. A better prescription is (Brookshaw, 1985)

$$(\nabla^2 f)_a = 2 \sum_b \frac{m_b}{\rho_b} (f_a - f_b) \frac{w_{ab}}{r_{ab}}, \quad (15)$$

where w_{ab} is related to the kernel by $\nabla W_{ab} = \hat{e}_{ab} w_{ab}$, \hat{e}_{ab} is the unit vector from particle b to particle a , $\hat{e}_{ab} = \vec{r}_{ab}/r_{ab}$ and $\vec{r}_{ab} = \vec{r}_a - \vec{r}_b$. For more information on higher order derivatives we refer to the existing literature (Brookshaw, 1985; Cleary and Monaghan, 1999; Espaol and Revenga, 2003; Monaghan, 2005).

2.2.3. The kernel function

To restrict the number of contributing particles in the sum of Eq. (12) to a local subset, the kernel should have compact support, otherwise the summation would extend over all n particles and produce a numerically intractable, completely inefficient n^2 -method. Although for geometries such as flattened disks non-radial kernels seem like a natural choice (Fulbright et al., 1995; Shapiro et al., 1996; Owen et al., 1998) they have the disadvantage that it is difficult to ensure exact angular momentum conservation, see below. Therefore, usually radial kernels with $W(\vec{r} - \vec{r}', h) = W(|\vec{r} - \vec{r}'|, h)$, are used in SPH.

The accuracy of the kernel interpolation is in practice rather difficult to quantify unless strongly simplifying assumptions about the particle distribution are made, which are usually not met in reality. One can expand $f(\vec{r})$ in the integral approximant, Eq. (9), into a Taylor series around \vec{r}

$$f(\vec{r}) = \sum_{k=0}^{\infty} \frac{(-1)^k h^k f^{(k)}(\vec{r})}{k!} \left(\frac{\vec{r} - \vec{r}'}{h} \right)^k. \quad (16)$$

By explicitly writing down the integrals over the different terms in the Taylor expansion on the RHS and comparing to the LHS, one can determine how well the approximation agrees with the original function. By requiring that error terms vanish, one can construct kernels of the desired order. In practice, however, such kernels may have unwanted properties such as negative values in certain

regions and this may, in extreme cases, lead to unphysical (negative!) density estimates from Eq. (13). Although substantial work has been invested into constructing more accurate kernels (Monaghan, 1985; Fulk and Quinn, 1996; Price, 2004; Cabezon et al., 2008), none has been found to overall perform substantially better in practice than the ‘‘standard’’ cubic spline SPH kernel (Monaghan, 1992) which is used in almost all SPH simulations. Particular higher-order kernels, however, may have advantages in the context of resolving Kelvin–Helmholtz instabilities near large density gradients (Read et al., 2009). In 3D, the cubic spline kernel reads

$$W(q) = \frac{1}{\pi h^3} \begin{cases} 1 - \frac{3}{2}q^2 + \frac{3}{4}q^3 & \text{for } 0 \leq q \leq 1, \\ \frac{1}{4}(2 - q)^3 & \text{for } 1 < q \leq 2, \\ 0 & \text{for } q > 2, \end{cases} \quad (17)$$

where $q = |\vec{r} - \vec{r}'|/h$. This kernel is *radial*, i.e. it depends only on the absolute value of $\vec{r} - \vec{r}'$. With this kernel the integral approximation, Eq. (9), is

$$\tilde{f}_h(\vec{r}) = f(\vec{r}) + Ch^2 + O(h^4), \quad (18)$$

where the quantity C contains the second derivatives of the function f . Therefore, constant and linear functions are reproduced exactly by the integral representation Eq. (9).

In practice, two approximations were applied: (i) the integral interpolation, Eq. (9), and (ii) the discretization, Eq. (12). The accuracy of the discretized equations depends on the distribution of the interpolation points (‘‘particles’’). In early work, error estimates were based on a purely statistical description assuming a random distribution of particles. In a simulation, however, the particle distribution is not random, but depends on both the kernel used and the dynamics of the considered system. For this reason, numerical experiments turned out to be far more accurate than predicted by these early estimates (Monaghan, 2005).

In the following box we collect some expressions for the derivatives of radial kernels that are frequently used throughout this text.

2.3. The ‘‘vanilla ice’’ SPH equations

2.3.1. Momentum equation

One could now proceed according to ‘‘discretize and hope for the best’’ and this was historically the first approach. A straightforward discretization of Eq. (4) (no body forces) yields

$$\frac{d\vec{v}_a}{dt} = -\frac{1}{\rho_a} \sum_b \frac{m_b}{\rho_b} P_b \nabla_a W_{ab}. \quad (19)$$

This form solves the Euler equation to the order of the method, but it does not conserve momentum. To see this, consider the force that particle b exerts on particle a ,

$$\vec{F}_{ba} = \left(m_a \frac{d\vec{v}_a}{dt} \right)_b = -\frac{m_a}{\rho_a} \frac{m_b}{\rho_b} P_b \nabla_a W_{ab}, \quad (20)$$

and similarly from a on b

$$\vec{F}_{ab} = \left(m_b \frac{d\vec{v}_b}{dt} \right)_a = -\frac{m_b}{\rho_b} \frac{m_a}{\rho_a} P_a \nabla_b W_{ba} = \frac{m_a}{\rho_a} \frac{m_b}{\rho_b} P_a \nabla_a W_{ab}, \quad (21)$$

where Eq. (26) was used. Since in general $P_a \neq P_b$, this momentum equation does not fulfill Newton’s third law (‘‘actio = reactio’’) by construction and therefore total momentum is not conserved.

Derivatives of radial kernels

Throughout the text, we use the notation $\vec{r}_{bk} = \vec{r}_b - \vec{r}_k$, $r_{bk} = |\vec{r}_{bk}|$ and $\vec{v}_{bk} = \vec{v}_b - \vec{v}_k$. Derivatives resulting from the smoothing lengths are ignored for the moment, they will receive particular attention in Section 3. By straight-forward component-wise differentiation one finds

$$\frac{\partial}{\partial \vec{r}_a} |\vec{r}_b - \vec{r}_k| = \frac{(\vec{r}_b - \vec{r}_k)(\delta_{ba} - \delta_{ka})}{|\vec{r}_b - \vec{r}_k|^2} = \hat{e}_{bk}(\delta_{ba} - \delta_{ka}), \quad (22)$$

where \hat{e}_{bk} is the unit vector from particle k to particle b ,

$$\frac{\partial}{\partial \vec{r}_a} \frac{1}{|\vec{r}_b - \vec{r}_k|} = -\frac{\hat{e}_{bk}(\delta_{ba} - \delta_{ka})}{|\vec{r}_b - \vec{r}_k|^2} \quad (23)$$

and δ_{ij} is the usual Kronecker symbol. Another frequently needed expression is

$$\begin{aligned} \frac{dr_{ab}}{dt} &= \frac{\partial r_{ab}}{\partial x_a} \frac{dx_a}{dt} + \frac{\partial r_{ab}}{\partial y_a} \frac{dy_a}{dt} + \frac{\partial r_{ab}}{\partial z_a} \frac{dz_a}{dt} + \frac{\partial r_{ab}}{\partial x_b} \frac{dx_b}{dt} + \frac{\partial r_{ab}}{\partial y_b} \\ &\quad \times \frac{dy_b}{dt} + \frac{\partial r_{ab}}{\partial z_b} \frac{dz_b}{dt} \\ &= \nabla_a r_{ab} \cdot \vec{v}_a + \nabla_b r_{ab} \cdot \vec{v}_b = \nabla_a r_{ab} \cdot \vec{v}_a - \nabla_a r_{ab} \cdot \vec{v}_b \\ &= \nabla_a r_{ab} \cdot \vec{v}_{ab} = \hat{e}_{ab} \cdot \vec{v}_{ab}, \end{aligned} \quad (24)$$

where $\partial r_{ab}/\partial x_b = -\partial r_{ab}/\partial x_a$ etc. was used. For kernels that only depend on the magnitude of the separation, $W(\vec{r}_b - \vec{r}_k) = W(|\vec{r}_b - \vec{r}_k|) \equiv W_{bk}$, the derivative with respect to the coordinate of an arbitrary particle a is

$$\begin{aligned} \nabla_a W_{bk} &= \frac{\partial}{\partial \vec{r}_a} W_{bk} = \frac{\partial W_{bk}}{\partial r_{bk}} \frac{\partial r_{bk}}{\partial \vec{r}_a} = \frac{\partial W_{bk}}{\partial r_{bk}} \hat{e}_{bk}(\delta_{ba} - \delta_{ka}) \\ &= \nabla_b W_{kb}(\delta_{ba} - \delta_{ka}), \end{aligned} \quad (25)$$

where Eq. (22) was used. This yields in particular the important property

$$\begin{aligned} \nabla_a W_{ab} &= \frac{\partial}{\partial \vec{r}_a} W_{ab} = \frac{\partial W_{ab}}{\partial r_{ab}} \frac{\partial r_{ab}}{\partial \vec{r}_a} = \frac{\partial W_{ab}}{\partial r_{ab}} \hat{e}_{ab} \\ &= -\frac{\partial W_{ab}}{\partial r_{ab}} \frac{\partial r_{ab}}{\partial \vec{r}_b} = -\frac{\partial}{\partial \vec{r}_b} W_{ab} = -\nabla_b W_{ab}. \end{aligned} \quad (26)$$

The time derivative of the kernel is given by

$$\begin{aligned} \frac{dW_{ab}}{dt} &= \frac{\partial W_{ab}}{\partial r_{ab}} \frac{dr_{ab}}{dt} = \frac{\partial W_{ab}}{\partial r_{ab}} \frac{(\vec{r}_a - \vec{r}_b) \cdot (\vec{v}_a - \vec{v}_b)}{r_{ab}} \\ &= \frac{\partial W_{ab}}{\partial r_{ab}} \hat{e}_{ab} \cdot \vec{v}_{ab} = \vec{v}_{ab} \cdot \nabla_a W_{ab}. \end{aligned} \quad (27)$$

But a slightly more sophisticated approach yields built-in conservation. If one starts from

$$\nabla \left(\frac{P}{\rho} \right) = \frac{\nabla P}{\rho} - P \frac{\nabla \rho}{\rho^2}, \quad (28)$$

solves for $\nabla P/\rho$ and applies the gradient formula (14), the momentum equation reads

$$\begin{aligned} \frac{d\vec{v}_a}{dt} &= -\frac{P_a}{\rho_a^2} \sum_b m_b \nabla_a W_{ab} - \sum_b \frac{m_b}{\rho_b} \frac{P_b}{\rho_b} \nabla_a W_{ab} \\ &= -\sum_b m_b \left(\frac{P_a}{\rho_a^2} + \frac{P_b}{\rho_b^2} \right) \nabla_a W_{ab}. \end{aligned} \quad (29)$$

Because the pressure part of the equation is now manifestly symmetric in a and b and $\nabla_a W_{ab} = -\nabla_b W_{ba}$, the forces are now equal and opposite and therefore total momentum and angular momen-

tum (see below) are conserved by construction. It is worth pointing out some issues:

- So far, any complications resulting from variable smoothing lengths have been ignored. Conservation is guaranteed if (a) constant smoothing lengths are used (which is a bad idea in practice!) or (b) “ $\nabla_a W_{ab}$ ” is symmetric in the smoothing lengths, which can be achieved, for example, by using $h_{ab} = (h_a + h_b)/2$ (Benz, 1990) or by replacing the gradient via $[\nabla_a W(r_{ab}, h_a) + \nabla_a W(r_{ab}, h_b)]/2$ (Hernquist and Katz, 1989).
- The conservation relies on the force being a term symmetric in a and b times \hat{e}_{ab} (keep in mind that $\nabla_a W_{ab} \propto \hat{e}_{ab}$, see Eq. (26)).
- SPH’s success largely relies on its excellent conservation properties which is guaranteed by the correct symmetry in the particle indices.

2.3.2. Energy equation

A suitable energy equation can be constructed from Eq. (5) in a straight forward manner:

$$\frac{du_a}{dt} = \frac{P_a}{\rho_a^2} \frac{d\rho_a}{dt} = \frac{P_a}{\rho_a^2} \frac{d}{dt} \left(\sum_b m_b W_{ab} \right) = \frac{P_a}{\rho_a^2} \sum_b m_b \vec{v}_{ab} \cdot \nabla_a W_{ab}, \quad (30)$$

where Eq. (27) was used. Together with an equation of state, the Eqs. (13), (29) and (30) form a complete set of SPH equations.

For later use we also note that the velocity divergence can be conveniently expressed by using Eqs. (3) and (27) as

$$(\nabla \cdot \vec{v})_a = -\frac{1}{\rho_a} \frac{d\rho_a}{dt} = -\frac{1}{\rho_a} \sum_b m_b \vec{v}_{ab} \cdot \nabla_a W_{ab}. \quad (31)$$

One can derive an alternative energy equation, and this will allow a smoother transition to the relativistic equations, by using the specific “thermokinetic” energy $\hat{e}_a = u_a + \frac{1}{2}v_a^2$ instead of the specific thermal energy u_a . The corresponding continuous evolution equation,

$$\frac{d\hat{e}}{dt} = -\frac{1}{\rho} \nabla \cdot (P\vec{v}), \quad (32)$$

can be written as

$$\frac{d\hat{e}}{dt} = -\frac{P}{\rho^2} \nabla \cdot (\rho\vec{v}) - \vec{v} \cdot \nabla \left(\frac{P}{\rho} \right). \quad (33)$$

Applying Eq. (14) yields

$$\begin{aligned} \frac{d\hat{e}_a}{dt} &= -\frac{P_a}{\rho_a^2} \sum_b \frac{m_b}{\rho_b} \rho_b \vec{v}_b \cdot \nabla_a W_{ab} - \vec{v}_a \cdot \sum_b \frac{m_b}{\rho_b} \frac{P_b}{\rho_b} \nabla_a W_{ab} \\ &= -\sum_b m_b \left(\frac{P_a \vec{v}_b}{\rho_a^2} + \frac{P_b \vec{v}_a}{\rho_b^2} \right) \cdot \nabla_a W_{ab}. \end{aligned} \quad (34)$$

As we will see later, this is similar to the relativistic form of the energy equation, see Eq. (167).

2.4. Conservation properties

We can easily check the numerical conservation of the physically conserved quantities. The change of the total particle momentum is

$$\begin{aligned} \sum_a m_a \frac{d\vec{v}_a}{dt} &= \sum_a \sum_b \vec{F}_{ba} = \frac{1}{2} \left(\sum_a \sum_b \vec{F}_{ba} + \sum_a \sum_b \vec{F}_{ba} \right) \\ &= \frac{1}{2} \left(\sum_{a,b} \vec{F}_{ab} + \sum_{b,a} \vec{F}_{ba} \right) = \frac{1}{2} \left(\sum_{a,b} (\vec{F}_{ab} + \vec{F}_{ba}) \right) = 0, \end{aligned} \quad (35)$$

where the (dummy) summation indices were relabeled after the third equal sign and the notation from Eq. (20) and $\vec{F}_{ab} = -\vec{F}_{ba}$ were used.

The proof for angular momentum is analogous. The torque on particle a is

$$\vec{M}_a = \vec{r}_a \times \vec{F}_a = \vec{r}_a \times \left(m_a \frac{d\vec{v}_a}{dt} \right) = \vec{r}_a \times \sum_b \vec{F}_{ba}, \quad (36)$$

and thus

$$\begin{aligned} \frac{d\vec{L}}{dt} &= \sum_a \vec{M}_a = \sum_{a,b} \vec{r}_a \times \vec{F}_{ba} = \frac{1}{2} \left(\sum_{a,b} \vec{r}_a \times \vec{F}_{ba} + \sum_{a,b} \vec{r}_a \times \vec{F}_{ba} \right) \\ &= \frac{1}{2} \left(\sum_{a,b} \vec{r}_a \times \vec{F}_{ba} + \sum_{b,a} \vec{r}_b \times \vec{F}_{ab} \right) = \frac{1}{2} \left(\sum_{a,b} (\vec{r}_a - \vec{r}_b) \times \vec{F}_{ba} \right) \\ &= 0. \end{aligned} \quad (37)$$

Again, the dummy indices were relabeled and $\vec{F}_{ab} = -\vec{F}_{ba}$ was used. The expression finally vanishes, because the forces between particles act along the line joining them: $\vec{F}_{ab} \propto \nabla_a W_{ab} \propto \hat{e}_{ab} \propto (\vec{r}_a - \vec{r}_b)$, see Eq. (26).

The total energy changes according to

$$\begin{aligned} \frac{dE}{dt} &= \frac{d}{dt} \sum_a \left(m_a u_a + \frac{1}{2} m_a v_a^2 \right) = \sum_a m_a \frac{d\hat{e}_a}{dt} \\ &= \sum_a m_a \left(\frac{du_a}{dt} + \vec{v}_a \cdot \frac{d\vec{v}_a}{dt} \right). \end{aligned} \quad (38)$$

Inserting Eqs. (30) and (29) we have

$$\begin{aligned} \frac{dE}{dt} &= \sum_a m_a \left[\frac{P_a}{\rho_a^2} \sum_b m_b \vec{v}_{ab} \cdot \nabla_a W_{ab} - \vec{v}_a \cdot \sum_b m_b \left(\frac{P_a}{\rho_a^2} + \frac{P_b}{\rho_b^2} \right) \nabla_a W_{ab} \right] \\ &= \sum_{a,b} m_a m_b \frac{P_a}{\rho_a^2} \vec{v}_a \cdot \nabla_a W_{ab} - \sum_{a,b} m_a m_b \frac{P_a}{\rho_a^2} \vec{v}_b \cdot \nabla_a W_{ab} \\ &\quad - \sum_{a,b} m_a m_b \frac{P_a}{\rho_a^2} \vec{v}_a \cdot \nabla_a W_{ab} - \sum_{a,b} m_a m_b \frac{P_b}{\rho_b^2} \vec{v}_a \cdot \nabla_a W_{ab} \\ &= - \sum_{a,b} m_a m_b \left(\frac{P_a \vec{v}_b}{\rho_a^2} + \frac{P_b \vec{v}_a}{\rho_b^2} \right) \cdot \nabla_a W_{ab}. \end{aligned} \quad (39)$$

From this equation we could have directly read off the evolution equation for the specific thermokinetic energy, Eq. (34). To show the conservation of the total energy we can apply the same procedure as in the case of the momentum equation since we have again a double sum over a quantity symmetric in the indices a, b multiplied by a quantity which is anti-symmetric in the indices a, b . Therefore, the double sum vanishes and total energy is conserved.

2.5. Alternative SPH discretizations

Like other numerical schemes, SPH offers some freedom in discretizing the continuum equations. At this point it is worth remembering that we had enforced momentum conservation by using a particular form of the gradient on the RHS of the momentum equation, see Eq. (28). Following the same reasoning one could as well have used (Monaghan, 1992)

$$\frac{\nabla P}{\rho} = \frac{P}{\rho^\lambda} \nabla \left(\frac{1}{\rho^{1-\lambda}} \right) + \frac{1}{\rho^{2-\lambda}} \nabla \left(\frac{P}{\rho^{\lambda-1}} \right), \quad (40)$$

which yields

$$\frac{d\vec{v}_a}{dt} = - \sum_b m_b \left(\frac{P_a}{\rho_a^\lambda \rho_b^{2-\lambda}} + \frac{P_b}{\rho_a^{2-\lambda} \rho_b^\lambda} \right) \nabla_a W_{ab}, \quad (41)$$

for the momentum equation. This form is symmetric in the particle indices for any value of λ and therefore also conserves momentum

by construction. This equation is consistent with the energy equation

$$\frac{du_a}{dt} = \frac{P_a}{\rho_a^\lambda} \sum_b m_b \frac{\vec{v}_{ab}}{\rho_b^{2-\lambda}} \cdot \nabla_a W_{ab}, \quad (42)$$

and the continuity equation

$$\frac{d\rho_a}{dt} = \rho_a^{2-\lambda} \sum_b m_b \frac{\vec{v}_{ab}}{\rho_b^{2-\lambda}} \cdot \nabla_a W_{ab}, \quad (43)$$

which is the SPH-discrete form of

$$\frac{d\rho_a}{dt} = \rho^{2-\lambda} [\vec{v} \cdot \nabla (\rho^{\lambda-1}) - \nabla \cdot (\vec{v} \rho^{\lambda-1})]. \quad (44)$$

The consistency of the above SPH equation set can be shown by using a generalized variational principle (Price, 2004) that does not assume that the density is given as a function of the coordinates, but instead assumes a given form of the continuity equation.

If $\lambda = 1$, the continuity equation only depends on the particle volumes m_b/ρ_b rather than the particle masses. This can reduce numerical noise in regions of large density contrasts where particles of very different masses interact (Ritchie and Thomas, 2001). Marri and White (2003) found improved results in their galaxy formation calculations by using (among other modifications) a value of $\lambda = 3/2$.

The SPH equations can be generalized even further after noting that the continuity equation can be written as (Price, 2004)

$$\frac{d\rho}{dt} = \Psi \left\{ \vec{v} \cdot \nabla \left(\frac{\rho}{\Psi} \right) - \nabla \cdot \left(\frac{\rho \vec{v}}{\Psi} \right) \right\}, \quad (45)$$

with Ψ being a scalar variable defined on the particle field. This leads to SPH equations of the form

$$\frac{d\rho_a}{dt} = \Psi_a \sum_b m_b \frac{\vec{v}_{ab}}{\Psi_b} \cdot \nabla_a W_{ab} \quad (46)$$

$$\frac{d\vec{v}_a}{dt} = - \sum_b m_b \left(\frac{P_a}{\rho_a^2} \frac{\Psi_a}{\Psi_b} + \frac{P_b}{\rho_b^2} \frac{\Psi_b}{\Psi_a} \right) \nabla_a W_{ab} \quad (47)$$

$$\frac{du_a}{dt} = \frac{P_a}{\rho_a^2} \sum_b m_b \frac{\Psi_a}{\Psi_b} \vec{v}_{ab} \cdot \nabla_a W_{ab}. \quad (48)$$

The ‘‘vanilla ice’’ equation set, Eqs. (29) and (30), is recovered for $\Psi = 1$, choosing $\Psi = \rho/\sqrt{P}$ one recovers the momentum equation of Hernquist and Katz (1989).

The above equation set has been used in recent work (Read et al., 2009) to address SPH’s weakness of resolving Kelvin–Helmholtz instabilities across large density jumps. The authors choose a different auxiliary function for each of the above equations, $\Psi^\rho, \Psi^v, \Psi^u$, and perform an error and stability analysis leading them to suggest $\Psi^\rho = \Psi^u = 1/A^\Gamma$ and $\Psi^v = \rho$. Here A is the entropy-dependent part of the polytropic equation of state, $P = A(s)\rho^\Gamma$ and Γ the polytropic exponent. This prescription leads to a sharper density transition that is more consistent with the entropy transitions between both parts of the fluid. Together with a higher-order kernel and large neighbor numbers they find convincing results in Kelvin–Helmholtz instability simulations.

2.6. Adaptive resolution

Whenever densities and length scales vary by large amounts, the smoothing length h should be adapted in space and time. Several ways to adjust the smoothing lengths have been used over the years (Gingold and Monaghan, 1977, 1978, 1982; Hernquist and Katz, 1989; Benz, 1990; Steinmetz and Müller, 1993). One of them seeks to keep the number of neighbors of each particle (approximately) constant (Hernquist and Katz, 1989), another to integrate

an additional equation that makes use of the continuity equation (Benz, 1990). One can use the ansatz

$$\frac{h(t)}{h_0} = \left(\frac{\rho_0}{\rho(t)} \right)^{1/3}, \quad (49)$$

where the index 0 labels the quantities at the beginning of the simulation. Taking Lagrangian time derivatives of both sides together with Eq. (3) yields

$$\frac{dh_a}{dt} = \frac{1}{3} h_a (\nabla \cdot \vec{v})_a. \quad (50)$$

Another convenient way is to evolve h according to

$$h_a = \eta \left(\frac{m_a}{\rho_a} \right)^{1/3}, \quad (51)$$

where η should be chosen in the range between 1.2 and 1.5 (Gingold and Monaghan, 1982; Price, 2004; Monaghan, 2005).

Note, that the above SPH equations were derived under the assumption that the smoothing lengths are constant. Varying the smoothing lengths while using the above equation set is strictly speaking inconsistent. A consistent formulation that involves extra-terms will be discussed in detail in Section 3.3. The importance of these corrective, or “grad-h” terms is problem- and resolution-dependent (Springel and Hernquist, 2002; Rosswog and Price, 2007).

2.7. Artificial dissipation

2.7.1. Purpose and general reasoning

In gas dynamics, even perfectly smooth initial conditions can steepen into discontinuous solutions, or “shocks”, see e.g. (Landau and Lifshitz, 1959; Whitham, 1974; Shu, 1992), which are nearly omnipresent in astrophysics. On length scales comparable to the gas mean free path these solutions are smooth (as a result of the *physical viscosity* that is always present to some extent), but on the macroscopic scales of a simulation (which is usually orders of magnitude larger), the very steep gradients appear as discontinuous.

The strategies to deal numerically with shocks are (broadly speaking) two-fold: (i) one can either make use of the analytical solution of a Riemann problem between two adjacent computational entities (either cells or particles) or (ii) add pseudo-microscopic terms that create entropy at the shock front, just as physical viscosity would do, but on a numerically resolvable scale. The latter is instantiated by adding extra, “artificial” dissipation to the flow. This can be achieved by choosing particular numerical discretization schemes that in fact solve continuum equations that are only similar to the original ones, but contain additional, higher-order deviatoric terms, such as, for example, the Lax scheme (Press et al., 1992). Alternatively, one may explicitly add pressure-like terms to the fluid equations. The addition of such “ad-hoc” terms is one of the oldest techniques (VonNeumann and Richtmyer, 1950) in the relatively young field of computational physics. Most astrophysical SPH implementations follow the latter strategy, e.g. (Hernquist and Katz, 1989; Wadsley et al., 2004; Springel, 2005; Rosswog and Price, 2007), but variants that use Riemann-solvers do also exist (Inutsuka, 2002; Cha and Whitworth, 2003).

Strictly speaking, real discontinuities with their infinite derivatives are no proper solutions of the ideal hydrodynamics equations Eqs. (3)–(5). The aim of artificial viscosity (AV) is, in the words of von Neumann and Richtmyer (from their seminal paper VonNeumann and Richtmyer, 1950) to introduce (artificial) dissipative terms into the equations so as to give the shocks a thickness comparable to (but preferentially larger than) the spacing ... [of the grid points]. Then the differential equations (more accurately, the

corresponding difference equations) may be used for the entire calculation, just as though there were no shocks at all.” Although guidance by physical viscosity can sometimes be helpful, artificial viscosity is not meant to mimic physical viscosity, it is instead an *ad hoc* method to produce on a resolvable scale what is the result of unresolvable, small-scale effects. In this sense one can think of it as a kind of sub-grid model.

AV should have a number of desirable properties (Caramana and Whalen, 1998) and must not introduce unphysical artifacts. It should always be dissipative, i.e. transfer kinetic energy into internal one and never vice versa, which is not a completely trivial task in 3D. AV should be absent in rigid and (shockless) differential rotation and in uniform compression. In other words, it should be “intelligent” in the sense that it distinguishes uniform compression from a shock. This can be done either via a tensor formulation of artificial viscosity, e.g. (Owen, 2004), or via “limiters” that detect such motion and subsequently suppress the action of AV. Generally, AV should go smoothly to zero as the compression vanishes and it should be absent for expansion. Moreover, to not destroy one of SPH’s most salient strength, it must be implemented consistently into momentum and energy equation, so that the conservation of energy, momentum and angular momentum is still guaranteed.

2.7.2. Bulk and von-Neumann–Richtmyer viscosity

Guided by the requirements that (i) no real discontinuities occur, (ii) the thickness of the “shock layer” is everywhere of the order of the resolvable length scale l , (iii) no noticeable effects occur away from shock layers, and (iv) the Rankine–Hugoniot relations (Landau and Lifshitz, 1959) hold when considering length scales that are large in comparison to the thickness of the shock layers, von Neumann and Richtmyer suggested an artificial pressure of the form

$$q_{NR} = c_2 \rho l^2 (\nabla \cdot \vec{v})^2, \quad (52)$$

where c_2 is a dimensionless parameter of order unity, to be added to the hydrodynamic pressure. Their approach yielded reasonably good results in strong shocks, yet it still allowed oscillations in the post-shock region to occur. To avoid them, usually an additional term (Landshoff, 1955) is introduced that vanishes less rapidly and has the form of a bulk viscosity (Landau and Lifshitz, 1959)

$$q_b = -c_1 \rho c_s l (\nabla \cdot \vec{v}). \quad (53)$$

Here c_s is the sound velocity and c_1 is a parameter of order unity. Often, the two contributions are combined into an artificial viscous pressure,

$$q_{visc} = -c_1 \rho c_s l (\nabla \cdot \vec{v}) + c_2 \rho l^2 (\nabla \cdot \vec{v})^2. \quad (54)$$

The term $l(\nabla \cdot \vec{v})$ is thereby an estimate for the velocity jump between adjacent cells or particles.

2.7.3. “Standard” SPH viscosity: reasoning and limitations

A straight-forward approach to transform these ideas into an SPH artificial viscosity prescription would be to insert Eq. (31) into (54), to use particle properties for the densities and sound velocities and identify the resolution length scale l with the smoothing length. Similar approaches have indeed been pursued (Hernquist and Katz, 1989), but we will focus here on an approach due to Monaghan and Gingold (1983) that is probably the most widespread form of SPH artificial viscosity and therefore often referred to as the “standard viscosity”.

Instead of just increasing the hydrodynamic pressures, P_a , by viscous contributions, q_{visc} , one augments the pressure terms in the momentum Eq. (29) by an artificial contribution Π_{ab} :

$$\left(\frac{P_a}{\rho_a^2} + \frac{P_b}{\rho_b^2}\right) \rightarrow \left(\frac{P_a}{\rho_a^2} + \frac{P_b}{\rho_b^2} + \Pi_{ab}\right). \quad (55)$$

For simplicity, let us consider the bulk viscosity contribution first and restrict ourselves to 1D. The bulk contribution to Π_{ab} is then of the form $-c_1 c_s (h/\rho) \partial v / \partial x$ and a Taylor expansion of the velocity field, $v(x_a + (x_b - x_a))$, yields

$$\left(\frac{\partial v}{\partial x}\right)_a = \frac{v_b - v_a}{x_b - x_a} + O((x_b - x_a)^2). \quad (56)$$

Inserting this approximation, replacing particle properties by their averages, $\bar{A}_{ab} = (A_a + A_b)/2$, using the notation $x_{ab} = x_a - x_b$ and $v_{ab} = v_a - v_b$ and replacing the possibly diverging denominator,

$$\frac{1}{x_{ab}} \rightarrow \frac{x_{ab}}{x_{ab}^2 + \epsilon \bar{h}_{ab}^2}, \quad (57)$$

the SPH prescription for the bulk viscosity reads

$$\Pi_{ab,\text{bulk}} = \begin{cases} -c_1 \frac{\bar{c}_{s,ab}}{\bar{\rho}_{ab}} \mu_{ab} & \text{for } x_{ab} v_{ab} < 0 \\ 0 & \text{otherwise} \end{cases}, \quad \text{where } \mu_{ab} = \frac{\bar{h}_{ab} x_{ab} v_{ab}}{x_{ab}^2 + \epsilon \bar{h}_{ab}^2}. \quad (58)$$

The product $x_{ab} v_{ab}$ thereby detects whether particles are approaching (< 0) and only in this case artificial viscosity becomes active. The quantity μ_{ab} has taken over the role of the term $l(\nabla \cdot \vec{v})$ in the original prescription of von Neumann and Richtmyer. Having said this, we can now treat the von Neumann–Richtmyer term, q_{NR} , in exactly the same way. Adapting to the usual SPH notation, $c_1 \rightarrow \alpha$, $c_2 \rightarrow \beta$, the artificial viscosity term reads

$$\Pi_{ab} = \Pi_{ab,\text{bulk}} + \Pi_{ab,\text{NR}} = \begin{cases} \frac{-\alpha \bar{c}_{ab} \mu_{ab} + \beta \mu_{ab}^2}{\bar{\rho}_{ab}} & \text{for } \vec{r}_{ab} \cdot \vec{v}_{ab} < 0 \\ 0 & \text{otherwise,} \end{cases} \quad (59)$$

with

$$\mu_{ab} = \frac{\bar{h}_{ab} \vec{r}_{ab} \cdot \vec{v}_{ab}}{r_{ab}^2 + \epsilon \bar{h}_{ab}^2}. \quad (60)$$

Note that the scalar quantities have now been replaced by vector quantities for the use in 3D. Numerical experiments suggest the following values for the involved parameters: $\alpha \approx 1$, $\beta \approx 2$ and $\epsilon \approx 0.01$.

Accounting for artificial viscosity, the momentum equation reads

$$\frac{d\vec{v}_a}{dt} = - \sum_b m_b \left(\frac{P_a}{\rho_a^2} + \frac{P_b}{\rho_b^2} + \Pi_{ab} \right) \nabla_a W_{ab}. \quad (61)$$

To have a consistent formulation, the energy equation must be modified according to

$$\frac{du_a}{dt} = \frac{P_a}{\rho_a^2} \sum_b m_b \vec{v}_{ab} \cdot \nabla_a W_{ab} + \frac{1}{2} \sum_b m_b \Pi_{ab} \vec{v}_{ab} \cdot \nabla_a W_{ab}. \quad (62)$$

This combination still conserves energy, linear and angular momentum by construction, the proofs are analogous to the ones outlined above.

To illustrate the performance of this artificial viscosity prescription, let us consider a standard test case for hydrodynamic schemes, the so-called ‘‘Sod shocktube’’ (Sod, 1978) which is a particular realization of a Riemann problem. A tube filled with gas, such as illustrated in Fig. 1, contains a high density ($\rho_1 = 1$)/high pressure ($p_1 = 1$) region that is separated by a wall from a low density ($\rho_2 = 0.25$)/low pressure ($p_2 = 0.1795$) region. For the Sod test a polytropic equation of state with exponent $\Gamma = 1.4$ is used. Once the wall is removed, the discontinuity decays into two elementary, non-linear waves that move in opposite directions: a shock moves into the unperturbed original low density region, while a rarefac-

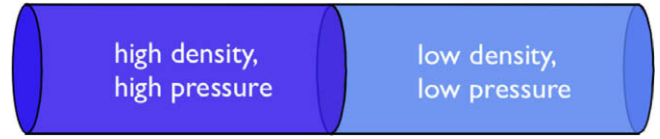


Fig. 1. Schematic illustration of the shock tube problem.

tion wave travels into the original high-density region. Between the shock and the tail of the rarefaction wave (the rightmost end of the rarefaction) two new states develop which are separated by a contact discontinuity across which the pressure is constant. The exact solution is sketched in Fig. 2.

If *no artificial viscosity* is applied in such a problem, strong post-shock oscillations occur as illustrated in Fig. 3 for the velocities in the Sod test. If the standard artificial viscosity prescription, Eq. (59) is used, the numerical solution agrees very well with the exact one, see Fig. 4, provided that the interesting regions of the flow are adequately resolved.³

While this artificial viscosity form performs very well in 1D, it suffers from deficiencies if used in multi-D: (i) for fixed parameters α and β it may affect the flow even if it is not really needed, and (ii) under certain conditions it can introduce spurious shear forces. Consider for example an idealized shear flow as sketched in Fig. 5. Assume that the velocity decreases vertically as sketched on the left and no shocks occur. For such a situation no artificial viscosity is needed. Nevertheless, as sketched for two example particles (‘‘1’’ and ‘‘2’’) the scalar product $\vec{r}_{ab} \cdot \vec{v}_{ab}$ is finite and thus, via μ_{ab} in Eq. (60), introduces a viscous force that is unwanted. Similar configurations are encountered for the (astrophysically important) cases of accretion disks.

2.7.4. Reducing artificial viscosity where unnecessary

Several recipes were suggested to cure the deficiencies that the standard artificial viscosity introduces in multi-D.

One such recipe is the so-called ‘‘Balsara-switch’’ (Balsara, 1991). Its strategy is to define a ‘‘limiter’’ that distinguishes shock from shear motion and suppresses AV in the latter case. One defines a quantity

$$f_a = \frac{|\langle \nabla \cdot \vec{v} \rangle_a|}{|\langle \nabla \cdot \vec{v} \rangle_a| + |\langle \nabla \times \vec{v} \rangle_a| + 0.0001 c_{s,a} / h_a}, \quad (63)$$

and, as before, applies a symmetrized average of the limiters f , $\Pi_{ab} = \Pi_{ab} \bar{f}_{ab}$. In pure compressional motion ($|\langle \nabla \cdot \vec{v} \rangle| \neq 0$ and $|\langle \nabla \times \vec{v} \rangle| = 0$) the limiter reduces to unity and the standard viscosity is recovered, and in pure shear flow ($|\langle \nabla \cdot \vec{v} \rangle| = 0$ and $|\langle \nabla \times \vec{v} \rangle| \neq 0$) the action of artificial viscosity is suppressed ($\bar{f}_{ab} \ll 1$). This limiter has been found very useful in many cases (Steinmetz, 1996; Navarro and Steinmetz, 1997; Rosswog et al., 2000), but it reaches its limitations if shocks occur in a shearing environment such as in an accretion disk (Owen, 2004).

Morris and Monaghan (1997) suggested the use of *time-dependent artificial viscosity parameters*. The main idea is to have α and β only at non-negligible levels where they are really needed. They suggested to fix β to 2α , to assign each particle its individual parameter, α_a , and to evolve it according to an additional differential equation,

$$\frac{d\alpha_a}{dt} = - \frac{\alpha_a - \alpha_{\min}}{\tau_a} + S_a, \quad (64)$$

³ Consistent with the finite resolution width of numerical shocks, we set up the initial density distribution as a Fermi function with a transition width of Δx : $\rho(x) = (\rho_1 - \rho_2) / (1 + \exp(\frac{x - x_s}{\Delta x})) + \rho_2$, where x_s is the initial position of the shock. For the presented test Δx was set to 1.5 times the average particle separation.

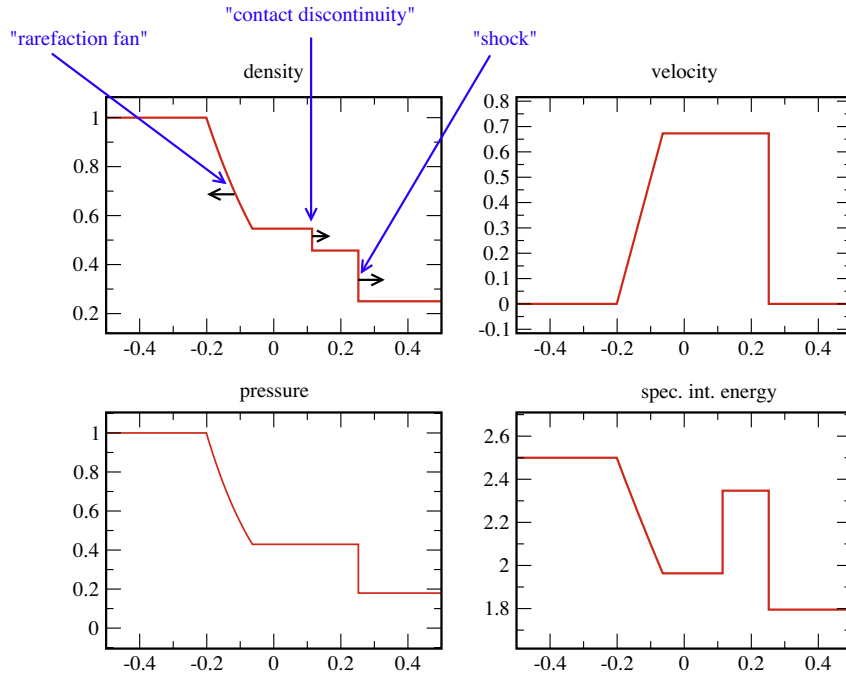


Fig. 2. The exact solution of the non-relativistic shock tube problem.

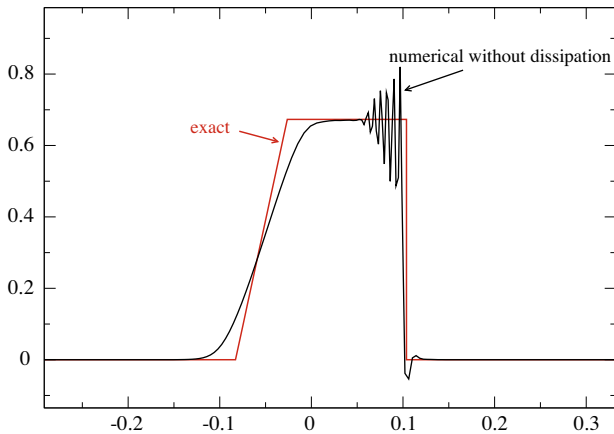


Fig. 3. Velocity snapshot of the Sod shock tube problem. Shown is the exact solution together with a numerical solution *without* artificial viscosity.

so that α_a decays exponentially with an e-folding time τ_a to a minimum value α_{\min} , unless it is triggered to rise by the source term S_a . The time scale τ_a should be chosen so that the viscosity persists for a few smoothing lengths behind the shock. This can be obtained by

$$\tau_a = \frac{h_a}{\xi c_{s,a}}, \quad (65)$$

where $\xi \approx 0.1^4$. Morris and Monaghan suggested $S_a = \max[-(\vec{\nabla} \cdot \vec{v})_a, 0]$ for the source term. If one wishes to restrict the growth of α to α_{\max} , one can use $S_a = \max[-(\vec{\nabla} \cdot \vec{v})_a(\alpha_{\max} - \alpha_a), 0]$ (Rosswog et al., 2000). Typical values for the numerical parameters are $\alpha_{\min} = 0.1$ and $\alpha_{\max} = 1.5$. In a Sod test this prescription leads to non-negligible values of α_a only in the vicinity of the shock front, elsewhere artificial viscosity is practically absent. This prescription has largely removed unwanted effects from AV in three-dimensional SPH simulations (Rosswog et al., 2000; Dolag et al., 2005). Note, however,

⁴ Note the similarity to the SPH-version of the Courant time step criterion.

that in homologous flow, $\vec{v} \propto \vec{r}$, α_a can still rise although it is not needed. This is counterbalanced to some extent by the increase of $c_{s,a}$ and the decrease of h_a , so that -via τ_a - the decay term in Eq. (64) becomes more dominant, but there is certainly still room for improvement.

2.7.5. New forms inspired by Riemann solvers

Monaghan used the analogy to Riemann solvers to motivate a new form of artificial dissipation which involves signal velocities and jumps in variables across characteristics (Monaghan, 1997). The main idea of these “discontinuity capturing terms” is that for any conserved scalar variable A with $\sum_a m_a dA_a/dt = 0$ a dissipative term of the form

$$\left(\frac{dA_a}{dt}\right)_{\text{diss}} = \sum_b m_b \frac{\alpha_{A,b} v_{\text{sig}}}{\rho_{ab}} (A_a - A_b) \hat{e}_{ab} \cdot \nabla_a W_{ab}, \quad (66)$$

should be added, where the parameter $\alpha_{A,b}$ determines the exact amount of dissipation and v_{sig} is the maximum signal velocity between particle a and b . Applied to velocity and thermokinetic energy this yields

$$\left(\frac{d\vec{v}_a}{dt}\right)_{\text{diss}} = \sum_b m_b \frac{\alpha v_{\text{sig}} (\vec{v}_a - \vec{v}_b) \cdot \hat{e}_{ab}}{\rho_{ab}} \nabla_a W_{ab}, \quad (67)$$

$$\left(\frac{d\hat{e}_a}{dt}\right)_{\text{diss}} = \sum_b m_b \frac{e_a^* - e_b^*}{\rho_{ab}} \hat{e}_{ab} \cdot \nabla_a W_{ab}, \quad (68)$$

where, following Price (2008), the energy including velocity components along the line of sight between particles a and b , $e_a^* = \frac{1}{2} \alpha v_{\text{sig}} (\vec{v}_a \cdot \hat{e}_{ab})^2 + \alpha_u v_{\text{sig}}^u u_a$, has been used and different signal velocities and dissipation parameters were explicitly allowed for. If one uses $du_a/dt = d\hat{e}_a/dt - \vec{v}_a \cdot d\vec{v}_a/dt$, one finds the dissipative terms of the thermal energy equation

$$\left(\frac{du_a}{dt}\right)_{\text{diss}} = - \sum_b \frac{m_b}{\rho_{ab}} \left[\alpha v_{\text{sig}} \frac{1}{2} (\vec{v}_{ab} \cdot \hat{e}_{ab})^2 + \alpha_u v_{\text{sig}}^u (u_a - u_b) \right] \hat{e}_{ab} \cdot \nabla_a W_{ab}. \quad (69)$$

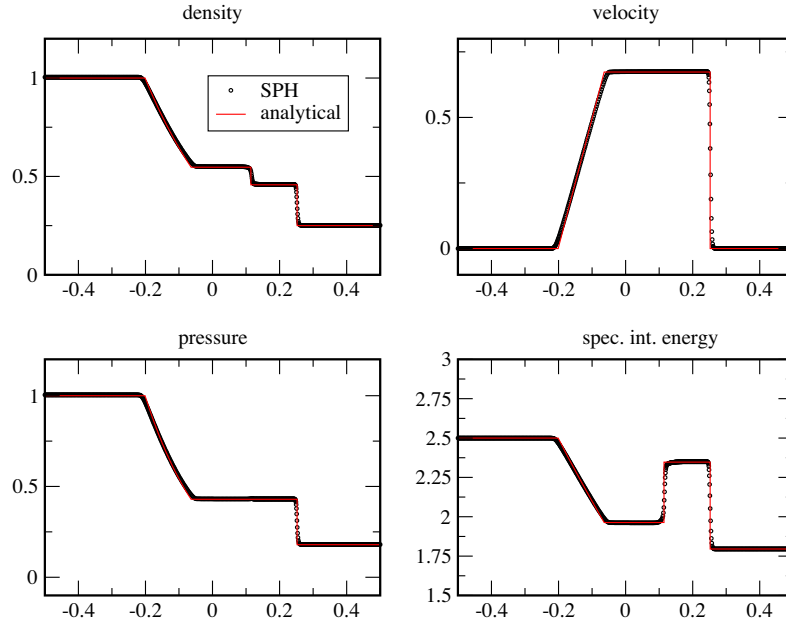


Fig. 4. Sod's shock tube: the exact solutions are shown by the red line, the numerical solution obtained with SPH are shown as circles. For this simulation 1000 particles were used, density was calculated via summation, and the smoothing lengths were updated according to $h_a = 1.4(m_a/\rho_a)$. For this test a second-order Runge–Kutta integrator was used.

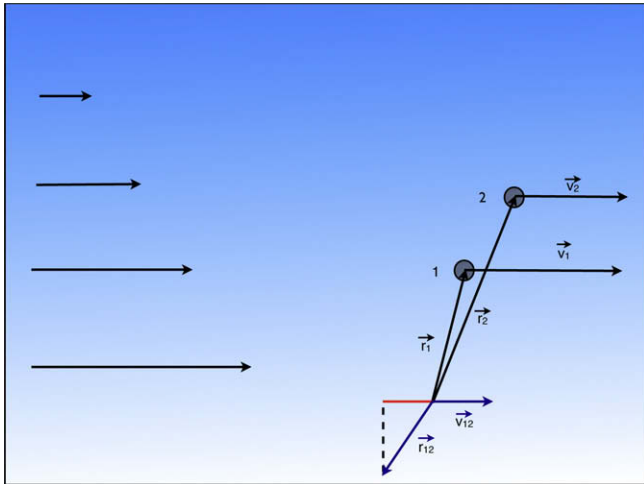


Fig. 5. Illustration how the “standard” SPH artificial viscosity introduces spurious shear forces: in this pure shear flow the difference position vector has a finite projection on the difference velocity vector (red) and thus introduces unwanted forces.

The first term in this equation bears similarities with the “standard” artificial viscosity prescription, see Eq. (62), the second one expresses the exchange of thermal energy between particles and therefore represents an artificial thermal conductivity which smoothes discontinuities in the specific energy. Such artificial conductivity had been suggested earlier to cure the so-called “wall heating problem” (Noh, 1987). Tests have shown that artificial conductivity substantially improves SPH's performance in simulating Sedov blast waves (Rosswog and Price, 2007).

For non-relativistic hydrodynamics the maximum signal velocity between two particles can be estimated as Monaghan (1997)

$$v_{\text{sig}} = c_{s,a} + c_{s,b} - \vec{v}_{ab} \cdot \hat{e}_{ab}, \quad (70)$$

where $c_{s,k}$ is the sound velocity of particle k . Price (2008) had realized that SPH's difficulty to treat Kelvin–Helmholtz instabilities across contact discontinuities with large density jumps (Agertz et al., 2007) is closely related to a “blip” that occurs in the pressure at the contact discontinuities.⁵ He suggested to use artificial conductivity only to eliminate spurious pressure gradients across contact discontinuities and to this end suggested

$$v_{\text{sig}}^u = \sqrt{\frac{|P_a - P_b|}{\bar{\rho}_{ab}}}. \quad (71)$$

Clearly, this quantity has the dimensions of a velocity and vanishes in pressure equilibrium. This approach has substantially improved SPH's ability to treat Kelvin–Helmholtz instabilities (Price, 2008).

To avoid conductivity where it is unwanted, one can follow again a strategy with time-dependent parameters. For the artificial viscosity one can use Eq. (64), and proceed in a similar way for α_u . One can use the second derivative of the thermal energy,

$$S_{u,a} = \frac{h_a |\nabla^2 u|_a}{\sqrt{u_a + \epsilon}}, \quad (72)$$

to control the growth α_u . The second derivative can be calculated as in Eq. (15), the parameter ϵ avoids that $S_{u,a}$ diverges as $u_a \rightarrow 0$.

According to a recent analysis (Read et al., 2009), SPH's difficulty to treat Kelvin–Helmholtz instabilities results from a mismatch in the sharpness of pressure and density across the density jump. This can be either cured by generating entropy at the boundary and thus smoothing the pressure as in Price (2008), or by obtaining a sharper density estimate. By a combination of using the freedom in discretization, see Section 2.5, a particular, higher-order kernel and an entropy-weighted density estimate together with large neighbor numbers, (Read et al., 2009) also find convincing results Kelvin–Helmholtz instability simulations.

⁵ It is not visible in our Sod shock tube in Fig. 4 since we had started from smoothed initial conditions.

2.8. Time integration in SPH

To integrate the ordinary differential equations of SPH one has to find a reasonable tradeoff between accuracy and efficiency of an integrator and most often the available computer power is better invested in larger particle numbers rather than in high-order integration schemes. Since the evaluation of derivatives is usually very expensive, and in particular so for self-gravitating fluids, one tries to minimize the number of force evaluations per time step, which gives preference to low-order integrators. If the storage of derivatives (from earlier time steps) is not a concern, one can resort to multi-step methods such as Adams–Bashforth-type integrators, e.g. (Press et al., 1992; Burden and Faires, 2001), giving higher-order time integration accuracy at moderate costs of force evaluations.

After a short collection of commonly used time step criteria, we want to discuss briefly two methods that we find particularly useful: the Störmer–Verlet/leap frog algorithm, which appeals by its conservation properties and the class of Fehlberg methods whose advantage is the appropriate choice of the time step size based on monitoring the quality of the numerical solution.

2.8.1. Time stepping

We will briefly collect here commonly used time step criteria, depending on the considered physical system, further criteria that capture the specific physical time scales have to be added. A criterion that triggers on accelerations, \bar{a}_a , is (Monaghan, 1992)

$$\Delta t_{f,a} \propto \sqrt{h_a/|\bar{a}_a|}, \quad (73)$$

and

$$\Delta t_{CV,a} \propto \frac{h_a}{v_{s,a} + 0.6(c_{s,a} + 2\max_b \mu_{ab})}, \quad (74)$$

is a combination of a Courant-type⁶ and viscous time step control, where μ_{ab} is the quantity defined in Eq. (60). If one wishes to restrict the change of the smoothing length over a time step, one can use additionally (Wetzstein et al., 2008)

$$\Delta t_{h,a} \propto \frac{h_a}{\dot{h}_a}. \quad (75)$$

In a simulation, the minimum of the different time step criteria (with a suitably chosen prefactor) determines the hydrodynamical time step. If further physical processes, say nuclear burning, occur on much shorter time scales, one may resort to an “operator splitting” approach and integrate different processes with separate integration schemes, e.g. (Rosswog et al., 2009).

For inexpensive test problems or cases where the physical time scales are (more or less) the same for each particle, it is easiest to evolve all the particles on the same (shortest particle) time step. In many astrophysical examples, say cosmological structure formation, the collapse of a molecular cloud or the tidal disruption of a star by a black hole, the required time steps in different parts of the fluid may span many orders of magnitude. In such cases it is beneficial to group particles into block time steps of $\Delta t_n = 2^n \Delta t_{\min}$, where n is an integer and Δt_{\min} is the smallest required time step, and to evolve each group of particles separately. In this way the number of (expensive) force evaluations can be reduced by orders of magnitude. Successful implementations of such individual time step schemes can be found, for example, in (Porter, 1985; Ewell, 1988; Hernquist and Katz, 1989; Bate et al., 1995; Klessen et al., 2000; Springel, 2005; Rosswog, 2005; Wetzstein et al., 2008).

⁶ The Courant or Courant–Friedrichs–Levi (or CFL for short) criterion ensures that the numerical propagation speed of information does not exceed the physical one. If a spatial scale of Δx can be resolved, the numerical time step has to be $\Delta t < \Delta x/c_s$ to ensure numerical stability (Press et al., 1992).

2.8.2. Störmer–Verlet and leap frog

The Verlet or leapfrog algorithm⁷ is particularly appealing due to its exact time reversibility. The original Verlet algorithm (Verlet, 1967) is very easy to derive: start from two Taylor expansions for $\vec{r}(t + \Delta t)$ and $\vec{r}(t - \Delta t)$, add them and solve for $\vec{r}(t + \Delta t)$ to find the position update prescription of the Verlet algorithm

$$\vec{r}(t + \Delta t) = 2\vec{r}(t) - \vec{r}(t - \Delta t) + \bar{a}(t)\Delta t^2 + O(\Delta t^3). \quad (76)$$

It is interesting to note that the position is updated without using the velocities. But this comes at a price: for a position update two positions at earlier time steps are needed. The velocity can be reconstructed from the positions via centered finite differences:

$$\vec{v}(t) = \frac{\vec{r}(t + \Delta t) - \vec{r}(t - \Delta t)}{2\Delta t} + O(\Delta t^3). \quad (77)$$

This simple integrator is only second-order accurate, but it is time reversible and has excellent conservation properties. To kick off a simulation at $t = 0$, one needs $\vec{r}(-\Delta t)$. It can be obtained by solving for $\vec{r}(-\Delta t)$ after inserting $t = 0$ into Eq. (77):

$$\vec{r}(-\Delta t) = \vec{r}(\Delta t) - 2\Delta t\vec{v}_0, \quad (78)$$

where $\vec{v}_0 = \vec{v}(t = 0)$. Inserting this into Eq. (76) provides the position update

$$\vec{r}(\Delta t) = \vec{r}_0 + \Delta t\vec{v}_0 + \frac{1}{2}\bar{a}_0\Delta t^2, \quad (79)$$

which looks like the first terms of a Taylor expansion around $t = 0$. The “leapfrog form” is obtained by defining velocities at half-steps, again via centered differences

$$\vec{v}\left(t - \frac{\Delta t}{2}\right) = \frac{\vec{r}(t) - \vec{r}(t - \Delta t)}{\Delta t} \quad \text{and} \quad \vec{v}\left(t + \frac{\Delta t}{2}\right) = \frac{\vec{r}(t + \Delta t) - \vec{r}(t)}{\Delta t}. \quad (80)$$

The last equation can be solved for the leapfrog form of the position equation

$$\vec{r}(t + \Delta t) = \vec{r}(t) + \Delta t\vec{v}\left(t + \frac{\Delta t}{2}\right). \quad (81)$$

Starting from Eq. (76) and inserting Eq. (80) we find the velocity update of the leapfrog algorithm

$$\vec{v}\left(t + \frac{\Delta t}{2}\right) = \vec{v}\left(t - \frac{\Delta t}{2}\right) + \bar{a}(t)\Delta t. \quad (82)$$

So positions and accelerations are always evaluated at “full” time steps t^n , while the velocities are evaluated in between, either at $t^{n-1/2}$ or $t^{n+1/2}$, so the velocities are always “leaping” over the positions. If velocities at t are needed, they can be calculated according to

$$\vec{v}(t) = \frac{\vec{v}\left(t + \frac{\Delta t}{2}\right) + \vec{v}\left(t - \frac{\Delta t}{2}\right)}{2}. \quad (83)$$

The “Störmer–Verlet form” is particularly useful, since all quantities are evaluated at the same point of time. Start from Eq. (77) and solve for

$$\vec{r}(t - \Delta t) = \vec{r}(t + \Delta t) - 2\Delta t\vec{v}(t). \quad (84)$$

Insert this into the Verlet position update, Eq. (76), to find the position update of the velocity Störmer–Verlet algorithm

$$\vec{r}(t + \Delta t) = \vec{r}(t) + \vec{v}(t)\Delta t + \frac{1}{2}\bar{a}(t)\Delta t^2. \quad (85)$$

⁷ This algorithm has many names: in astronomy it is often called *Störmer method*, in molecular dynamics it is usually named *Verlet method* in the context of partial differential equations it is usually referred to as *leap-frog method*. Note that the scheme needs modification if the acceleration depends on the velocity.

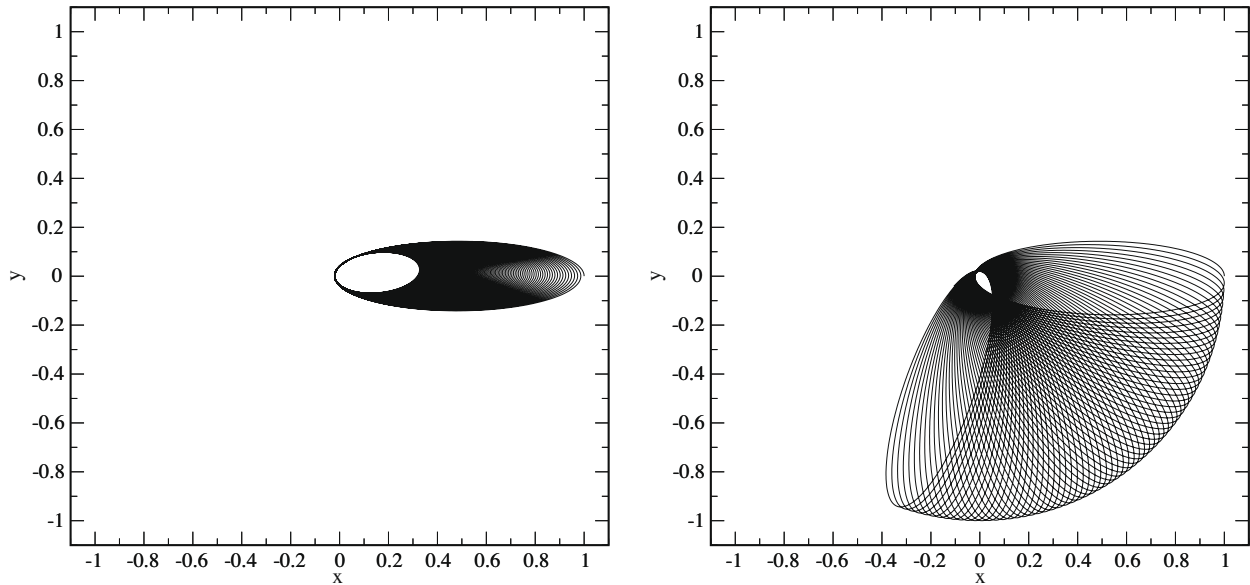


Fig. 6. Integration of the test particle orbit up to $t = 150$ for an eccentric orbit ($\vec{v}_0 = (0, 0.2)$, $\Delta t = 10^{-3}$). Left: fourth-order Runge–Kutta. Right: velocity Störmer–Verlet.

To find the velocity update for the algorithm start from Eq. (77) and insert the Verlet position update, Eq. (76),

$$\vec{v}(t) = \frac{\vec{r}(t) - \vec{r}(t - \Delta t)}{\Delta t} + \frac{\vec{a}(t)}{2} \Delta t. \quad (86)$$

Completely analogous one finds for the velocity at $t + \Delta t$

$$\vec{v}(t + \Delta t) = \frac{\vec{r}(t + \Delta t) - \vec{r}(t)}{\Delta t} + \frac{\vec{a}(t + \Delta t)}{2} \Delta t. \quad (87)$$

Adding the last two equations and using Eq. (77) gives

$$\vec{v}(t + \Delta t) = \vec{v}(t) + \Delta t \frac{\vec{a}(t) + \vec{a}(t + \Delta t)}{2}. \quad (88)$$

Together with Eq. (85) this update forms the Störmer–Verlet algorithm. It is a simple example of a “geometric integrator” which preserves qualitative features of the exact flow of the ODE by construction (Leimkuhler and Reich, 2004; Hairer et al., 2006). In particular, it conserves angular momentum exactly.⁸

The integration of an elliptical Kepler orbit represents a simple, yet significant numerical experiment. As long as no deviations from purely Newtonian point mass gravity are considered, bound orbits are closed ellipses, e.g. (Landau and Lifshitz, 1976; Goldstein et al., 2002), any “non-closure” is a numerical artifact due to finite integration accuracy.

To define the problem, we use units in which a test body (“planet”) is accelerated by

$$\vec{a} = -\frac{\vec{r}}{r^3}, \quad (89)$$

and, since angular momentum is conserved in a central force field, one only needs to consider two spatial dimensions. We choose $\vec{r}_0 = (1, 0)$ and $\vec{v}_0 = (0, 0.2)$ as initial conditions. We perform a simulation up to $t = 150$ with a slightly too large time step, $\Delta t = 10^{-3}$. For comparison we also use a fourth-order Runge–Kutta scheme with the same time step. The results are displayed in Fig. 6. Due to the inappropriate time step the numerical inaccuracies in the velocity Störmer–Verlet case lead to a perihelion shift, but otherwise the behavior is physical: the test particle orbits the center of gravity on an eccentric orbit. In the Runge–Kutta case a qualita-

tively different and unphysical effect occurs: energy and angular momentum are dissipated for purely numerical reasons. The evolution of angular momentum is shown in Fig. 7. The “steps” in the Runge–Kutta case occur at perihelion since here the time steps are much too large. Therefore, the test particle drifts into a more circular, lower energy orbit. This illustrates that *exact conservation can be more important than high order!*

2.8.3. Time stepping with quality control: Fehlberg methods

The size of the time step Δt is crucial for the accuracy (and stability!) of the numerical solution of an ODE. It has to be a small fraction of the shortest physical time scale of the problem at hand. For a complex multi-physics system this may require to determine the time scales of every involved physical process. In the worst case, these may not be known and, on top, the meaning of “a small fraction” may subject to trial and error.

Ideally, a method should decide itself which step size to take. This is the philosophy behind *adaptive step size control* or *Fehlberg*

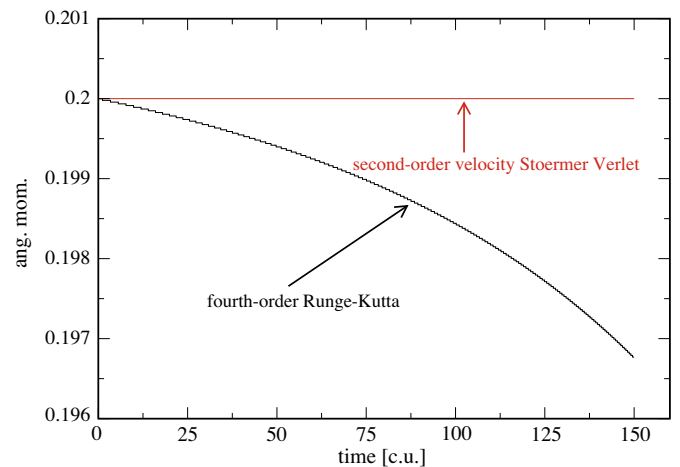


Fig. 7. Angular momentum evolution of the long-term comparison. While the velocity Störmer–Verlet method conserves angular momentum to machine precision, the fourth-order Runge–Kutta method loses about 2%. As a result of this purely numerical dissipation the planet spirals inward.

⁸ For an elegant proof based on Newton’s *Principia* see (Hairer et al., 2006).

methods (Fehlberg, 1964, 1966, 1969; Press et al., 1992). The main idea is to use two estimates of different order for the solution and use them to estimate the error growth rate. Based on the comparison of the estimated and the tolerable growth rate, the chosen time step may be accepted or rejected. Independent of whether the time step was accepted or not, the growth rate can provide an educated guess for the size of the next time step.

The procedure is the following:

- Choose a trial time step Δt .
- Use two different methods to obtain results at the end of the time step, a_1 and a_2 . To be reasonably efficient, the two methods should use nearly the same evaluations of the RHS of the ODE.
- Use a_1 and a_2 to calculate an approximate local truncation error E .
- Compare the error growth rate $\epsilon \approx E/\Delta t$ with some acceptable error growth rate, ϵ^{acc} . If the rate is small enough, $\epsilon < \epsilon^{\text{acc}}$, accept the time step, $t^{n+1} = t^n + \Delta t$ and $y^{n+1} = a_2$, where a_2 is the more accurate method. Otherwise, re-take the step with a reduced step size determined from ϵ and the previously tried step size.

Obviously, the above strategy can be applied to a large variety of integrator combinations. An often used example is the combination of fourth- and fifth-order Runge–Kutta schemes (Fehlberg, 1969). As a low-order example, we apply the outlined strategy to a second- and a third-order method. Let $\Phi(t)$ be the exact solution of the differential equation and assume that an approximation to the solution at t^n is known: $\Phi(t^n) \simeq y^n$. Take three RHS evaluations of the ODE:

$$f_1 = f(t^n, y^n), \quad (90)$$

$$f_2 = f(t^n + \Delta t, y^n + \Delta t f_1), \quad (91)$$

$$f_3 = f\left(t^n + \frac{\Delta t}{2}, y^n + \frac{\Delta t}{4} [f_1 + f_2]\right), \quad (92)$$

to produce a second-order (this is just the modified Euler method)

$$a_1 = y^n + \Delta t \frac{f_1 + f_2}{2}, \quad (93)$$

and a third-order method

$$a_2 = y^n + \frac{\Delta t}{6} [f_1 + f_2 + 4f_3]. \quad (94)$$

Thus, we have

$$\Phi(t^n + \Delta t) = a_1 + K\Delta t^3 + O(\Delta t^4) = a_2 + O(\Delta t^4). \quad (95)$$

Therefore, the leading error is

$$E = |a_2 - a_1| = K\Delta t^3 + O(\Delta t^4), \quad (96)$$

and the error grows at a rate

$$\epsilon \approx \frac{E}{\Delta t} \approx K\Delta t^2. \quad (97)$$

The step can either be accepted ($\epsilon < \epsilon^{\text{acc}}$), $t^{n+1} = t^n + \Delta t$, $y^{n+1} = a_2$, or rejected ($\epsilon > \epsilon^{\text{acc}}$) and re-taken. In both cases one can use the error measure to estimate the new time step. Since $\epsilon \propto \Delta t^2$, one finds

$$\frac{\epsilon^{\text{new}}}{\epsilon^{\text{tried}}} = \left(\frac{\Delta t^{\text{new}}}{\Delta t^{\text{tried}}}\right)^2, \quad (98)$$

and the suggestion for the new time step is

$$\Delta t^{\text{new}} = s \left(\frac{\epsilon^{\text{acc}}}{\epsilon^{\text{tried}}}\right)^{1/2} \Delta t^{\text{tried}}, \quad (99)$$

where $s < 1$ is a “safety factor” for a conservative choice of the next time step.

For further reading on ODE-integration the excellent text books of (Hockney and Eastwood, 1988; Leimkuhler and Reich, 2004; Hairer et al., 2006; Griebel et al., 2007) are recommended.

2.9. “Best practice” suggestions

We want to collect here a couple of suggestions born from practical experience that should help to carry out reliable simulations and to avoid numerical artifacts. This is somewhat “soft”, yet hopefully still useful knowledge.

2.9.1. Neighbor numbers and resolution

We recommend a large neighbor number, typically 100 or more. This somewhat increases the smoothing lengths and thus deteriorates the integral approximation, Eq. (18). On the other hand, it can substantially reduce numerical noise, i.e. fluctuations around the true solution. To compensate, it is advisable to run simulations at the highest affordable particle number, numerical resolution *does* matter. Substructures can only be considered resolved if they are substantially larger than the local smoothing lengths. If just an idea about the mass distribution is required, one may get away with a small particle number, say a few thousand particles, but reliable thermodynamic properties usually require *much* larger particle numbers. Contrary to some prejudices, SPH *can* resolve shocks properly, but since shocks are spread across a few smoothing lengths an appropriate numerical resolution is required.

2.9.2. Particle masses

If at all possible, equal-mass particles should be used. Light particles that interact with much more massive ones easily become “nervous” (“ping pong and cannon ball effect”), i.e. they can exhibit large fluctuations. In some problems different particle numbers are unavoidable, if, for example, a highly centrally condensed star is considered, the Courant time step criterion may restrict the central time steps to prohibitively small values. In such cases one should make sure that interacting particles only differ in masses by factors of very few.

2.9.3. Initial conditions

Accurate initial conditions are absolutely crucial for reliable simulations. The SPH particles should start out from their true numerical equilibrium positions. This can be obtained by applying an artificial damping term $\propto \bar{v}_a$ in the momentum equation that drags the particles to the desired initial conditions. Once equilibrium is found the particles should not move considerably during a few dynamical time scales after the damping has been switched off.

2.9.4. Time integration

Ideally, an integration scheme should monitor the achieved accuracy for the tried time step and *reject* it if the error becomes unacceptably large. Just estimating a time step that seems reasonable and then hope for the best, may produce noisy, or in the worst case, spurious results. The rejection of time steps in individual time step schemes may, however, pose bookkeeping challenges. A simple workaround has been proposed by Saitoh and Makino (2009). For each and every simulation the conservation of energy, momentum and angular momentum should be monitored. Reducing the time step size and increasing the force accuracy, say, if a tree is used for gravity, should improve the conservation properties. A correct code should ensure conservation to better than 1% over several thousand time steps.

2.9.5. Artificial dissipation

Artificial dissipation should only be applied where really necessary. Schemes with time-dependent parameters are highly

recommended. Modern versions of artificial dissipation terms such as Eqs. (67) and (68) should be used. Recent years have seen a large leap forward in eliminating unwanted effects from artificial dissipation, yet, there is certainly room for further improvement.

2.9.6. Displaying results

Generally, display continuous quantities and avoid particle plots to present physical results. The particles are just auxiliary constructs, “moving interpolation points” that represent a continuum. Just showing particle positions projected on a plane may mimic a “resolution” that does not exist, a contour plot is a more honest presentation. To check that the numerics is well behaved, it may, however, be useful to inspect the particle distribution. A noisy particle distribution should always raise doubts about the quality of a simulation.

Summary of “vanilla ice” SPH

We summarize here the most basic form of the SPH equations. As the particle masses are kept fix, there is no need to solve the continuity equation. Densities can be obtained via summation from

$$\rho_a = \sum_b m_b W_{ab}. \quad (100)$$

Alternatively, the continuity equation can be integrated, see Eq. (3). The evolution equation for the specific internal energy can be written as

$$\frac{du_a}{dt} = \sum_b m_b \left(\frac{P_a}{\rho_a^2} + \frac{1}{2} \Pi_{ab} \right) \vec{v}_{ab} \cdot \nabla_a W_{ab}, \quad (101)$$

and the momentum equation as

$$\frac{d\vec{v}_a}{dt} = - \sum_b m_b \left(\frac{P_a}{\rho_a^2} + \frac{P_b}{\rho_b^2} + \Pi_{ab} \right) \nabla_a W_{ab}. \quad (102)$$

Particles are advanced in time according to this equation. Π_{ab} is the “standard” artificial viscosity term given in Eq. (59), more modern prescriptions are given in Eqs. (67) and (68). Alternative forms of energy may be integrated forward in time, see, for example, Eq. (34).

3. SPH from a variational principle

In the previous section we had seen how the “vanilla ice” SPH equations can be derived directly from the Lagrangian form of the inviscid hydrodynamic equations. Although this form ensures conservation of energy, linear and angular momentum and works well in practice, the corresponding symmetries were enforced somewhat ad hoc. SPH can also be derived using nothing more than a suitable fluid Lagrangian, the first law of thermodynamics and a prescription on how to obtain a density estimate via summation (Gingold and Monaghan, 1982; Monaghan and Price, 2001; Springel and Hernquist, 2002).

3.1. The Lagrangian and the Euler–Lagrange equations

The Lagrangian of a perfect fluid is given by (Eckart, 1960)

$$L = \int \rho \left(\frac{v^2}{2} - u(\rho, s) \right) dV, \quad (103)$$

where ρ is the mass density, v the fluid velocity, u the specific energy and s the specific entropy. In SPH-discretization it reads

$$L_{\text{SPH,h}} = \sum_b m_b \left(\frac{v_b^2}{2} - u(\rho_b, s_b) \right). \quad (104)$$

The discretized equations for the fluid are then derived by applying the Euler–Lagrange equations

$$\frac{d}{dt} \left(\frac{\partial L}{\partial \vec{v}_a} \right) - \frac{\partial L}{\partial \vec{r}_a} = 0, \quad (105)$$

where \vec{r}_a and \vec{v}_a refer to the position and velocity of particle a . The term in brackets yields the canonical particle momentum (like usual, we keep the particle mass fixed in time)

$$\frac{\partial L}{\partial \vec{v}_a} = \frac{\partial}{\partial \vec{v}_a} \left[\sum_b m_b \left(\frac{v_b^2}{2} - u(\rho_b, s_b) \right) \right] = m_a \vec{v}_a, \quad (106)$$

and therefore, the first term in Eq. (105) yields the change of particle momentum $m_a \frac{d\vec{v}_a}{dt}$.

The second term in the Lagrangian acts like a potential, and if self-gravity is considered, $-\sum_b m_b u_b$ has to be replaced by $-\sum_b m_b (u_b + \Phi_b)$, where Φ_b is the gravitational potential (Price and Monaghan, 2007). In the following, we will only consider $\Phi_b = 0$. The second term in Eq. (105) becomes

$$\frac{\partial L}{\partial \vec{r}_a} = \frac{\partial}{\partial \vec{r}_a} \left[\sum_b m_b \left(\frac{v_b^2}{2} - u(\rho_b, s_b) \right) \right] = - \sum_b m_b \frac{\partial u_b}{\partial \rho_b} \bigg|_s \cdot \frac{\partial \rho_b}{\partial \vec{r}_a}. \quad (107)$$

We can make use of the first law of thermodynamics, Eq. (7), to find

$$m_a \frac{d\vec{v}_a}{dt} = - \sum_b m_b \frac{P_b}{\rho_b^2} \frac{\partial \rho_b}{\partial \vec{r}_a}. \quad (108)$$

3.2. The density, its derivatives and “grad- h ”-terms

So far, we had ignored all extra terms that result from variable smoothing lengths (Nelson and Papaloizou, 1994; Springel and Hernquist, 2002; Monaghan, 2002), this is what we address now. From now on, we use the smoothing length of the particle itself in the density summation,

$$\rho_a = \sum_b m_b W(r_{ab}, h_a). \quad (109)$$

and use Eq. (51) to adapt the smoothing length. Thus, ρ_a depends on h_a and vice versa, which requires an iteration to reach consistency.

If we take the changes of h into account, the Lagrangian time derivative of the density is given by

$$\begin{aligned} \frac{d\rho_a}{dt} &= \frac{d}{dt} \left(\sum_b m_b W_{ab}(h_a) \right) \\ &= \sum_b m_b \left\{ \frac{\partial W_{ab}(h_a)}{\partial r_{ab}} \frac{dr_{ab}}{dt} + \frac{\partial W_{ab}(h_a)}{\partial h_a} \frac{dh_a}{dt} \right\} \\ &= \sum_b m_b \frac{\partial W_{ab}(h_a)}{\partial r_{ab}} \hat{e}_{ab} \cdot \vec{v}_{ab} + \sum_b m_b \frac{\partial W_{ab}(h_a)}{\partial h_a} \cdot \frac{\partial h_a}{\partial \rho_a} \frac{d\rho_a}{dt} \\ &= \sum_b m_b \vec{v}_{ab} \cdot \nabla_a W_{ab}(h_a) + \frac{\partial h_a}{\partial \rho_a} \frac{d\rho_a}{dt} \sum_b m_b \frac{\partial W_{ab}(h_a)}{\partial h_a}, \end{aligned} \quad (110)$$

where we have used Eqs. (24) and (26). If we collect the $d\rho_a/dt$ -terms and introduce

$$\Omega_a \equiv \left(1 - \frac{\partial h_a}{\partial \rho_a} \sum_b m_b \frac{\partial W_{ab}(h_a)}{\partial h_a} \right), \quad (111)$$

the time derivative of the density reads

$$\frac{d\rho_a}{dt} = \frac{1}{\Omega_a} \sum_b m_b \vec{v}_{ab} \cdot \nabla_a W_{ab}(h_a). \quad (112)$$

This is the generalization of the SPH expression for the density change that follows from Eq. (31). In a similar way, the spatial derivatives can be calculated

$$\begin{aligned} \frac{\partial \rho_b}{\partial \vec{r}_a} &= \sum_k m_k \left\{ \nabla_a W_{bk}(h_b) + \frac{\partial W_{bk}(h_b)}{\partial h_b} \frac{\partial h_b}{\partial \rho_b} \frac{\partial \rho_b}{\partial \vec{r}_a} \right\} \\ &= \frac{1}{\Omega_b} \sum_k m_k \nabla_a W_{bk}(h_b). \end{aligned} \quad (113)$$

To summarize: if derivatives of the smoothing length h are accounted for, the “standard” SPH expressions for the density derivatives have to be corrected by factors $1/\Omega$, see Eqs. (111)–(113).

3.3. The SPH equations with “grad- h ”-terms

We keep again the masses fixed in time, so there is no need to solve the continuity equation. By inserting Eq. (112) into Eq. (30) we find the energy equation

$$\frac{du_a}{dt} = \frac{1}{\Omega_a} \frac{P_a}{\rho_a^2} \sum_b m_b \vec{v}_{ab} \cdot \nabla_a W_{ab}(h_a). \quad (114)$$

For the momentum equation we need to insert the density gradient, Eq. (113), into Eq. (108)

$$\begin{aligned} m_a \frac{d\vec{v}_a}{dt} &= - \sum_b m_b \frac{P_b}{\rho_b^2} \nabla_a \rho_b \\ &= - \sum_b m_b \frac{P_b}{\rho_b^2} \left(\frac{1}{\Omega_b} \sum_k m_k \nabla_a W_{bk}(h_b) \right). \end{aligned} \quad (115)$$

Using Eq. (25), the above equation becomes

$$\begin{aligned} m_a \frac{d\vec{v}_a}{dt} &= - \sum_b m_b \frac{P_b}{\rho_b^2} \frac{1}{\Omega_b} \sum_k m_k \nabla_b W_{kb}(h_b) (\delta_{ba} - \delta_{ka}) \\ &= -m_a \frac{P_a}{\rho_a^2} \frac{1}{\Omega_a} \sum_k m_k \nabla_a W_{ka}(h_a) + \sum_b m_b \frac{P_b}{\rho_b^2} \frac{1}{\Omega_b} m_a \nabla_b W_{ab}(h_b) \\ &= -m_a \frac{P_a}{\rho_a^2} \frac{1}{\Omega_a} \sum_b m_b \nabla_a W_{ba}(h_a) - m_a \sum_b m_b \frac{P_b}{\rho_b^2} \frac{1}{\Omega_b} \nabla_a W_{ab}(h_b) \\ &= -m_a \sum_b m_b \left(\frac{P_a}{\Omega_a \rho_a^2} \nabla_a W_{ab}(h_a) + \frac{P_b}{\Omega_b \rho_b^2} \nabla_a W_{ab}(h_b) \right). \end{aligned} \quad (116)$$

Thus the final momentum equation reads

$$\frac{d\vec{v}_a}{dt} = - \sum_b m_b \left(\frac{P_a}{\Omega_a \rho_a^2} \nabla_a W_{ab}(h_a) + \frac{P_b}{\Omega_b \rho_b^2} \nabla_a W_{ab}(h_b) \right). \quad (117)$$

Note that now all arbitrariness (such as the particular form of Eq. (28)) has been eliminated from the derivation. The “grad- h ” terms increase the accuracy of SPH and the conservation properties in the presence of varying smoothing lengths. How important they are in practice depends on both the problem and the numerical resolution (Springel and Hernquist, 2002; Rosswog and Price, 2007).

SPH equations from a variational principle
With

$$\rho_a = \sum_b m_b W(r_{ab}, h_a) \quad \text{and} \quad h_a = \eta \left(\frac{m_a}{\rho_a} \right)^{1/3}, \quad (118)$$

the energy equation reads

$$\frac{du_a}{dt} = \frac{1}{\Omega_a} \frac{P_a}{\rho_a^2} \sum_b m_b \vec{v}_{ab} \cdot \nabla_a W_{ab}(h_a), \quad (119)$$

and the momentum equation is

$$\frac{d\vec{v}_a}{dt} = - \sum_b m_b \left(\frac{P_a}{\Omega_a \rho_a^2} \nabla_a W_{ab}(h_a) + \frac{P_b}{\Omega_b \rho_b^2} \nabla_a W_{ab}(h_b) \right), \quad (120)$$

where

$$\Omega_a \equiv \left(1 - \frac{\partial h_a}{\partial \rho_a} \sum_b m_b \frac{\partial}{\partial h_a} W_{ab}(h_a) \right), \quad (121)$$

are the so-called “grad- h -terms”. Additional artificial dissipation terms as discussed in Section 2 need to be applied in order to resolve shocks.

4. Relativistic SPH

Several relativistic versions of SPH exist. Early formulations due to Mann (1991) and Mann (1993) were able to capture the overall solutions, but they were – by today’s standards – not particularly accurate.

Laguna et al. (1993) developed a 3D, general-relativistic SPH code. Due to their choice of variables their continuity equation contains a gravitational source term. This term requires to introduce SPH kernel functions for curved space-times which are in general not isotropic and invariant under translations. Moreover, they did not use a conservative form of the equations and their approach requires additional time derivatives of Lorentz factors which they approximated by first order finite differences. Similar to the approach of Mann, only mildly relativistic shocks could be treated. The approach of Laguna et al. (1993) is also the basis of the more recent code described in Rantsiou et al. (2008).

Kheyfets et al. (1990) suggested an alternative approach in which they define the spatial kernel function in a local rest frame and assume that space is approximately flat in this frame. The interaction between particles requires the choice of a particular frame whose calculation requires the solution of four coupled algebraic equations. While this approach is completely covariant, it requires a large computational effort.

Like in grid-based methods, a conservative formulation is crucial to handle strong shocks. As we had seen in Section 2.7, concepts of Riemann solvers were used as a guide to improve SPH’s artificial viscosity by treating the interaction between two particles as a local Riemann problem (Monaghan, 1997). This approach replaces wave propagation speeds by an appropriately chosen signal velocity. With this approach (together with evolving the total energy rather than the thermal energy) Chow and Monaghan (1997) obtained accurate results even for ultra-relativistic flows.

More recently, Siegler and Riffert (2000) and Siegler (2000) have suggested a set of equations for both the special- and general-relativistic (fixed background metric) case. It is based on a formulation of the Lagrangian hydrodynamics equations in conservative form. By a particular choice of dynamical variables they avoid many complications that have plagued earlier relativistic SPH for-

mulations. In particular, by choosing the relativistic rest mass density for the SPH formalism the continuity equation has the same form as in non-relativistic SPH, time derivatives of Lorentz factors do not appear and flat space kernels can be used. This comes at the price of inverting the dynamically evolved variables into the physical variables. Sieglér (2000) was able to accurately simulate some test cases with Lorentz factors up to $\gamma = 1000$.

A more elegant approach is based on the use of the discretized Lagrangian of a perfect fluid (Monaghan and Price, 2001). Guided by the canonical momentum and energy, suitable numerical variables can be chosen which lead to evolution equations that are similar to the Newtonian ones. Due to the consistent derivation from a Lagrangian the conservation of mass, energy, linear and angular momentum are guaranteed. This approach can be applied both to the special- and the general-relativistic case.

In recent years, SPH has also been applied to study flows in time-varying space-times. The first approaches used post-Newtonian approximations (Ayal et al., 2001; Faber and Rasio, 2000, 2002; Faber et al., 2001), more recently the conformal flatness approximation (Isenberg, unpublished; Wilson et al., 1996) has been implemented (Oechslin et al., 2002; Faber et al., 2004, 2006).

In the following subsections we derive the special- and general-relativistic SPH equations from a variational principle similar to Monaghan and Price (2001).

4.1. Special-relativistic SPH

Here, we generalize the approach of Monaghan and Price (2001) to include the special-relativistic “grad-h” terms. We use the conventions that the metric tensor has the signature $(-, +, +, +)$, Latin indices run from 1 to 3, Greek ones from 0 to 3 with the zero component being time. In addition, the usual Einstein sum convention and $c = G = 1$ are used and the flat spacetime metric is denoted by $\eta_{\mu\nu}$.

With these conventions, the line element reads

$$ds^2 = \eta_{\mu\nu} dx^\mu dx^\nu, \quad (122)$$

and the proper time is given by $d\tau^2 = -ds^2$. The 4-velocity is defined as

$$U^\mu = \frac{dx^\mu}{d\tau}, \quad (123)$$

and, due to the above two relations, it is normalized to -1 :

$$U_\mu U^\mu = \eta_{\mu\nu} \frac{dx^\nu}{d\tau} \frac{dx^\mu}{d\tau} = \frac{ds^2}{d\tau^2} = -1. \quad (124)$$

The velocity components can be written as

$$(U^\mu) = (\gamma, \gamma\vec{v}), \quad (125)$$

where γ is the Lorentz factor

$$\gamma = \frac{1}{\sqrt{1 - v^2}}, \quad (126)$$

with \vec{v} being the 3-velocity. Due to Eq. (125) the 3-velocity can be expressed as

$$v^i = \frac{U^i}{U^0}. \quad (127)$$

The 4-momentum of a particle with rest mass m is given by

$$(p^\mu) = (mU^\mu) = (\gamma m, \gamma m\vec{v}) = (E, \vec{p}), \quad (128)$$

where E is the particle energy and \vec{p} its relativistic momentum. The last expression is also correct for particles with vanishing rest mass.

4.1.1. The Lagrangian

Consistent with our overall strategy, we derive the SPH equations from a Lagrangian to ensure exact conservation. We start from the Lagrangian of a perfect fluid (Fock, 1964)

$$L_{\text{pf, sr}} = - \int T^{\mu\nu} U_\mu U_\nu dV. \quad (129)$$

The energy momentum tensor of a perfect fluid

The energy-momentum tensor, $T^{\mu\nu}$, is a key element of relativistic hydrodynamics as it contains the sources of the relativistic gravitational field. Its components $T^{\mu\nu}$ are defined as “flux of μ -component of the 4-momentum in ν -direction”. Thus, the T^{00} -component is the *energy density*, the T^{0j} component is the *energy flux*, the T^{i0} component is the *momentum density* and the T^{ij} is the *momentum flux*. For a perfect fluid with zero viscosity and heat conduction it is given by

$$T^{\mu\nu} = (P + e)U^\mu U^\nu + P\eta^{\mu\nu}, \quad (130)$$

where P is the fluid pressure, U^μ the 4-velocity and e the energy density in the local rest frame. The conservation of energy and momentum can be expressed as

$$T^{\mu\nu},_{\nu} = 0, \quad (131)$$

where the comma denotes the partial derivative (in general relativity it has to be replaced by the covariant derivative, usually denoted by a semicolon). $\mu = 0$ expresses energy and $\mu = i$ momentum conservation. In the Newtonian limit (with $c = 1$) the following relations hold $U^0 = \gamma \approx 1$, $U^i \approx v^i$, $e \approx \rho$ and $P/e \ll 1$. Thus the components read

$$T^{00} = (P + e)U^0 U^0 + P \approx \rho, \quad (132)$$

$$T^{0j} = (P + e)U^0 U^j \approx \rho v^j, \quad (133)$$

$$T^{ij} = (P + e)U^i U^j + P\delta^{ij} \approx \rho v^i v^j + P\delta^{ij}. \quad (134)$$

Therefore, $T^{0\mu},_{\mu} = 0$ reduces to the usual continuity equation

$$T^{0\mu},_{\mu} = T^{00},_0 + T^{0j},_j = \frac{\partial \rho}{\partial t} + \frac{\partial(\rho v^j)}{\partial x^j} = 0, \quad (135)$$

and $T^{i\mu},_{\mu} = 0$ becomes

$$T^{i\mu},_{\mu} = T^{i0},_0 + T^{ij},_j = \frac{\partial(\rho v^i)}{\partial t} + \frac{\partial(\rho v^i v^j)}{\partial x^j} + \frac{\partial P}{\partial x^i} = 0, \quad (136)$$

which is the Euler equation.

This Lagrangian is, apart from the flat space volume element, the same as the general-relativistic one, see Section 4.2. The energy density, e^9 , that is needed in the energy-momentum tensor, see Eq. (130), has contributions from the rest mass and the thermal energy:

$$e = e_{\text{rest}} + e_{\text{therm}} = \rho_{\text{rest}} c^2 + u \rho_{\text{rest}} = n m_0 c^2 (1 + u/c^2), \quad (137)$$

where m_0 is the baryon mass¹⁰ and u is again the specific thermal energy and n is the baryon number density, the latter two are measured in the local rest frame. Here, we have kept the c^2 s for clarity. From now on we will measure all our energies in units of $m_0 c^2$ (and use $c \equiv 1$). With these conventions the energy momentum tensor reads

$$T^{\mu\nu} = (n[1 + u(n, s)] + P)U^\mu U^\nu + P\eta^{\mu\nu}. \quad (138)$$

⁹ This quantity is usually denoted by ρ in the literature. To avoid confusion with the non-relativistic mass density that we have used previously, we choose a different symbol here.

¹⁰ Note that this quantity depends on the relative number of neutrons and protons, i.e. on the nuclear composition.

Here s is the specific entropy per baryon in the local fluid rest frame and P the fluid pressure. For a practical computation we fix a particular frame (“computing frame”) and transform the quantities into this frame where necessary.

Using Eq. (124), we can considerably simplify the above Lagrangian. The quantity under the integral becomes

$$T^{\mu\nu}U_\mu U_\nu = \{(n[1+u] + P)U^\mu U^\nu\}U_\mu U_\nu + P\eta^{\mu\nu}U_\mu U_\nu = n(1+u), \quad (139)$$

and the Lagrangian simplifies to

$$L_{\text{pf},\text{sr}} = - \int n(1+u)dV. \quad (140)$$

The baryon number density in the rest frame of a fluid element, n , is related to the number density in our computing frame, N , by a Lorentz factor, γ . To see this, assume a volume in the local rest frame of a fluid element, V_{lrf} , that contains k baryons. In general, this fluid element will move with some velocity with respect to our computing frame. If we assume that the motion is in, say, x -direction, the x -component of the volume element in the computing frame, V_{cf} , appears Lorentz-contracted by a factor γ : $V_{\text{cf}} = V_{\text{lrf}}/\gamma$. Since this volume element contains the same number of baryons, k , the density in the computing frame is

$$N = \frac{k}{V_{\text{cf}}} = \frac{k\gamma}{V_{\text{lrf}}} = \gamma n. \quad (141)$$

As before, see Eq. (104), we want to discretize the Lagrangian to derive the SPH equations. We subdivide space in volumes ΔV_b , so that a volume labeled by index b contains $v_b = \Delta V_b N_b$ baryons, where N_b is the baryon density at particle b (all quantities measured in the computing frame). Or, the other way around, if a fluid parcel labeled by b contains v_b baryons, it has a volume

$$\Delta V_b = \frac{v_b}{N_b}. \quad (142)$$

Similar to Eq. (12), we can use this volume element in the SPH-approximation of a quantity f^{11} :

$$f(\vec{r}) = \sum_b f_b \frac{v_b}{N_b} W(|\vec{r} - \vec{r}_b|, h). \quad (143)$$

With this prescription the baryon number density in the computing frame at position of particle a reads

$$N_a = N(\vec{r}_a) = \sum_b v_b W(|\vec{r}_a - \vec{r}_b|, h_a), \quad (144)$$

where we have used h_a to conform with the non-relativistic version, Eq. (109). The latter can be recovered by the following replacements: $m_b \rightarrow v_b$ and $\rho_b \rightarrow N_b$. If we keep the baryon number per SPH particle, v_b , fixed, the total baryon number is conserved and there is no need to evolve a continuity equation. Analogously to Eq. (31) one could also discretize the continuity equation and calculate the density by integration. We adapt the smoothing length similar to the Newtonian case, see Eq. (51),

$$h_a = \eta \left(\frac{v_a}{N_a} \right)^{1/3}, \quad (145)$$

which, again, requires an iteration for consistent values of N_a and h_a . We can now discretize the Lagrangian of Eq. (140)

$$L_{\text{SPH},\text{sr}} = - \sum_b \frac{v_b}{N_b} n_b [1 + u(n_b, s_b)], \quad (146)$$

or, by using Eq. (141),

$$L_{\text{SPH},\text{sr}} = - \sum_b \frac{v_b}{\gamma_b} [1 + u(n_b, s_b)] = - \sum_b v_b \sqrt{1 - v_b^2} [1 + u_b]. \quad (147)$$

4.1.2. The momentum equation

The Euler–Lagrange equations, Eq. (105), determine the evolution of special-relativistic momentum:

$$\vec{p}_a \equiv \frac{\partial L_{\text{SPH},\text{sr}}}{\partial \vec{v}_a} = - \sum_b v_b \frac{\partial}{\partial \vec{v}_a} \left(\frac{1 + u(n_b, s_b)}{\gamma_b} \right). \quad (148)$$

The specific energy u depends, via the density, on the velocity:

$$\frac{\partial u_b}{\partial \vec{v}_a} = \left(\frac{\partial u_b}{\partial n_b} \right)_s \frac{\partial n_b}{\partial \vec{v}_a} = \frac{P_b}{n_b^2} \frac{\partial n_b}{\partial \vec{v}_a}, \quad (149)$$

where we have used Eq. (8). Via Eq. (141) we have

$$\frac{\partial n_b}{\partial \vec{v}_a} = N_b \frac{\partial}{\partial \vec{v}_a} \left(\frac{1}{\gamma_b} \right) = N_b \frac{\partial}{\partial \vec{v}_a} (1 - v_b^2)^{1/2} = -N_b \gamma_b \vec{v}_b \delta_{ab}. \quad (150)$$

Thus, the canonical momentum is

$$\begin{aligned} \vec{p}_a &\equiv \frac{\partial L_{\text{SPH},\text{sr}}}{\partial \vec{v}_a} = - \sum_b v_b [1 + u_b] \frac{\partial}{\partial \vec{v}_a} \left(\frac{1}{\gamma_b} \right) - \sum_b \frac{v_b}{\gamma_b} \frac{\partial u_b}{\partial \vec{v}_a} \\ &= \sum_b v_b (\vec{v}_b \gamma_b \delta_{ab}) [1 + u_b] + \sum_b \frac{v_b}{\gamma_b} \left(\frac{P_b}{n_b^2} \right) (N_b \gamma_b \vec{v}_b \delta_{ab}) \\ &= v_a \gamma_a \vec{v}_a \left(1 + u_a + \frac{P_a}{n_a} \right), \end{aligned} \quad (151)$$

where we have again used Eq. (141), the term in brackets after the last equal sign is the enthalpy per baryon. Obviously, in relativity the pressure contributes to the momentum density. We define the canonical momentum per baryon as

$$\vec{s}_a \equiv \gamma_a \vec{v}_a \left(1 + u_a + \frac{P_a}{n_a} \right), \quad (152)$$

whose time evolution is governed by $\partial L_{\text{SPH},\text{sr}}/\partial \vec{r}_a$, see Eq. (105), and which requires the gradient of the number density. The latter is obtained similar to the Newtonian case, see Eq. (113),

$$\begin{aligned} \frac{\partial N_b}{\partial \vec{r}_a} &= \sum_k v_k \left\{ \frac{\partial W(r_{bk}, h_b)}{\partial r_{bk}} \frac{\partial r_{bk}}{\partial \vec{r}_a} + \frac{\partial W(r_{bk}, h_b)}{\partial h_b} \frac{\partial h_b}{\partial N_b} \frac{\partial N_b}{\partial \vec{r}_a} \right\} \\ &= \frac{1}{\Omega_b} \sum_k v_k \nabla_a W_{bk}(h_b) (\delta_{ba} - \delta_{ka}), \end{aligned} \quad (153)$$

with

$$\tilde{\Omega}_b = 1 - \frac{\partial h_b}{\partial N_b} \sum_k v_k \frac{\partial W(r_{bk}, h_b)}{\partial h_b}. \quad (154)$$

Thus

$$\begin{aligned} \frac{\partial L_{\text{SPH},\text{sr}}}{\partial \vec{r}_a} &= - \sum_b \frac{v_b}{\gamma_b} \frac{\partial u_b}{\partial \vec{r}_a} = - \sum_b \frac{v_b}{\gamma_b} \frac{P_b}{n_b^2} \frac{\partial n_b}{\partial \vec{r}_a} = - \sum_b \frac{v_b}{\gamma_b^2} \frac{P_b}{n_b^2} \frac{\partial N_b}{\partial \vec{r}_a} \\ &= - \sum_{b,k} \frac{v_b v_k}{\gamma_b^2} \frac{P_b}{\tilde{\Omega}_b n_b^2} \nabla_a W_{bk}(h_b) (\delta_{ba} - \delta_{ka}) \\ &= - v_a \sum_b v_b \left\{ \frac{P_a}{\tilde{\Omega}_a N_a^2} \nabla_a W_{ab}(h_a) + \frac{P_b}{\tilde{\Omega}_b N_b^2} \nabla_a W_{ab}(h_b) \right\}, \end{aligned} \quad (155)$$

where we have used Eqs. (8), (141), (144), (153) and (26). With Eqs. (155) and (151), the special-relativistic SPH momentum equation becomes

¹¹ For ease of notation we have again dropped the distinction between the function to be interpolated and the interpolant.

$$\frac{d\vec{S}_a}{dt} = - \sum_b v_b \left\{ \frac{P_a}{\Omega_a N_a^2} \nabla_a W_{ab}(h_a) + \frac{P_b}{\Omega_b N_b^2} \nabla_a W_{ab}(h_b) \right\}. \quad (156)$$

This form can be obtained from the non-relativistic case, Eq. (117), by the following replacements: $\vec{v}_a \rightarrow \vec{S}_a$, $m_k \rightarrow v_k$, $\Omega_k \rightarrow \tilde{\Omega}_k$ and $\rho_k \rightarrow N_k$.

Since the Lagrangian is invariant under infinitesimal translation the total canonical momentum

$$\vec{P} = \sum_b \vec{p}_b = \sum_b v_b \vec{S}_b = \sum_b v_b \gamma_b \vec{v}_b \left(1 + u_b + \frac{P_b}{n_b} \right), \quad (157)$$

is conserved. Similarly, due to invariance under rotation, the angular momentum

$$\begin{aligned} \vec{L} &= \sum_b \vec{r}_b \times \vec{p}_b = \sum_b v_b \vec{r}_b \times \vec{S}_b \\ &= \sum_b v_b \gamma_b \left(1 + u_b + \frac{P_b}{n_b} \right) \vec{r}_b \times \vec{v}_b, \end{aligned} \quad (158)$$

is conserved by construction.

4.1.3. The energy equation

To choose a suitable numerical energy variable we start from the conserved canonical energy (no explicit time dependence in the Lagrangian)

$$E \equiv \sum_a \frac{\partial L_{\text{SPH},sr}}{\partial \vec{v}_a} \cdot \vec{v}_a - L_{\text{SPH},sr}. \quad (159)$$

With Eqs. (147) and (151) the energy reads

$$E = \sum_a v_a \left(\vec{v}_a \cdot \vec{S}_a + \frac{1 + u_a}{\gamma_a} \right) = \sum_a v_a \hat{\epsilon}_a, \quad (160)$$

where, we have defined

$$\hat{\epsilon}_a \equiv \vec{v}_a \cdot \vec{S}_a + \frac{1 + u_a}{\gamma_a}. \quad (161)$$

For later use, we note that by using $v_a^2 = 1 - 1/\gamma_a^2$ and Eq. (141) we can express $\hat{\epsilon}_a$ as

$$\hat{\epsilon}_a = \gamma_a v_a^2 \left(1 + u_a + \frac{P_a}{n_a} \right) + \frac{1 + u_a}{\gamma_a} = \gamma_a \left(1 + u_a + \frac{P_a}{n_a} \right) - \frac{P_a}{N_a}. \quad (162)$$

To find the evolution equation for $\hat{\epsilon}_a$, we need the time derivative of the second term in Eq. (161). Ideally, it should not contain a time derivative of the Lorentz factor since such terms are known to destabilize numerical schemes (Norman and Winkler, 1986). Using

$$\begin{aligned} \frac{d\gamma_a}{dt} &= \gamma_a^3 \vec{v}_a \cdot \frac{d\vec{v}_a}{dt} \quad \text{and} \quad \frac{dn_a}{dt} = \frac{d}{dt} \left(\frac{N_a}{\gamma_a} \right) \\ &= \frac{1}{\gamma_a} \frac{dN_a}{dt} - N_a \gamma_a \vec{v}_a \cdot \frac{d\vec{v}_a}{dt}, \end{aligned} \quad (163)$$

we find

$$\begin{aligned} \frac{d}{dt} \left(\frac{1 + u_a}{\gamma_a} \right) &= \frac{1}{\gamma_a^2} \left(\gamma_a \frac{du_a}{dt} - (1 + u_a) \frac{d\gamma_a}{dt} \right) \\ &= \frac{1}{\gamma_a} \frac{P_a}{n_a^2} \frac{dn_a}{dt} - \frac{1 + u_a}{\gamma_a^2} \gamma_a^3 \vec{v}_a \cdot \frac{d\vec{v}_a}{dt} \\ &= \frac{P_a}{N_a^2} \frac{dN_a}{dt} - \left(1 + u_a + \frac{P_a}{n_a} \right) \gamma_a \vec{v}_a \cdot \frac{d\vec{v}_a}{dt} \\ &= \frac{P_a}{N_a^2} \frac{dN_a}{dt} - \vec{S}_a \cdot \frac{d\vec{v}_a}{dt}, \end{aligned} \quad (164)$$

where we used Eqs. (8), (141) and (163). With Eq. (164) at hand, we can take the derivative of Eq. (161)

$$\begin{aligned} \frac{d\hat{\epsilon}_a}{dt} &= \frac{d}{dt} \left\{ \vec{v}_a \cdot \vec{S}_a + \frac{1 + u_a}{\gamma_a} \right\} \\ &= \vec{S}_a \cdot \frac{d\vec{v}_a}{dt} + \vec{v}_a \cdot \frac{d\vec{S}_a}{dt} + \frac{P_a}{N_a^2} \frac{dN_a}{dt} - \vec{S}_a \cdot \frac{d\vec{v}_a}{dt} \\ &= \vec{v}_a \cdot \frac{d\vec{S}_a}{dt} + \frac{P_a}{N_a^2} \frac{dN_a}{dt}, \end{aligned} \quad (165)$$

i.e. apart from the relativistic momentum Eq. (156), we need the Lagrangian time derivative of the number density in the computing frame:

$$\begin{aligned} \frac{dN_a}{dt} &= \sum_b v_b \left\{ \frac{\partial W_{ab}(h_a)}{\partial r_{ab}} \frac{dr_{ab}}{dt} + \frac{\partial W_{ab}}{\partial h_a} \frac{dh_a}{dt} \frac{dN_a}{dt} \right\} \\ &= \frac{1}{\Omega_a} \sum_b v_b \vec{v}_{ab} \cdot \nabla_a W_{ab}(h_a), \end{aligned} \quad (166)$$

where we have used Eq. (154). If we insert Eqs. (156) and (166) into Eq. (165) the energy evolution equation becomes

$$\frac{d\hat{\epsilon}_a}{dt} = - \sum_b v_b \left(\frac{P_a \vec{v}_b}{\Omega_a N_a^2} \cdot \nabla_a W_{ab}(h_a) + \frac{P_b \vec{v}_a}{\Omega_b N_b^2} \cdot \nabla_a W_{ab}(h_b) \right). \quad (167)$$

This relativistic energy equation looks similar to the non-relativistic equation for the thermokinetic energy, see Eq. (34).

4.1.4. Recovery of the primitive variables

Due to our choice of the numerical variables neither the momentum nor the energy equation contain time derivatives of Lorentz factors. Such terms restricted earlier versions of relativistic SPH to moderate Lorentz factors only. But this comes at the price that the physical variables need to be recovered at every time step from the numerical ones, a price that relativistic Eulerian codes also have to pay.

At the end of a time step γ , v , u and n need to be calculated from the updated numerical quantities N , \vec{S} and $\hat{\epsilon}$. One can express all variables in the equation of state

$$P_a = (\Gamma - 1) n_a u_a, \quad (168)$$

as a function of the updated numerical variables and the pressure P_a . The resulting equation is solved numerically for P_a and once it is found, the other physical variables can be recovered (Marti and Müller, 1996; Monaghan, 1997). From Eqs. (152) and (162) one finds

$$\vec{v}_a = \frac{\vec{S}_a}{\hat{\epsilon}_a + P_a/N_a}, \quad (169)$$

and thus the Lorentz factor is

$$\gamma_a = \frac{1}{\sqrt{1 - \vec{S}_a^2 / (\hat{\epsilon}_a + P_a/N_a)^2}}. \quad (170)$$

From Eq. (169) we have

$$\left(\hat{\epsilon}_a + \frac{P_a}{\gamma_a n_a} \right) \vec{v}_a = \vec{S}_a = \gamma_a \vec{v}_a \left(1 + u_a + \frac{P_a}{n_a} \right), \quad (171)$$

which can be solved for

$$u_a = \frac{\hat{\epsilon}_a}{\gamma_a} + \frac{P_a}{\gamma_a N_a} (1 - \gamma_a^2) - 1. \quad (172)$$

With aid of Eqs. (141) and (172), Eq. (168) can be solved, e.g. via a Newton–Raphson scheme, for the new pressure P_a . Once P_a is known, the Lorentz factor can be calculated from Eq. (170), the specific energy from Eq. (172) and the velocity from Eq. (169).

4.1.5. Numerical tests

To explore the performance of this SPH formulation we show a numerical test that can be considered a special-relativistic generalization of Sod’s shock tube test, see Section 2.7. This test has become a widespread benchmark for relativistic hydrodynamics codes, see for example (Marti and Müller, 1996; Chow and Monaghan, 1997; Siegler and Riffert, 2000; Del Zanna and Bucciantini, 2002; Marti and Müller, 2003). The test is performed with a polytropic equation of state with exponent $\Gamma = 5/3$, vanishing initial velocities everywhere, the left state has a pressure $P_L = 40/3$ and

a density $N_L = 10$, while the right state is prepared with $P_R = 10^{-6}$ and $N_R = 1$. Although the resulting velocities are only mildly relativistic ($\gamma_{\max} \approx 1.4$), the deviations from the purely Newtonian result are already substantial. This is demonstrated in Fig. 8, where we compare the exact solutions for these initial conditions for the Newtonian (dashed) and the special-relativistic case (solid).

Fig. 9 shows the SPH result (black circles, about 3000 particles) at $t = 0.35$ together with the exact solution (red, solid line). The general agreement is excellent, noticeable deviations are only ob-

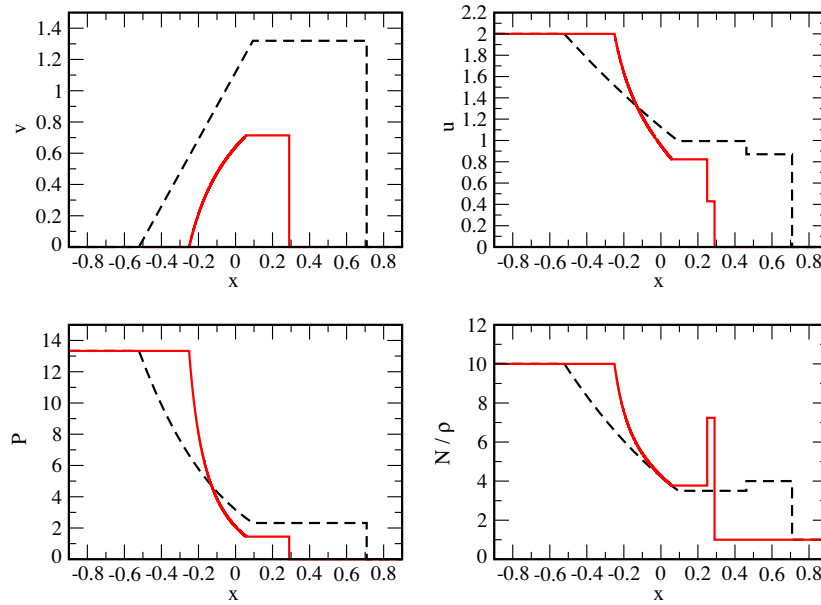


Fig. 8. Mildly relativistic ($\gamma_{\max} \approx 1.4$) shock tube test: comparison between the Newtonian (dashed) and the special-relativistic results (solid, red). Upper left: velocity in units of c , upper right: thermal energy, lower left: pressure, lower right: (computing frame) number density N and Newtonian mass density ρ .

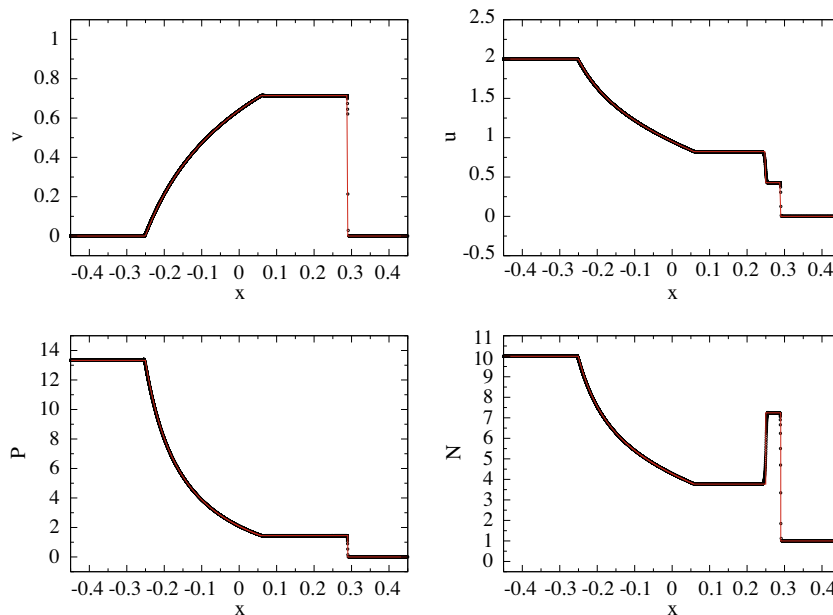


Fig. 9. SPH solution of the relativistic shock tube test of Marti and Müller (1996) (shown are 3000 particles; upper left: velocity in units of c , upper right: thermal energy, lower left: pressure, lower right: (computing frame) number density N). The black circles show the SPH solution, the red line marks the exact solution (Marti and Müller, 2003).

served in the form of a slightly smeared out contact discontinuity at $x \approx 0.25$. A striking difference to earlier SPH formulations (Laguna et al., 1993; Siegler and Riffert, 2000) is the absence of any spike in u and P at the contact discontinuity.

This SPH formulation has been further explored in a large set of special-relativistic benchmark tests (Rosswog, 2009). As expected, it performs very well in pure advection problems. Maybe more remarkable, it also shows convincing results in extremely strong, relativistic shocks. For example, it yields accurate solutions in a wall shock test with a Lorentz factor of $\gamma = 50,000$. The special-relativistic “grad-h”-terms generally improve the accuracy, but (at least in the performed set of tests) only to a moderate extent. For more details we refer to Rosswog (2009).

Summary of the special-relativistic SPH equations

The momentum equation derived from the special-relativistic Lagrangian reads

$$\frac{d\vec{S}_a}{dt} = - \sum_b v_b \left\{ \frac{P_a}{\tilde{\Omega}_a N_a^2} \nabla_a W_{ab}(h_a) + \frac{P_b}{\tilde{\Omega}_b N_b^2} \nabla_a W_{ab}(h_b) \right\}, \quad (173)$$

where

$$\vec{S}_a = \gamma_a \vec{v}_a \left(1 + u_a + \frac{P_a}{n_a} \right), \quad (174)$$

and

$$\tilde{\Omega}_b = 1 - \frac{\partial h_b}{\partial N_b} \sum_k v_k \frac{\partial W(r_{bk}, h_b)}{\partial h_b}. \quad (175)$$

The (canonical) energy variable

$$\hat{e}_a = \vec{v}_a \cdot \vec{S}_a + \frac{1 + u_a}{\gamma_a}, \quad (176)$$

is evolved according to

$$\frac{d\hat{e}_a}{dt} = - \sum_b v_b \left(\frac{P_a \vec{v}_b}{\tilde{\Omega}_a N_a^2} \cdot \nabla_a W_{ab}(h_a) + \frac{P_b \vec{v}_a}{\tilde{\Omega}_b N_b^2} \cdot \nabla_a W_{ab}(h_b) \right). \quad (177)$$

The computing frame number density can be found either by summation,

$$N_a = \sum_b v_b W_{ab}(h_a), \quad (178)$$

or, alternatively, by integration of

$$\frac{dN_a}{dt} = \frac{1}{\tilde{\Omega}_a} \sum_b v_b \vec{v}_{ab} \cdot \nabla_a W_{ab}(h_a). \quad (179)$$

4.2. General-relativistic SPH on a fixed background metric

4.2.1. The strategy

We now generalize the previous approach by assuming that a fixed metric is given as a function of the coordinates and that corrections to the metric induced by the fluid are negligible. Such a situation occurs, for example, during the tidal disruption of a star by a supermassive black hole in the center of a galaxy. Again, we start from the discretized Lagrangian of an ideal fluid and use the canonical momentum/energy as a guide for the choice of the numerical variables. As a matter of course, this new set of equations should reduce in the flat-space limit to the special-relativistic equations, see Eqs. (173)–(178), which, in their low-velocity limit, should be equivalent to the non-relativistic, standard SPH equations.

4.2.2. The Lagrangian

We start from the general-relativistic Lagrangian of a perfect fluid (Fock, 1964)

$$L_{\text{pf,GR}} = - \int T^{\mu\nu} U_\mu U_\nu \sqrt{-g} dV, \quad (180)$$

where $\sqrt{-g} dV$ is the proper volume element and $g = \det(g_{\mu\nu})$ is the determinant of the metric tensor, $g_{\mu\nu}$. As before, the energy momentum tensor is defined by

$$T^{\mu\nu} = \{n[1 + u(n, s)] + P\} U^\mu U^\nu + P g^{\mu\nu}, \quad (181)$$

where the fluid quantities are measured in their local rest frame and the four-velocity is defined as in Eq. (125). Obviously,

$$\frac{d\tau}{dt} = \left(-g_{\mu\nu} \frac{dx^\mu}{dt} \frac{dx^\nu}{dt} \right)^{\frac{1}{2}} = \left(-g_{\mu\nu} v^\mu v^\nu \right)^{\frac{1}{2}}, \quad (182)$$

where we used $v^\rho = dx^\rho/dt$. Comparing with the special-relativistic relation $d\tau/dt = 1/\gamma$, one sees that the quantity

$$\Theta \equiv \left(-g_{\mu\nu} v^\mu v^\nu \right)^{\frac{1}{2}} \quad (183)$$

takes over the role of and reduces in the flat spacetime limit to the special-relativistic Lorentz factor $\gamma = 1/\sqrt{1 - v^2}$. Similar to Eq. (127) we can also write

$$v^\mu = \frac{dx^\mu}{dt} = \frac{dx^\mu}{d\tau} \frac{d\tau}{dt} = \frac{U^\mu}{U^0}, \quad (184)$$

where we have used $dt/d\tau = U^0 = \Theta$, see Eq. (182). Using the normalization condition of the four-velocity, Eq. (124), the Lagrangian reduces to

$$\begin{aligned} L_{\text{pf,GR}} &= - \int [\{n(1 + u) + P\} U^\mu U^\nu U_\mu U_\nu + P g^{\mu\nu} U_\mu U_\nu] \sqrt{-g} dV \\ &= - \int n[1 + u(n, s)] \sqrt{-g} dV, \end{aligned} \quad (185)$$

which is, of course, up to the volume element, the same result as in special relativity, Eq. (140).

To discretize the Lagrangian, we first have to find a suitable density variable so that we can apply the usual SPH discretization prescription. The general-relativistic baryon number conservation equation reads

$$\frac{1}{\sqrt{-g}} \frac{\partial}{\partial x^\nu} (\sqrt{-g} U^\nu n) = 0, \quad (186)$$

see e.g. (Schutz, 1989), and this suggests to use the modified number density

$$N^* = \sqrt{-g} U^0 n = \sqrt{-g} \Theta n, \quad (187)$$

since it can be written with the help of Eq. (184) as

$$\frac{\partial N^*}{\partial t} + \frac{\partial(N^* v^i)}{\partial x^i} = 0. \quad (188)$$

Eq. (187) generalizes the earlier relation between the computing frame and the local rest frame, Eq. (141). We use N^* in the SPH interpolations

$$f(\vec{r}) = \sum_b f_b \frac{v_b}{N_b^*} W(|\vec{r} - \vec{r}_b|), \quad (189)$$

where

$$v_b = N_b^* \Delta V_b = n_b \Theta_b \sqrt{-g_b} \Delta V_b, \quad (190)$$

is the number of baryons contained in the volume $\sqrt{-g_b} \Delta V_b$. Applying Eq. (189) to N^* one obtains a density estimate by summation

$$N_a^* = \sum_b v_b W_{ab}(h_a), \quad (191)$$

similar to the earlier results, Eqs. (109) and (144). We can now use the relation between N^* and n , Eq. (187), to write the Lagrangian as

$$L_{\text{pf,GR}} = - \int \frac{N^*}{\sqrt{-g}} \Theta [1 + u(n, s)] \sqrt{-g} dV = - \int \frac{N^*}{\Theta} [1 + u(n, s)] dV, \quad (192)$$

i.e. the metric tensor contribution $\sqrt{-g}$ drops out, and using $\Delta V_b = v_b/N_b^*$, the SPH form of the Lagrangian reads

$$L_{\text{SPH,GR}} = - \sum_b \frac{v_b}{\Theta_b} [1 + u(n_b, s_b)]. \quad (193)$$

In the flat spacetime limit $\Theta_b \rightarrow \gamma_b$ and we recover the discretized, special-relativistic Lagrangian, Eq. (147).

4.2.3. The momentum equation

To identify a suitable numerical variable, we use like before, see Eq. (152), the canonical momentum

$$\frac{\partial L}{\partial v_a^i} = - \sum_b v_b \left(\frac{\partial}{\partial v_a^i} \frac{1}{\Theta_b} \right) [1 + u_b] - \sum_b \frac{v_b}{\Theta_b} \left(\frac{\partial}{\partial v_a^i} u_b \right). \quad (194)$$

We thus need

$$\frac{\partial}{\partial v_a^i} \left(\frac{1}{\Theta_b} \right) = \frac{\partial}{\partial v_a^i} (-g_{\mu\nu} v^\mu v^\nu)^{1/2} = -\Theta_b (g_{i\mu} v^\mu)_a \delta_{ab}, \quad (195)$$

and the derivative $\partial u_b / \partial v_a^i$, where, like in the special-relativistic case, the velocity dependence comes from the Lorentz-factor-like quantity Θ relating the densities in the local frame and the computing frame

$$\begin{aligned} \frac{\partial u_b}{\partial v_a^i} &= \frac{\partial u_b}{\partial n_b} \frac{\partial n_b}{\partial v_a^i} = \frac{P_b}{n_b^2} \frac{\partial}{\partial v_a^i} \left(\frac{N_b^*}{\sqrt{-g_b} \Theta_b} \right) = \frac{P_b}{n_b^2} \frac{N_b^*}{\sqrt{-g_b}} \frac{\partial}{\partial v_a^i} \left(\frac{1}{\Theta_b} \right) \\ &= - \frac{P_b}{n_b^2} \frac{N_b^*}{\sqrt{-g_b}} \Theta_b (g_{i\mu} v^\mu)_a \delta_{ab}. \end{aligned} \quad (196)$$

Here, we have used Eqs. (8), (187) and (195). By inserting Eqs. (195) and (196) into Eq. (194) we find

$$\begin{aligned} \frac{\partial L}{\partial v_a^i} &= - \sum_b v_b [1 + u_b] (-\Theta_b (g_{i\mu} v^\mu)_a \delta_{ab}) - \sum_b \\ &\quad \times \frac{v_b}{\Theta_b} \left(- \frac{P_b}{n_b^2} \frac{N_b^*}{\sqrt{-g_b}} \Theta_b (g_{i\mu} v^\mu)_a \delta_{ab} \right) \\ &= v_a \Theta_a \left(1 + u_a + \frac{P_a}{n_a^2} \frac{N_a^*}{\sqrt{-g_a} \Theta_a} \right) (g_{i\mu} v^\mu)_a \\ &= v_a \Theta_a \left(1 + u_a + \frac{P_a}{n_a} \right) (g_{i\mu} v^\mu)_a, \end{aligned} \quad (197)$$

where Eq. (187) has been used. This is the i -component of the canonical momentum and, like before, we use the canonical momentum per baryon,

$$S_{i,a} \equiv \frac{1}{v_a} \frac{\partial L}{\partial v_a^i} = \Theta_a \left(1 + u_a + \frac{P_a}{n_a} \right) (g_{i\mu} v^\mu)_a, \quad (198)$$

as numerical variable. Again, the term in the first bracket is the specific enthalpy. In the flat-space limit, $\Theta_a \rightarrow \gamma_a$, $g_{\mu\nu} \rightarrow \eta_{\mu\nu}$ and $g_{i\mu} v^\mu \rightarrow v_i = v^i$, this expression reduces exactly to the special-relativistic case, Eq. (174), as it should.

The evolution of $S_{i,a}$ is determined by the Euler–Lagrange equations, so we need

$$\frac{\partial L}{\partial x_a^i} = - \sum_b v_b \left(\frac{\partial}{\partial x_a^i} \frac{1}{\Theta_b} \right) [1 + u_b] - \sum_b \frac{v_b}{\Theta_b} \left(\frac{\partial u_b}{\partial x_a^i} \right). \quad (199)$$

The first derivative can be written as

$$\left(\frac{\partial}{\partial x_a^i} \frac{1}{\Theta_b} \right) = \frac{\partial}{\partial x_a^i} (-g_{\mu\nu} v^\mu v^\nu)^{1/2} = - \frac{\Theta_b}{2} \left(\frac{\partial g_{\mu\nu}}{\partial x_a^i} \right)_b v_b^\mu v_b^\nu \delta_{ab}, \quad (200)$$

and due to Eq. (184)

$$v^\mu v^\nu = \frac{U^\mu U^\nu}{\Theta^2}, \quad (201)$$

so it becomes

$$\left(\frac{\partial}{\partial x_a^i} \frac{1}{\Theta_b} \right) = - \left(\frac{U^\mu U^\nu}{2\Theta} \right)_b \left(\frac{\partial g_{\mu\nu}}{\partial x_a^i} \right)_b \delta_{ab}. \quad (202)$$

The derivative of the internal energy is

$$\begin{aligned} \frac{\partial u_b}{\partial x_a^i} &= \frac{\partial u_b}{\partial n_b} \frac{\partial n_b}{\partial x_a^i} = \frac{P_b}{n_b^2} \frac{\partial}{\partial x_a^i} \left(\frac{N_b^*}{\sqrt{-g_b} \Theta_b} \right) = \frac{P_b}{n_b^2 \sqrt{-g_b} \Theta_b} \left(\frac{\partial N_b^*}{\partial x_a^i} \right) \\ &\quad + \frac{P_b N_b^*}{n_b^2 \sqrt{-g_b}} \left(\frac{\partial}{\partial x_a^i} \frac{1}{\Theta_b} \right) + \frac{P_b N_b^*}{n_b^2 \Theta_b} \left(\frac{\partial}{\partial x_a^i} \frac{1}{\sqrt{-g_b}} \right), \end{aligned} \quad (203)$$

where we have used the first law of thermodynamics, Eq. (8). By using Eq. (25), the derivative of the number density becomes

$$\frac{\partial N_b^*}{\partial x_a^i} = \frac{\partial}{\partial x_a^i} \left(\sum_k v_k W_{bk} \right) = \sum_k v_k \frac{\partial W_{bk}}{\partial x_a^i} (\delta_{ba} - \delta_{ka}). \quad (204)$$

The last remaining derivative is

$$\left(\frac{\partial}{\partial x_a^i} \frac{1}{\sqrt{-g_b}} \right) = - \left(\frac{g^{\alpha\beta}}{2\sqrt{-g}} \frac{\partial g_{\alpha\beta}}{\partial x_a^i} \right)_b \delta_{ab}, \quad (205)$$

see the box on the derivatives of the metric tensor determinant.

Derivatives of the metric tensor determinant g

We will collect here some formulae related to the quantity g that are needed in several places. The derivative of the metric tensor determinant is generally given by (see e.g. Schutz, 1989)

$$\frac{\partial g}{\partial x^\mu} = g g^{\alpha\beta} \frac{\partial g_{\alpha\beta}}{\partial x^\mu}. \quad (206)$$

Therefore

$$\frac{\partial \sqrt{-g}}{\partial x^i} = \frac{\sqrt{-g}}{2} g^{\alpha\beta} \frac{\partial g_{\alpha\beta}}{\partial x^i}, \quad \frac{\partial}{\partial x^i} \left(\frac{1}{\sqrt{-g}} \right) = - \frac{g^{\alpha\beta}}{2\sqrt{-g}} \frac{\partial g_{\alpha\beta}}{\partial x^i} \quad (207)$$

and

$$\begin{aligned} \frac{d}{dt} (\sqrt{-g}) &= \frac{\partial}{\partial x^\mu} (\sqrt{-g}) \frac{dx^\mu}{dt} = \frac{\sqrt{-g}}{2} g^{\alpha\beta} \frac{\partial g_{\alpha\beta}}{\partial x^\mu} v^\mu \\ &= \frac{\sqrt{-g}}{2} g^{\alpha\beta} \frac{dg_{\alpha\beta}}{dt}. \end{aligned} \quad (208)$$

Of course, if the metric tensor at the position of particle b is to be differentiated with respect to a property of particle a , the appropriate Kronecker deltas, δ_{ab} , have to be applied.

With the help of Eqs. (202), (203), (204) and (207) Eq. (199) becomes

$$\begin{aligned} \frac{\partial L}{\partial x_a^i} &= + \sum_b v_b [1 + u_b] \left(\frac{U^\mu U^\nu}{2\Theta} \right)_b \left(\frac{\partial g_{\mu\nu}}{\partial x_a^i} \right)_b \delta_{ab} \\ &\quad - \sum_b \frac{v_b}{\Theta_b} \left\{ \frac{P_b}{n_b^2 \sqrt{-g_b} \Theta_b} \sum_k v_k \frac{\partial W_{bk}}{\partial x_a^i} (\delta_{ba} - \delta_{ka}) \right. \\ &\quad \left. + \frac{P_b N_b^*}{n_b^2 \sqrt{-g_b}} \left[- \left(\frac{U^\mu U^\nu}{2\Theta} \right)_b \left(\frac{\partial g_{\mu\nu}}{\partial x_a^i} \right)_b \delta_{ab} \right] \right. \\ &\quad \left. + \frac{P_b N_b^*}{n_b^2 \Theta_b} \left[- \left(\frac{g^{\mu\nu}}{2\sqrt{-g}} \frac{\partial g_{\mu\nu}}{\partial x_a^i} \right)_b \delta_{ab} \right] \right\}. \end{aligned} \quad (209)$$

The terms that involve the derivatives of the kernel represent the hydrodynamic part of the equations, the others the action of gravity. After eliminating one sum in the hydrodynamic terms via the Kronecker symbol, relabeling the summation index from k to b and using kernel property Eq. (26) they read

$$\left(\frac{\partial L}{\partial \mathbf{x}_a^i}\right)_h = -v_a \sum_b v_b \left(\frac{P_a}{n_a^2 \sqrt{-g_a} \Theta_a^2} + \frac{P_b}{n_b^2 \sqrt{-g_b} \Theta_b^2} \right) \frac{\partial W_{ab}}{\partial \mathbf{x}_a^i}. \quad (210)$$

and on using Eq. (187)

$$\left(\frac{\partial L}{\partial \mathbf{x}_a^i}\right)_h = -v_a \sum_b v_b \left(\frac{\sqrt{-g_a} P_a}{N_a^{*2}} + \frac{\sqrt{-g_b} P_b}{N_b^{*2}} \right) \frac{\partial W_{ab}}{\partial \mathbf{x}_a^i}. \quad (211)$$

The terms that involve derivatives of the metric (“gravity terms”) can be written as

$$\left(\frac{\partial L}{\partial \mathbf{x}_a^i}\right)_g = \frac{v_a}{2\Theta_a} \left[\left(1 + u_a + \frac{P_a}{n_a^2} \frac{N_a^*}{\sqrt{-g_a} \Theta_a}\right) U^\mu U^\nu + \frac{P_a}{n_a^2} \frac{N_a^*}{\sqrt{-g_a} \Theta_a} g^{\mu\nu} \right] \left(\frac{\partial g_{\mu\nu}}{\partial \mathbf{x}_a^i}\right)_a. \quad (212)$$

If we apply once more Eq. (187) and remember the form of the energy-momentum tensor of the fluid, Eq. (181), the above term simply becomes

$$\left(\frac{\partial L}{\partial \mathbf{x}_a^i}\right)_g = \frac{v_a \sqrt{-g_a}}{2N_a^*} \left(T^{\mu\nu} \frac{\partial g_{\mu\nu}}{\partial \mathbf{x}_a^i} \right)_a. \quad (213)$$

Putting all together, the spatial derivative of the Lagrangian reads

$$\frac{\partial L}{\partial \mathbf{x}_a^i} = v_a \left\{ -\sum_b v_b \left(\frac{\sqrt{-g_a} P_a}{N_a^{*2}} + \frac{\sqrt{-g_b} P_b}{N_b^{*2}} \right) \frac{\partial W_{ab}}{\partial \mathbf{x}_a^i} + \frac{\sqrt{-g_a}}{2N_a^*} \left(T^{\mu\nu} \frac{\partial g_{\mu\nu}}{\partial \mathbf{x}_a^i} \right)_a \right\}. \quad (214)$$

Note that the first, hydrodynamical term has the symmetry in the particle indices, a and b , that we know from previous forms of SPH equations, while the gravity term is exclusively evaluated at the position of the particle under consideration, a .

Inserting Eqs. (197), (198) and (214) into the Euler–Lagrange equations yields the final, general-relativistic momentum equation

$$\frac{dS_{i,a}}{dt} = -\sum_b v_b \left(\frac{\sqrt{-g_a} P_a}{N_a^{*2}} + \frac{\sqrt{-g_b} P_b}{N_b^{*2}} \right) \frac{\partial W_{ab}}{\partial \mathbf{x}_a^i} + \frac{\sqrt{-g_a}}{2N_a^*} \left(T^{\mu\nu} \frac{\partial g_{\mu\nu}}{\partial \mathbf{x}_a^i} \right)_a. \quad (215)$$

4.2.4. The energy equation

We use once more guidance from the canonical energy to choose the numerical energy variable:

$$\begin{aligned} E &\equiv \sum_a \frac{\partial L}{\partial \vec{v}_a} \cdot \vec{v}_a - L = \sum_a v_a S_{i,a} v_a^i + \frac{v_a}{\Theta_a} [1 + u_a] \\ &= \sum_a v_a \left[\Theta_a \left(1 + u_a + \frac{P_a}{n_a} \right) (g_{i\mu} v^\mu v^i)_a + \frac{1 + u_a}{\Theta_a} \right] = \sum_a v_a \hat{e}_a. \end{aligned} \quad (216)$$

Here we have introduced the energy per baryon

$$\hat{e}_a \equiv \Theta_a \left(1 + u_a + \frac{P_a}{n_a} \right) (g_{i\mu} v^\mu v^i)_a + \frac{1 + u_a}{\Theta_a} = S_{i,a} v_a^i + \frac{1 + u_a}{\Theta_a}, \quad (217)$$

very similar to the special-relativistic energy variable, Eq. (161). Its temporal change is given by

$$\frac{d\hat{e}_a}{dt} = \frac{dS_{i,a}}{dt} v_a^i + S_{i,a} \frac{dv_a^i}{dt} + \frac{d}{dt} \left(\frac{1 + u_a}{\Theta_a} \right). \quad (218)$$

The first time derivative is known from the momentum equation, the second can be hoped to cancel out with a term resulting from the last term, as in the special-relativistic case, see Eq. (164). For this last term we need du_a/dt and $d\Theta_a/dt$. To obtain the time derivative of u_a we use the first law of thermodynamics, Eq. (8), the num-

ber density relation between the frames, Eq. (187), and $d(\sqrt{-g})/dt$, Eq. (208). This delivers

$$\frac{du_a}{dt} = \frac{P_a}{n_a^2} \frac{d}{dt} \left(\frac{N^*}{\sqrt{-g} \Theta} \right)_a = \frac{P_a \sqrt{-g_a} \Theta_a}{N_a^{*2}} \frac{dN_a^*}{dt} + \frac{P_a N_a^*}{n_a^2} \frac{d}{dt} \left(\frac{1}{\sqrt{-g} \Theta} \right)_a. \quad (219)$$

The last derivative is given by

$$\frac{d}{dt} \left(\frac{1}{\sqrt{-g} \Theta} \right)_a = - \left(\frac{1}{2\sqrt{-g} \Theta} g^{\alpha\beta} \frac{dg_{\alpha\beta}}{dt} \right)_a - \left(\frac{1}{\sqrt{-g} \Theta^2} \frac{d\Theta}{dt} \right)_a, \quad (220)$$

thus the change in u_a becomes

$$\frac{du_a}{dt} = \frac{P_a \sqrt{-g_a} \Theta_a}{N_a^{*2}} \frac{dN_a^*}{dt} - \frac{P_a}{2n_a} g^{\alpha\beta} \frac{dg_{\alpha\beta}}{dt} - \frac{P_a}{n_a \Theta_a} \frac{d\Theta_a}{dt}. \quad (221)$$

It remains to calculate the derivative of the generalized Lorentz-factor

$$\frac{d\Theta_a}{dt} = \frac{d}{dt} \left(-g_{\alpha\beta} v^\alpha v^\beta \right)_a^{-1/2} = \left(\frac{\Theta^3}{2} v^\alpha v^\beta \frac{dg_{\alpha\beta}}{dt} + \Theta^3 g_{\alpha\beta} \frac{dv^\alpha}{dt} v^\beta \right)_a. \quad (222)$$

On using Eqs. (221) and (222) we find

$$\begin{aligned} \frac{d}{dt} \left(\frac{1 + u_a}{\Theta_a} \right) &= \frac{1}{\Theta_a} \left\{ \frac{P_a \sqrt{-g_a} \Theta_a}{N_a^{*2}} \frac{dN_a^*}{dt} - \frac{P_a}{2n_a} g^{\alpha\beta} \frac{dg_{\alpha\beta}}{dt} - \frac{P_a}{n_a \Theta_a} \frac{d\Theta_a}{dt} \right\} \\ &\quad - \frac{1 + u_a}{\Theta_a^2} \frac{d\Theta_a}{dt} = \frac{P_a \sqrt{-g_a}}{N_a^{*2}} \frac{dN_a^*}{dt} - \Theta_a \left(1 + u_a + \frac{P_a}{n_a} \right) \left(g_{\alpha\beta} v^\alpha \frac{dv^\beta}{dt} \right)_a \\ &\quad - \left(\frac{P_a}{2n_a \Theta_a} g_a^{\alpha\beta} + \frac{\Theta_a}{2} \left[1 + u_a + \frac{P_a}{n_a} \right] v^\alpha v^\beta \right) \left(\frac{dg_{\alpha\beta}}{dt} \right)_a. \end{aligned} \quad (223)$$

If we replace the velocities via Eq. (184) by four-velocities and use the definition of the energy momentum tensor, Eq. (181), the equation simplifies to

$$\begin{aligned} \frac{d}{dt} \left(\frac{1 + u_a}{\Theta_a} \right) &= \frac{P_a \sqrt{-g_a}}{N_a^{*2}} \frac{dN_a^*}{dt} - \Theta_a \left(1 + u_a + \frac{P_a}{n_a} \right) \left(g_{\alpha\beta} v^\alpha \frac{dv^\beta}{dt} \right)_a \\ &\quad - \left(\frac{\sqrt{-g} T^{\alpha\beta}}{2N^*} \frac{dg_{\alpha\beta}}{dt} \right)_a = \frac{P_a \sqrt{-g_a}}{N_a^{*2}} \frac{dN_a^*}{dt} - (S_i)_a \frac{dv_a^i}{dt} \\ &\quad - \left(\frac{\sqrt{-g} T^{\alpha\beta}}{2N^*} \frac{dg_{\alpha\beta}}{dt} \right)_a. \end{aligned} \quad (224)$$

Here we have split the contraction in the term containing dv^β/dt into a spatial and a temporal part and we made use of $v^0 = 1$, see Eq. (184). This equation is very similar the special-relativistic one, Eq. (164), but it also contains a gravity contribution. If we insert Eq. (224) into the energy evolution Eq. (218), use the SPH prescription for dN^*/dt and collect terms into “hydro” (kernels) and “gravity” (metric derivatives) we find

$$\begin{aligned} \frac{d\hat{e}_a}{dt} &= -\sum_b v_b \left(\frac{\sqrt{-g_a} P_a \vec{v}_b}{N_a^{*2}} + \frac{\sqrt{-g_b} P_b \vec{v}_a}{N_b^{*2}} \right) \cdot \nabla_a W_{ab} \\ &\quad + \frac{\sqrt{-g_a}}{2N_a^*} T_a^{\alpha\beta} \left(\frac{\partial g_{\alpha\beta}}{\partial \mathbf{x}^i} v^i - \frac{dg_{\alpha\beta}}{dt} \right)_a \\ &= -\sum_b v_b \left(\frac{\sqrt{-g_a} P_a \vec{v}_b}{N_a^{*2}} + \frac{\sqrt{-g_b} P_b \vec{v}_a}{N_b^{*2}} \right) \cdot \nabla_a W_{ab} \\ &\quad - \frac{\sqrt{-g_a}}{2N_a^*} \left(T^{\alpha\beta} \frac{\partial g_{\alpha\beta}}{\partial t} \right)_a. \end{aligned} \quad (225)$$

This is the final, general-relativistic SPH energy equation. The Eqs. (191), (215) and (225) together with an equation of state form the set of general-relativistic SPH equations in a fixed background metric.

Summary of the general-relativistic SPH equations on a fixed background metric

Ignoring derivatives from the smoothing lengths, the momentum equation reads

$$\frac{dS_{i,a}}{dt} = - \sum_b v_b \left(\frac{\sqrt{-g_a} P_a}{N_a^{s_2}} + \frac{\sqrt{-g_b} P_b}{N_b^{s_2}} \right) \frac{\partial W_{ab}}{\partial x_a^i} + \frac{\sqrt{-g_a}}{2N_a} \left(T^{\mu\nu} \frac{\partial g_{\mu\nu}}{\partial x^i} \right)_a, \quad (226)$$

where

$$S_{i,a} = \Theta_a \left(1 + u_a + \frac{P_a}{n_a} \right) (g_{i\mu} v^\mu)_a, \quad (227)$$

is the canonical momentum per baryon and

$$\Theta_a = \left(-g_{\mu\nu} v^\mu v^\nu \right)_a^{-\frac{1}{2}}, \quad (228)$$

the generalized Lorentz factor. The energy equation reads

$$\frac{d\hat{e}_a}{dt} = - \sum_b v_b \left(\frac{\sqrt{-g_a} P_a}{N_a^{s_2}} \vec{v}_b + \frac{\sqrt{-g_b} P_b}{N_b^{s_2}} \vec{v}_a \right) \cdot \nabla_a W_{ab} - \frac{\sqrt{-g_a}}{2N_a} \left(T^{\mu\nu} \frac{\partial g_{\mu\nu}}{\partial t} \right)_a, \quad (229)$$

where

$$\hat{e}_a = S_{i,a} v_a^i + \frac{1 + u_a}{\Theta_a}, \quad (230)$$

is the canonical energy per nucleon. The number density can again be calculated via summation,

$$N_a^s = \sum_b v_b W_{ab}(h_a). \quad (231)$$

5. Summary

Since the Smooth Particle Hydrodynamics method was suggested in the late seventies it has undergone a long sequence of technical improvements. In parallel, the method has been applied to a large variety of problems both inside and outside astrophysics, and consequently a slew of different physical processes has been included in SPH-based simulations.

In this review we have only very briefly touched upon this latter development, we merely provided pointers to the current literature. Instead we have focused on what we hope is a pedagogical introduction leading to an in-depth understanding of how the method works. All essential equations were derived, and in particular, a commonly used (“vanilla ice”) set of SPH equations that directly discretizes the Lagrangian equations of an ideal fluid. We have also reviewed concepts such as adaptive numerical resolution, the reasoning behind artificial viscosity and basic aspects of the ODE integration in the SPH context.

The “vanilla ice” equation set works well in practice and possesses the property of “hard-wired” conservation of mass, energy, linear and angular momentum. The symmetrization in the particle indices is, however, somewhat arbitrary and was enforced ad hoc. In Section 3, a modern form of the SPH equations was derived that improves on this weakness: it uses nothing more than the Lagrangian of an ideal fluid, the first law of thermodynamics and a prescription how to obtain the density by a summation over particles. After the Lagrangian has been written in its SPH-discrete

form, there is no more arbitrariness left in the rest of the derivation: the equations follow stringently from the Euler–Lagrange equations. In addition to curing the aesthetical shortcoming of the previous approach, the latter also naturally leads to corrective terms due to the derivatives of the smoothing lengths, in SPH usually called “grad-h-terms”.

The elegant variational concept naturally carries over to both the special- and general-relativistic (fixed-metric) case. Here, we derived for the first time the special-relativistic SPH equations that include “grad-h-terms”. The numerical variables are chosen as canonical momentum and energy per baryon. While this has obvious numerical advantages, it comes at the price of recovering the physical variables from the numerical ones at each time step, a tribute that is also paid in modern grid-based relativistic approaches, see e.g. (Marti and Müller, 2003). The performance of this new equation set has been briefly illustrated at the example of a relativistic shock tube test, for a more exhaustive set of tests we refer to Rosswog (2009).

We concluded this review with a derivation of the general-relativistic case in which the space-time metric can be considered unperturbed by the self-gravity of the fluid, a case that is realized, for example, in the tidal disruption of a star by a supermassive black hole. The resulting equations are a natural generalization of the special-relativistic case and do not introduce much of an additional numerical burden. The resulting extra terms can be analytically calculated from the metric that is assumed to be known.

In the future, more physical processes and their corresponding numerical schemes will certainly find their ways into SPH. On the numerical hydrodynamics side the recent past has seen a couple suggestions on how to improve on known weaknesses of SPH. One of them was SPH’s unsatisfactory performance on fluid instabilities across discontinuities with large density jumps (Agertz et al., 2007). A modification of artificial dissipation terms (Price, 2008) or, alternatively, a more general formulation of the SPH equations (Read et al., 2009) have been suggested as cures for this problem. In terms of artificial dissipation, a tensor artificial viscosity approach such as the one suggested in Owen (2004) should definitely be explored further for its potential and usability in astrophysics. While the special-relativistic SPH equations as derived in Section 4 have been carefully tested, the general-relativistic equation set has so far not been implemented and applied to astrophysical problems. This task is left for future investigations.

Acknowledgments

It is a great pleasure to thank Marcus Brüggen, Marius Dan, James Guillochon and Roland Speith for their careful reading of the manuscript. This work has been supported by DFG under Grant RO 3399/5-1.

References

- Agertz, O., Moore, B., Stadel, J., Potter, D., Miniati, F., Read, J., Mayer, L., Gawryszczak, A., Kravtsov, A., Nordlund, Å., Pearce, F., Quilis, V., Rudd, D., Springel, V., Stone, J., Tasker, E., Teyssier, R., Wadsley, J., Walder, R., 2007. Fundamental differences between SPH and grid methods. *MNRAS* 380, 963–978.
- Altay, G., Croft, R.A.C., Pelupessy, I., 2008. SPHAY: a smoothed particle hydrodynamics ray tracer for radiative transfer. *MNRAS* 386, 1931–1946.
- Alvarez, M.A., Bromm, V., Shapiro, P.R., 2006. The H II region of the first star. *ApJ* 639, 621–632.
- Ascasibar, Y., Yepes, G., Gottlöber, S., Müller, V., 2002. Numerical simulations of the cosmic star formation history. *A&A* 387, 396–405.
- Asphaug, E., Benz, W., 1996. Size, density, and structure of comet Shoemaker-Levy 9 inferred from the physics of tidal breakup. *Icarus* 121, 225–248.
- Ayal, S., Piran, T., Oechslin, R., Davies, M.B., Rosswog, S., 2001. Post-Newtonian smoothed particle hydrodynamics. *ApJ* 550, 846–859.
- Balsara, D.S., 1991. Asymmetries in extragalactic radio sources, Ph.D. Thesis, AA (Illinois Univ., Urbana-Champaign).
- Barnes, J., Hut, P., 1986. A hierarchical O(NlogN) force-calculation algorithm. *Nature* 324, 446–449.

- Bate, M.R., Bonnell, I.A., Price, N.M., 1995. Modelling accretion in protobinary systems. *MNRAS* 277, 362–376.
- Bate, M.R., Bonnell, I.A., Bromm, V., 2003. The formation of a star cluster: predicting the properties of stars and brown dwarfs. *MNRAS* 339, 577–599.
- Benz, W., 1990. Smooth particle hydrodynamics: a review. In: Buchler, J. (Ed.), *Numerical Modeling of Stellar Pulsations*. Kluwer Academic Publishers, Dordrecht, p. 269.
- Benz, W., Asphaug, E., 1994. Impact simulations with fracture. I – Method and tests. *Icarus* 107, 98.
- Benz, W., Asphaug, E., 1995. Simulations of brittle solids using smooth particle hydrodynamics. *Computer Physics Communications* 87, 253–265.
- Benz, W., Thielemann, F.-K., Hills, J.G., 1989. Three-dimensional hydrodynamical simulations of stellar collisions. II – White dwarfs. *ApJ* 342, 986–998.
- Benz, W., Bowers, R., Cameron, A., Press, W., 1990. Dynamic mass exchange in doubly degenerate binaries. I. – 0.9 and 1.2 solar mass stars. *ApJ* 348, 647.
- Berczik, P., 1999. Chemo-dynamical smoothed particle hydrodynamic code for evolution of star forming disk galaxies. *A&A* 348, 371–380.
- Bethe, H.A., Wilson, J.R., 1985. Revival of a stalled supernova shock by neutrino heating. *ApJ* 295, 14–23.
- Bode, P., Ostriker, J.P., 2003. Tree particle-mesh: an adaptive, efficient, and parallel code for collisionless cosmological simulation. *ApJS* 145, 1–13.
- Bode, P., Ostriker, J.P., Xu, G., 2000. The tree particle-mesh N-body gravity solver. *ApJS* 128, 561–569.
- Bonnell, I.A., Bate, M.R., Vine, S.G., 2003. The hierarchical formation of a stellar cluster. *MNRAS* 343, 413–418.
- Børve, S., Omang, M., Trulsen, J., 2001. Regularized smoothed particle hydrodynamics: a new approach to simulating magnetohydrodynamic shocks. *ApJ* 561, 82–93.
- Børve, S., Omang, M., Trulsen, J., 2004. Two-dimensional MHD smoothed particle hydrodynamics stability analysis. *ApJS* 153, 447–462.
- Børve, S., Omang, M., Trulsen, J., 2005. Regularized smoothed particle hydrodynamics with improved multi-resolution handling. *Journal of Computational Physics* 208, 345–367.
- Børve, S., Omang, M., Trulsen, J., 2006. Multidimensional MHD shock tests of regularized smoothed particle hydrodynamics. *ApJ* 652, 1306–1317.
- Brookshaw, L., 1985. A method of calculating radiative heat diffusion in particle simulations. *Proceedings of the Astronomical Society of Australia* 6, 207–210.
- Burden, R.L., Faires, J.D., 2001. *Numerical analysis*, 7th ed. Pacific Grove, CA: Brooks/Cole, 2001. ISBN 0534382169.
- Cabezón, R.M., García-Senz, D., Relano, A., 2008. A one-parameter family of interpolating kernels for smoothed particle hydrodynamics studies. *Journal of Computational Physics* 227, 8523–8540.
- Caramana, S.M., Whalen, E.P., 1998. Formulations of artificial viscosity for multi-dimensional shock wave computations. *Journal of Computational Physics* 144, 70–97.
- Carraro, G., Ng, Y.K., Portinari, L., 1998. On the galactic disc age-metallicity relation. *MNRAS* 296, 1045–1056.
- Carraro, G., Lia, C., Chiosi, C., 1998. Galaxy formation and evolution – I. The Padua tree-sph code (pd-sph). *MNRAS* 297, 1021–1040.
- Cattaneo, A., Blaizot, J., Weinberg, D.H., Kere, S. D., Colombi, S., Davé, R., Devriendt, J., Guiderdoni, B., Katz, N., 2007. Accretion, feedback and galaxy bimodality: a comparison of the GALCS semi-analytic model and cosmological SPH simulations. *MNRAS* 377, 63–76.
- Cha, S.-H., Whitworth, A.P., 2003. Implementations and tests of Godunov-type particle hydrodynamics. *MNRAS* 340, 73–90.
- Chow, J.E., Monaghan, J., 1997. Ultrarelativistic sph. *Journal of Computational Physics* 134, 296.
- Clark, P.C., Bonnell, I.A., 2004. Star formation in transient molecular clouds. *MNRAS* 347, L36–L40.
- Cleary, P.W., Monaghan, J.J., 1999. Conduction modelling using smoothed particle hydrodynamics. *Journal of Computational Physics* 148, 227–264.
- Cox, T.J., Primack, J., Jonsson, P., Somerville, R.S., 2004. Generating hot gas in simulations of disk-galaxy major mergers. *ApJL* 607, L87–L90.
- Croft, R.A.C., Altay, G., 2008. Radiation-induced large-scale structure during the reionization epoch: the autocorrelation function. *MNRAS* 388, 1501–1520.
- Dale, J.E., Bonnell, I.A., Clarke, C.J., Bate, M.R., 2005. Photoionizing feedback in star cluster formation. *MNRAS* 358, 291–304.
- Dale, J.E., Ercolano, B., Clarke, C.J., 2007. A new algorithm for modelling photoionizing radiation in smoothed particle hydrodynamics. *MNRAS* 382, 1759–1767.
- Dan, M., Rosswog, S., Brügggen, M., 2009. Mass transfer dynamics in double degenerate binary systems. *Journal of Physics Conference Series* 172 (1), 012034.
- Dave, R., Dubinski, J., Hernquist, L., 1997. Parallel TreeSPH. *New Astronomy* 2, 277–297.
- Dehnen, W., 2000. A very fast and momentum-conserving tree code. *ApJL* 536, L39–L42.
- Dehnen, W., 2002. A hierarchical O(N) force calculation algorithm. *Journal of Computational Physics* 179, 27–42.
- Del Zanna, L., Bucciantini, N., 2002. An efficient shock-capturing central-type scheme for multidimensional relativistic flows. I. Hydrodynamics. *A&A* 390, 1177–1186.
- Di Matteo, T., Springel, V., Hernquist, L., 2005. Energy input from quasars regulates the growth and activity of black holes and their host galaxies. *Nature* 433, 604–607.
- Dolag, K., Stasyszyn, F.A., 2009. An MHD gadget for cosmological simulations. *MNRAS*. doi:10.1111/j.1365-2966.2009.15181.x.
- Dolag, K., Bartelmann, M., Lesch, H., 2002. Evolution and structure of magnetic fields in simulated galaxy clusters. *A&A* 387, 383–395.
- Dolag, K., Vazza, F., Brunetti, G., Tormen, G., 2005. Turbulent gas motions in galaxy cluster simulations: the role of smoothed particle hydrodynamics viscosity. *MNRAS* 364, 753–772.
- Dubinski, J., Kim, J., Park, C., Humble, R., 2004. GOTPM: a parallel hybrid particle-mesh treecode. *New Astronomy* 9, 111–126.
- Eckart, C., 1960. Variation principles of hydrodynamics. *Physics of Fluids* 3, 421.
- Enßlin, T.A., Pfrommer, C., Springel, V., Jubelgas, M., 2007. Cosmic ray physics in calculations of cosmological structure formation. *A&A* 473, 41–57.
- Español, P., Revenga, M., 2003. Smoothed dissipative particle dynamics. *Physics Review E* 67 (2), 026705.
- Ewell, M.W.J., 1988. Dissipative N-body simulations of the formation of single galaxies in a cold dark matter cosmology. Ph.D. Thesis, AA (Princeton Univ., NJ).
- Faber, J.A., Rasio, F.A., 2000. Post-Newtonian SPH calculations of binary neutron star coalescence: method and first results. *Physics Review D* 62 (6), 064012.
- Faber, J.A., Rasio, F.A., 2002. Post-Newtonian SPH calculations of binary neutron star coalescence. III. Irrotational systems and gravitational wave spectra. *Physics Review D* 65 (8), 084042.
- Faber, J.A., Rasio, F.A., Manor, J.B., 2001. Post-Newtonian smoothed particle hydrodynamics calculations of binary neutron star coalescence. II. Binary mass ratio, equation of state, and spin dependence. *Physics Review D* 63 (4), 044012.
- Faber, J.A., Grandclément, P., Rasio, F.A., 2004. Mergers of irrotational neutron star binaries in conformally flat gravity. *Physics Review D* 69 (12), 124036.
- Faber, J.A., Baumgarte, T.W., Shapiro, S.L., Taniguchi, K., Rasio, F.A., 2006. Dynamical evolution of black hole-neutron star binaries in general relativity: simulations of tidal disruption. *Physics Review D* 73 (2), 024012.
- Fabian, A.C., Sanders, J.S., Crawford, C.S., Conselice, C.J., Gallagher, J.S., Wyse, R.F.G., 2003. The relationship between the optical Hz filaments and the X-ray emission in the core of the Perseus cluster. *MNRAS* 344, L48–L52.
- Fehlberg, E., 1966. New one-step integration methods of high order accuracy applied to some problems in celestial mechanics. Tech. Rep., NASA technical report TR R-248.
- Fehlberg, E., 1969. Low-order classical Runge–Kutta formulas with step size control and their application to some heat transfer problems. Tech. Rep., NASA Technical Report TR R-315.
- Fehlberg, E., 1964. New high-order Runge–Kutta formulas with step size control for systems of first- and second-order differential equations. *Zeitschrift Fur Angewandte Mathematik Und Mechanik* 44, T17–T29.
- Flebbe, O., Muenzel, S., Herold, H., Riffert, H., Ruder, H., 1994. Smoothed particle hydrodynamics: physical viscosity and the simulation of accretion disks. *ApJ* 431, 754–760.
- Fock, V., 1964. *Theory of Space, Time and Gravitation*. Pergamon, Oxford.
- Forgan, D., Rice, K., Stamatellos, A., 2009. Whitworth, introducing a hybrid radiative transfer method for smoothed particle hydrodynamics. *MNRAS* 392, 1381–1387.
- Frank, J., King, A., Raine, D.J., 2002. *Accretion Power in Astrophysics*, third ed. Cambridge University Press, Cambridge, UK, p. 398. ISBN 0521620538.
- Fryer, C., Benz, W., Herant, M., Colgate, S.A., 1999. What can the accretion-induced collapse of white dwarfs really explain? *ApJ* 516, 892–899.
- Fryer, C.L., Rockefeller, G., Warren, M.S., 2006. SNSPH: a parallel three-dimensional smoothed particle radiation hydrodynamics code. *ApJ* 643, 292–305.
- Fulbright, M.S., Benz, W., Davies, M.B., 1995. A method of smoothed particle hydrodynamics using spheroidal kernels. *ApJ* 440, 254–262.
- Fulk, D., Quinn, D., 1996. An analysis of 1D smoothed particle hydrodynamics kernels. *Journal of Computational Physics* 126, 165–180.
- Gerritsen, J.P.E., Icke, V., 1997. Star formation in N-body simulations. I. The impact of the stellar ultraviolet radiation on star formation. *A&A* 325, 972–986.
- Gingold, R.A., Monaghan, J.J., 1977. Smoothed particle hydrodynamics – theory and application to non-spherical stars. *MNRAS* 181, 375–389.
- Gingold, R.A., Monaghan, J.J., 1978. Binary fission in damped rotating polytropes. *MNRAS* 184, 481–499.
- Gingold, R.A., Monaghan, J.J., 1982. Kernel estimates as a basis for general particle methods in hydrodynamics. *Journal of Computational Physics* 46, 429–453.
- Goldstein, H., Poole, C., Safko, J. (Eds.), 2002. *Classical Mechanics*, third ed. Addison-Wesley, San Francisco.
- Greengard, L., Rokhlin, V., 1987. A fast algorithm for particle simulations. *Journal of Computational Physics* 73, 325–348.
- Greif, T.H., Glover, S.C.O., Bromm, V., Klessen, R.S., 2009. Chemical mixing in smoothed particle hydrodynamics simulations. *MNRAS* 392, 1381–1387.
- Griebel, M., Knapek, S., Zumbusch, G., 2007. *Numerical Simulation in Molecular Dynamics*, first ed. Springer, Berlin.
- Gritschneider, M., Naab, T., Burkert, A., Walch, S., Heitsch, F., Wetzstein, M., 2009. iVINE - Ionization in the parallel TREE/SPH code VINE: first results on the observed age-spread Around O-stars. *MNRAS* 393, 21–31.
- Guerrero, J., García-Berro, E., Isern, J., 2004. Smoothed particle hydrodynamics simulations of merging white dwarfs. *A&A* 413, 257–272.
- Hairer, E., Lubich, C., Wanner, G., 2006. *Geometric Numerical Integration*, second ed. Springer, Berlin.
- Herant, M., Benz, W., Hix, W.R., Fryer, C.L., Colgate, S.A., 1994. Inside the supernova: a powerful convective engine. *ApJ* 435, 339–361.
- Hernquist, L., Katz, N., 1989. Treeshp – a unification of sph with the hierarchical tree method. *ApJS* 70, 419.

- Hicks, D.A., Swegle, J.W., Attaway, S.W., 1997. Conservative smoothing stabilizes discrete-numerical instabilities in SPH material dynamics computations. *Applied Mathematics and Computation* 85, 209–226.
- Hix, W.R., Khokhlov, A.M., Wheeler, J.C., Thielemann, F.-K., 1998. The quasi-equilibrium-reduced alpha-network. *ApJ* 503, 332.
- Hockney, R.W., Eastwood, J.W., 1988. *Computer Simulation Using Particles*, first ed. McGraw-Hill, New York.
- Hoefl, M., Yepes, G., Gottlöber, S., Springel, V., 2006. Dwarf galaxies in voids: suppressing star formation with photoheating. *MNRAS* 371, 401–414.
- Inutsuka, S.-I., 2002. Reformulation of smoothed particle hydrodynamics with riemann solver. *Journal of Computational Physics* 179, 238–267.
- Isenberg, J., unpublished. Waveless approximation theories of gravity.
- Johnson, J.L., Greif, T.H., Bromm, V., 2007. Local radiative feedback in the formation of the first protogalaxies. *ApJ* 665, 85–95.
- Jubelgas, M., Springel, V., Dolag, K., 2004. Thermal conduction in cosmological SPH simulations. *MNRAS* 351, 423–435.
- Jubelgas, M., Springel, V., Enßlin, T., Pfrommer, C., 2008. Cosmic ray feedback in hydrodynamical simulations of galaxy formation. *A&A* 481, 33–63.
- Jutzi, M., Benz, W., Michel, P., 2008. Numerical simulations of impacts involving porous bodies. I. Implementing sub-resolution porosity in a 3D SPH hydrocode. *Icarus* 198, 242–255.
- Katz, N., Weinberg, D.H., Hernquist, L., 1996. Cosmological simulations with TreeSPH. *ApJS* 105, 19.
- Kawata, D., Gibson, B.K., 2003. GCD+: a new chemodynamical approach to modelling supernovae and chemical enrichment in elliptical galaxies. *MNRAS* 340, 908–922.
- Kay, S.T., 2004. The entropy distribution in clusters: evidence of feedback? *MNRAS* 347, L13–L17.
- Kay, S.T., Pearce, F.R., Frenk, C.S., Jenkins, A., 2002. Including star formation and supernova feedback within cosmological simulations of galaxy formation. *MNRAS* 330, 113–128.
- Kessel-Deynet, O., Burkert, A., 2000. Ionizing radiation in smoothed particle hydrodynamics. *MNRAS* 315, 713–721.
- Kheyfets, A., Miller, W.A., Zurek, W.H., 1990. Covariant smoothed particle hydrodynamics on a curved background. *Physical Review D* 41, 451–454.
- Klessen, R.S., Burkert, A., 2000. The formation of stellar clusters: Gaussian cloud conditions I. *ApJS* 128, 287–319.
- Klessen, R.S., Heitsch, F., Mac Low, M.-M., 2000. Gravitational collapse in turbulent molecular clouds. I. Gas dynamical turbulence. *ApJ* 535, 887–906.
- Klypin, A., Holtzman, J., 1997. Particle-mesh code for cosmological simulations. *ArXiv Astrophysics e-prints*, <arXiv:astro-ph/9712217>.
- Knebe, A., Green, A., Binney, J., 2001. Multi-level adaptive particle mesh (MLAPM): a code for cosmological simulations. *MNRAS* 325, 845–864.
- Kobayashi, C., 2004. GRAPE-SPH chemodynamical simulation of elliptical galaxies – I. Evolution of metallicity gradients. *MNRAS* 347, 740–758.
- Kunze, S., Speith, R., Riffert, H., 1997. Reproducing superhumps and gamma-shifts of SU UMa stars with SPH simulations. *MNRAS* 289, 889–897.
- Laguna, P., Miller, W.A., Zurek, W.H., 1993. Smoothed particle hydrodynamics near a black hole. *ApJ* 404, 678–685.
- Landau, L.D., Lifshitz, E.M., 1959. *Fluid Mechanics, Course of Theoretical Physics*. Pergamon Press, Oxford.
- Landau, L., Lifshitz, E., 1976. *Mechanics*, 12th ed. Akademie-Verlag, Berlin.
- Landshoff, R., 1955. A numerical method for treating fluid flow in the presence of shocks. Los Alamos National Laboratory Report, LA-1930.
- Lee, W.H., Ramirez-Ruiz, E., 2002. Accretion disks around black holes: dynamical evolution, meridional circulations, and gamma-ray bursts. *ApJ* 577, 893–903.
- Lee, W.H., Ramirez-Ruiz, E., Page, D., 2004. Opaque or transparent? A link between neutrino optical depths and the characteristic duration of short gamma-ray bursts. *ApJ* 608, L5–L8.
- Lee, W.H., Ramirez-Ruiz, E., Page, D., 2005. Dynamical evolution of neutrino-cooled accretion disks: detailed microphysics, lepton-driven convection, and global energetics. *ApJ* 632, 421–437.
- Leimkuhler, B., Reich, S., 2004. *Simulating Hamiltonian Dynamics*, first ed. Cambridge University Press, Cambridge.
- Libersky, L.D., Petschek, A.G., 1990. Smooth particle hydrodynamics with strength of materials. In: Trease, H.E., Fritts, M.J., Crowley, W.P. (Eds.), *Advances in the Free-Lagrange Method*. Springer-Verlag, pp. 248–257.
- Libersky, L.D., Petschek, A.G., Carney, T.C., Hipp, J.R., Allahdadi, F.A., 1993. High strain lagrangian hydrodynamics. *Journal of Computational Physics* 109, 67–75.
- Lucy, L., 1977. A numerical approach to the testing of the fission hypothesis. *The Astronomical Journal* 82, 1013.
- Mann, P., 1993. Smoothed particle hydrodynamics applied to relativistic spherical collapse. *Journal of Computational Physics* 107, 188–198.
- Mann, P., 1991. A relativistic smoothed particle hydrodynamics method tested with the shock tube. *Computer Physics Communications* 67, 245–260.
- Marri, S., White, S.D.M., 2003. Smoothed particle hydrodynamics for galaxy-formation simulations: improved treatments of multiphase gas, of star formation and of supernovae feedback. *MNRAS* 345, 561–574.
- Marti, J., Müller, E., 1996. *Journal of Computational Physics* 123, 1.
- Marti, J.M., Müller, E., 2003. Numerical hydrodynamics in special relativity. *Living Reviews in Relativity* 6, 7.
- Martinez-Serrano, F.J., Serna, A., Dominguez-Tenreiro, R., Molla, M., 2008. Chemical evolution of galaxies – I. A composition-dependent SPH model for chemical evolution and cooling. *MNRAS* 388, 39–55.
- Mayer, L., Lufkin, G., Quinn, T., Wadsley, J., 2007. Fragmentation of gravitationally unstable gaseous protoplanetary disks with radiative transfer. *ApJ* 661, L77–L80.
- Mihos, J.C., Hernquist, L., 1994. Star-forming galaxy models: blending star formation into TREE-SPH. *ApJ* 437, 611–624.
- Monaghan, J.J., 1985. Extrapolating B-Splines for interpolation. *Journal of Computational Physics* 60, 253.
- Monaghan, J.J., 1989. On the problem of penetration in particle methods. *Journal of Computational Physics* 82, 1–15.
- Monaghan, J.J., 1992. Smoothed particle hydrodynamics. *Annual Review of Astronomy and Astrophysics* 30, 543.
- Monaghan, J.J., 1997. SPH and Riemann solvers. *Journal of Computational Physics* 136, 298–307.
- Monaghan, J.J., 2002. SPH compressible turbulence. *MNRAS* 335, 843–852.
- Monaghan, J.J., 2005. Smoothed particle hydrodynamics. *Reports on Progress in Physics* 68, 1703–1759.
- Monaghan, J., Gingold, R., 1983. *Journal of Computational Physics* 52, 374.
- Monaghan, J.J., Price, D.J., 2001. Variational principles for relativistic smoothed particle hydrodynamics. *MNRAS* 328, 381–392.
- Morris, J., Monaghan, J., 1997. A switch to reduce sph viscosity. *Journal of Computational Physics* 136, 41.
- Navarro, J.F., Steinmetz, M., 1997. The effects of a photoionizing ultraviolet background on the formation of disk galaxies. *ApJ* 478, 13.
- Navarro, J.F., White, S.D.M., 1993. Simulations of dissipative galaxy formation in hierarchically clustering universes – Part one – Tests of the code. *MNRAS* 265, 271.
- Nelson, R., Papaloizou, J., 1994. Variable smoothing lengths and energy conservation in smooth particle hydrodynamics. *MNRAS* 270, 1.
- Nelson, A.F., Wetzstein, M., Naab, T., 2008. VINE – a numerical code for simulating astrophysical systems using particles II: Implementation and performance characteristics. *ArXiv e-prints*, 0802.4253.
- Noh, W.F., 1987. Errors for calculations of strong shocks using an artificial viscosity and an artificial heat flux. *Journal of Computational Physics* 72, 78–120.
- Norman, M.L., Winkler, K.-H., 1986. Why ultrarelativistic numerical hydrodynamics is difficult. In: Winkler, K.-H., Norman, M.L. (Eds.), *Astrophysical Radiation Hydrodynamics*. Reidel, Berlin.
- Oechslein, R., Rosswog, S., Thielemann, F.-K., 2002. Conformally flat smoothed particle hydrodynamics application to neutron star mergers. *Physics Review D* 65 (10), 103005.
- Owen, J.M., 2004. A tensor artificial viscosity for SPH. *Journal of Computational Physics* 201, 601–629.
- Owen, J.M., Villumsen, J.V., Shapiro, P.R., Martel, H., 1998. Adaptive smoothed particle hydrodynamics: methodology II. *ApJS* 116, 155.
- Oxley, S., Woolfson, M.M., 2003. Smoothed particle hydrodynamics with radiation transfer. *MNRAS* 343, 900–912.
- Pawlik, A.H., Schaye, J., 2008. TRAPHIC – radiative transfer for smoothed particle hydrodynamics simulations. *MNRAS* 389, 651–677.
- Pfrommer, C., 2008b. Simulating cosmic rays in clusters of galaxies – III. Non-thermal scaling relations and comparison to observations. *MNRAS* 385, 1242–1256.
- Pfrommer, C., Enßlin, T.A., Springel, V., 2008a. Simulating cosmic rays in clusters of galaxies – II. A unified scheme for radio haloes and relics with predictions of the γ -ray emission. *MNRAS* 385, 1211–1241.
- Phillips, G.J., Monaghan, J.J., 1985. A numerical method for three-dimensional simulations of collapsing, isothermal, magnetic gas clouds. *MNRAS* 216, 883–895.
- Porter, D.H., 1985. A study of hierarchical clustering of galaxies in an expanding universe. Ph.D. Thesis, AA(California Univ., Berkeley).
- Press, W.H., Flannery, B.P., Teukolsky, S.A., Vetterling, W.T., 1992. *Numerical Recipes*. Cambridge University Press, New York.
- Price, D., 2004. *Magnetic fields in astrophysics*. Ph.D. Thesis, University of Cambridge. Available from: [arXiv:astro-ph/0507472](http://arXiv.org/abs/astro-ph/0507472).
- Price, D.J., 2008. Modelling discontinuities and Kelvin–Helmholtz instabilities in SPH. *Journal of Computational Physics* 227, 10040–10057.
- Price, D.J., Monaghan, J.J., 2004a. Smoothed Particle Magnetohydrodynamics – I. Algorithm and tests in one dimension. *MNRAS* 348, 123–138.
- Price, D.J., Monaghan, J.J., 2004b. Smoothed Particle Magnetohydrodynamics – II. Variational principles and variable smoothing-length terms. *MNRAS* 348, 139–152.
- Price, D.J., Monaghan, J.J., 2005. Smoothed particle magnetohydrodynamics – III. Multidimensional tests and the $\nabla \cdot \mathbf{B} = 0$ constraint. *MNRAS* 364, 384–406.
- Price, D., Monaghan, J., 2007. An energy-conserving formalism for adaptive gravitational force softening in sph and n-body codes. *MNRAS* 374, 1347.
- Raiteri, C.M., Villata, M., Navarro, J.F., 1996. Simulations of galactic chemical evolution. I.O and Fe abundances in a simple collapse model. *A&A* 315, 105–115.
- Randles, P.W., Libersky, L.D., 1996. Smoothed particle hydrodynamics: some recent improvements and applications. *Computational Methods and Application in Mechanical Engineering* 139, 375–408.
- Rantsiou, E., Kobayashi, S., Laguna, P., Rasio, F., 2008. Mergers of black hole – neutron star binaries. I. Methods and first results. *ApJ* 680, 1326–1349.
- Raskin, C., Timmes, F.X., Scannapieco, E., Diehl, S., Fryer, C., 2009. On type Ia supernovae from the collisions of two white dwarfs. *MNRAS*. doi:10.1111/j.1745-3933.2009.00743.x.
- Read, J.I., Hayfield, T., Agertz, O., 2009. Resolving mixing in smoothed particle hydrodynamics. *ArXiv e-prints*, 0906.0774.
- Ritchie, B.W., Thomas, P.A., 2001. Multiphase smoothed-particle hydrodynamics. *MNRAS* 323, 743–756.
- Rosswog, S., 2005. Mergers of neutron star-black hole binaries with small mass ratios: nucleosynthesis, gamma-ray bursts, and electromagnetic transients. *ApJ* 634, 1202–1213.

- Rosswog, S., Davies, M.B., 2002. High-resolution calculations of merging neutron stars – I. Model description and hydrodynamic evolution. *MNRAS* 334, 481–497.
- Rosswog, S., Liebendörfer, M., 2003. High-resolution calculations of merging neutron stars – II. Neutrino emission. *MNRAS* 342, 673–689.
- Rosswog, S., Price, D., 2007. Magma: a magnetohydrodynamics code for merger applications. *MNRAS* 379, 915–931.
- Rosswog, S., Price, D., 2008. Meshless magnetohydrodynamics. *Springer Lecture Notes in Computational Science and Engineering*, 247–275.
- Rosswog, S., Liebendörfer, M., Thielemann, F.-K., Davies, M., Benz, W., Piran, T., 1999. Mass ejection in neutron star mergers. *A&A* 341, 499–526.
- Rosswog, S., Davies, M.B., Thielemann, F.-K., Piran, T., 2000. Merging neutron stars: asymmetric systems. *A&A* 360, 171–184.
- Rosswog, S., Ramirez-Ruiz, E., Hix, W.R., Dan, M., 2008. Simulating black hole white dwarf encounters. *Computer Physics Communications* 179, 184–189.
- Rosswog, S., Ramirez-Ruiz, E., Hix, R., 2008. Atypical thermonuclear supernovae from tidally crushed white dwarfs. *ApJ* 679, 1385.
- Rosswog, S., Ramirez-Ruiz, E., Hix, R., 2009. Tidal disruption and ignition of white dwarfs by moderately massive black holes. *ApJ* 695, 404–419.
- Rosswog, S., Kasen, D., Guillochon, J., Ramirez-Ruiz, E., 2009. Collisions of white dwarfs as a new progenitor channel for type Ia supernovae. *ArXiv e-prints*, 0907.3196.
- Rosswog, S., 2009. Conservative, special-relativistic smooth particle hydrodynamics. *ArXiv e-prints*, 0907.4890.
- Saitoh, T.R., Makino, J., 2009. A necessary condition for individual time steps in SPH simulations. *ApJL* 697, L99–L102.
- Scannapieco, E., Thacker, R.J., Davis, M., 2001. High-redshift galaxy outflows and the formation of dwarf galaxies. *ApJ* 557, 605–615.
- Scannapieco, C., Tissera, P.B., White, S.D.M., Springel, V., 2005. Feedback and metal enrichment in cosmological smoothed particle hydrodynamics simulations – I. A model for chemical enrichment. *MNRAS* 364, 552–564.
- Schäfer, C., Speith, R., Günther, R., Kley, W., 2004. Simulations of planet-disc interactions with SPH. *Astronomische Nachrichten Supplement* 325, 85.
- Schäfer, C., Speith, R., Kley, W., 2007. Collisions between equal-sized ice grain agglomerates. *A&A* 470, 733–739.
- Schutz, B., 1989. *A First Course in General Relativity*, first ed. Cambridge University Press, Cambridge.
- Semelin, B., Combes, F., Baek, S., 2007. Lyman-alpha radiative transfer during the epoch of reionization: contribution to 21-cm signal fluctuations. *A&A* 474, 365–374.
- Shapiro, P.R., Martel, H., Villumsen, J.V., Owen, J.M., 1996. Adaptive smoothed particle hydrodynamics, with application to cosmology: methodology. *ApJS* 103, 269.
- Shu, F., 1992. *Gas Dynamics*. University Science Books.
- Siegler, S., 2000. Entwicklung und untersuchung eines smoothed particle hydrodynamics verfahrens für relativistische strömungen. Ph.D. Thesis, Eberhard-Karls-Universität Tübingen.
- Siegler, S., Riffert, H., 2000. Smoothed particle hydrodynamics simulations of ultrarelativistic shocks with artificial viscosity. *ApJ* 531, 1053–1066.
- Sijacki, D., Springel, V., 2006. Physical viscosity in smoothed particle hydrodynamics simulations of galaxy clusters. *MNRAS* 371, 1025–1046.
- Sijacki, D., Frommer, C., Springel, V., Enßlin, T.A., 2008. Simulations of cosmic-ray feedback by active galactic nuclei in galaxy clusters. *MNRAS* 387, 1403–1415.
- Sirono, S., 2004. Conditions for collisional growth of a grain aggregate. *Icarus* 167, 431–452.
- Sod, G., 1978. A survey of several finite difference methods for systems of nonlinear hyperbolic conservation laws. *Journal of Computational Physics* 43, 1–31.
- Sommer-Larsen, J., Gelato, S., Vedel, H., 1999. Formation of disk galaxies: feedback and the angular momentum problem. *ApJ* 519, 501–512.
- Springel, V., 2000. Modelling star formation and feedback in simulations of interacting galaxies. *MNRAS* 312, 859–879.
- Springel, V., 2005. The cosmological simulation code GADGET-2. *MNRAS* 364, 1105–1134.
- Springel, V., Hernquist, L., 2002. Cosmological smoothed particle hydrodynamics simulations: the entropy equation. *MNRAS* 333, 649–664.
- Springel, V., Hernquist, L., 2003. Cosmological smoothed particle hydrodynamics simulations: a hybrid multiphase model for star formation. *MNRAS* 339, 289–311.
- Springel, V., Yoshida, N., White, S.D.M., 2001. GADGET: a code for collisionless and gas dynamical cosmological simulations. *New Astronomy* 6, 79–117.
- Springel, V., White, M., Hernquist, L., 2001. Hydrodynamic simulations of the Sunyaev-Zeldovich Effect(s). *ApJ* 549, 681–687.
- Springel, V., Di Matteo, T., Hernquist, L., 2005. Modelling feedback from stars and black holes in galaxy mergers. *MNRAS* 361, 776–794.
- Stamatellos, D., Whitworth, A.P., 2005. Monte Carlo radiative transfer in SPH density fields. *A&A* 439, 153–158.
- Steinmetz, M., 1996. GRAPESPH: cosmological smoothed particle hydrodynamics simulations with the special-purpose hardware GRAPE. *MNRAS* 278, 1005–1017.
- Steinmetz, M., Müller, E., 1993. On the capabilities and limits of smoothed particle hydrodynamics. *A&A* 268, 391–410.
- Steinmetz, M., Müller, E., 1994. The formation of disk galaxies in a cosmological context: populations, metallicities and metallicity gradients. *A&A* 281, L97–L100.
- Steinmetz, M., Müller, E., 1995. The formation of disc galaxies in a cosmological context: structure and kinematics. *MNRAS* 276, 549–562.
- Susa, H., 2006. Smoothed particle hydrodynamics coupled with radiation transfer. *Publications of the Astronomical Society of Japan* 58, 445–460.
- Takeda, H., Miyama, S.M., Sekiya, M., 1994. Numerical simulation of viscous flow by smoothed particle hydrodynamics. *Progress of Theoretical Physics* 92 (5), 939–960.
- Thacker, R.J., Couchman, H.M.P., 2000. Implementing feedback in simulations of galaxy formation: a survey of methods. *ApJ* 545, 728–752.
- Thacker, R.J., Couchman, H.M.P., 2001. Star formation supernova feedback and the angular momentum problem in numerical cold dark matter cosmogony: halfway there? *ApJL* 555, L17–L20.
- Theuns, T., 1994. Parallel P3M with exact calculation of short range forces. *Computer Physics Communications* 78, 238–246.
- Theuns, T., Leonard, A., Efstathiou, G., Pearce, F.R., Thomas, P.A., 1998. P³M-SPH simulations of the Ly α forest. *MNRAS* 301, 478–502.
- Theuns, T., Viel, M., Kay, S., Schaye, J., Carswell, R.F., Tzanavaris, P., 2002. Galactic winds in the intergalactic medium. *ApJL* 578, L5–L8.
- Thomas, P.A., Couchman, H.M.P., 1992. Simulating the formation of a cluster of galaxies. *MNRAS* 257, 11–31.
- Timmes, F.X., 1999. Integration of nuclear reaction networks for stellar hydrodynamics. *ApJS* 124, 241–263.
- Tornatore, L., Borgani, S., Springel, V., Matteucci, F., Menci, N., Murante, G., 2003. Cooling and heating the intracluster medium in hydrodynamical simulations. *MNRAS* 342, 1025–1040.
- Tornatore, L., Borgani, S., Matteucci, F., Recchi, S., Tozzi, P., 2004. Simulating the metal enrichment of the intracluster medium. *MNRAS* 349, L19–L24.
- van den Bosch, F.C., Abel, T., Hernquist, L., 2003. The angular momentum of gas in protogalaxies – II. The impact of pre-heating. *MNRAS* 346, 177–185.
- Verlet, L., 1967. Computer experiments on classical fluids. I. Thermodynamical properties of Lennard-Jones molecules. *Physics Review* 159, 98–103.
- Viau, S., Bastien, P., Cha, S.-H., 2006. An implicit method for radiative transfer with the diffusion approximation in smooth particle hydrodynamics. *ApJ* 639, 559–570.
- Vignjevic, R., Campbell, J., Libersky, L., 2000. A treatment of zero-energy modes in the smoothed particle hydrodynamics method. *Computation Methods and Application in Mechanical Engineering* 184, 67–85.
- VonNeumann, J., Richtmyer, R.D., 1950. A method for the numerical calculation of hydrodynamic shocks. *Journal of Applied Physics* 21, 232–237.
- Wadsley, J.W., Stadel, J., Quinn, T., 2004. Gasoline: a flexible, parallel implementation of TreeSPH. *New Astronomy* 9, 137–158.
- Warren, M.S., Salmon, J.K., 1995. A parallel, portable and versatile treecode. In: *Parallel Processing for Scientific Computing*, 319–324.
- Watkins, S., Bhattal, A., Francis, N., Turner, J., Whitworth, A., 1996. A new prescription for viscosity in smoothed particle hydrodynamics. *A&AS* 119, 177.
- Wetzstein, M., Nelson, A.F., Naab, T., Burkert, A., 2008. VINE – a numerical code for simulating astrophysical systems using particles I: description of the physics and the numerical methods. *ArXiv e-prints*, 0808.4245.
- Whitehouse, S.C., Bate, M.R., 2006. The thermodynamics of collapsing molecular cloud cores using smoothed particle hydrodynamics with radiative transfer. *MNRAS* 367, 32–38.
- Whitehouse, S.C., Bate, M.R., Monaghan, J.J., 2005. A faster algorithm for smoothed particle hydrodynamics with radiative transfer in the flux-limited diffusion approximation. *MNRAS* 364, 1367–1377.
- Whitham, G., 1974. *Linear and Non-linear Waves*. John Wiley, New York.
- Wiersma, R.P.C., Schaye, J., Theuns, T., Dalla Vecchia, C., Tornatore, L., 2009. Chemical enrichment in cosmological, smoothed particle hydrodynamics simulations. *MNRAS*. doi:10.1111/j.1365-2966.2009.15331.x.
- Wilson, J.R., 1982. In: *Centrella, J.M., LeBlanc, J.M., Bowers, R.L. (Eds.), Numerical Astrophysics*. Jones and Bartlett, Boston, p. 422.
- Wilson, J.R., Mathews, G., Marronetti, P., 1996. *Physics Review D* 54, 1317.
- Yoon, S., Podsiadlowski, P., Rosswog, S., 2007. Remnant evolution after a carbon-oxygen white dwarf merger. *MNRAS* 380, 933.